The Pennsylvania State University

Graduate School

Department of Chemistry

STRUCTURAL CHARACTERIZATION OF THE TRUNCATED HEMOGLOBIN FROM *SYNECHOCYSTIS* SP. PCC 6803

A Thesis in

Chemistry

by

Bao-Han Christie Vu

Submitted in Partial Fulfillment
of the Requirements
for the Degree of

Doctor of Philosophy

December 2004

The thesis of Bao-Han Christie Vu was reviewed and approved* by the following:

Juliette T.J. Lecomte
Associate Professor of Chemistry
Thesis Advisor
Chair of Committee

Alan J. Benesi
Lecturer in Chemistry

Philip C. Bevilacqua
Associate Professor of Chemistry

J. Martin Bollinger
Associate Professor of Biochemistry
and Molecular Biology

Ayusman Sen
Professor of Chemistry
Head of the Department of Chemistry

*Signatures are on file in the Graduate School

ABSTRACT

This thesis details studies of the heme pocket structure from the truncated hemoglobin (Hb) from the cyanobacterium *Synechocystis* sp. PCC 6803. *Synechocystis* sp. PCC 6803 Hb contains an endogenously hexacoordinate heme iron, with His46 (distal) and His70 (proximal) serving as axial ligands. The solution structure of the ferric form (hemichrome), revealed a highly α-helical protein with a fold similar to that of other truncated hemoglobins [Falzone, C. J. et al. (2002) *J. Mol. Biol*. *324*, 1015]. Characterization of the protein in solution showed that it is able to undergo a post-translational modification of the heme 2-vinyl group [Scott, N. L. et al. (2002) *Biochemistry* 41, 6902]. The reaction was facilitated by sodium dithionite reduction of the iron. Optical and NMR data indicated that the heme iron in the product remained low-spin Fe(III). Mass spectrometry and NMR spectroscopy established that a covalent link was formed between His117 and the α-position of the 2-vinyl group. Optical methods showed that covalent attachment of the heme group stabilized the protein by >20 °C with respect to thermal denaturation and 1.1 pH units with respect to acid denaturation. The unique reactivity of His117 was confirmed by mutagenesis. Thus His117Ala *Synechocystis* sp. PCC 6803 Hb was incapable of forming the cross-link. Cyanide binding experiments were performed on this mutant to characterize the metcyano form in the absence of the cross-link. It was found that His46 (distal) was displaced from the heme iron. A hydrogen bonding network involving the cyanide ion, Tyr22, Gln43 and Gln47 was detected, likely mimicking that in the related hemoglobins from *Chlamydomonas eugametos* and *Mycobacterium tuberculosis*. Kinetic data indicated that the variant bound cyanide more slowly than the wild-type protein and

suggested that position 117 had an influence on the properties of the heme pocket. Ligand binding in hemoglobins is known to be modulated by structural interactions at the proximal and distal ligand sites. Here, hyperfine chemical shifts were used to probe the relationship between heme electronic structure and axial ligand orientation. The data indicated that the covalent modification perturbed moderately the orientation of the axial ligands and overall heme electronic structure. The heme pocket structure in the ligand dissociated state was probed by incorporation of Zn(II) protoporphyrin IX in place of heme. NMR studies on the pentacoordinate zinc protein revealed that His46 moved away from the porphyrin ring; however, the conformation was neither that observed in the hemichrome, nor that in the metcyano complex. The hemoglobin characterization presented here demonstrated new reactivity and conformational properties expanding in unexpected ways the structure-function relationship within this family of proteins.

TABLE OF CONTENTS

LIST OF FIGURES

LIST OF TABLES

LIST OF ABBREVIATIONS

2,4-DPIX	2,4-dimethyldeuteroheme
Ala, A	Alanine
Arg, R	Arginine
Asn, N	Asparagine
Asp, D	Aspartic Acid
Ce	*Chlamydomonas eugametos*
Cys, C	Cysteine
ddH_2O	Distilled-deionized water
DEAE	Diethylaminoethyl
DNA	Deoxyribonucleic acid
DQF-COSY	Double-quantum-filtered correlation spectroscopy
EDTA	Ethylenediaminetetraacetic acid
GlbN	Cyanoglobin
Gln, Q	Glutamine
Glu, E	Glutamic Acid
Gly, G	Glycine
Hb	Hemoglobin
HbCN	Metcyano hemoglobin
His, H	Histidine
HMQC	Heteronuclear multiple quantum coherence
HPLC	High performance liquid chromatography
HSQC	Heteronuclear single quantum coherence
hxHb	Hexacoordinate hemoglobin
Ile, I	Isoleucine
IPTG	Isopropyl β-D-thiogalactopyranoside
LC	Liquid chromatography
Leu, L	Leucine
Lys, K	Lysine
MALDI	Matrix-assisted laser desorption/ionization
Mb	Myoglobin
Met, M	Methionine
MS/MS	Tandem mass spectrometry
Mt	*Mycobacterium tuberculosis*
NMR	Nuclear magnetic resonance
NOE	Nuclear Overhauser effect
NOESY	Nuclear Overhauser effect spectroscopy (multi-dimensional)
nsHb	Nonsymbiotic plant hemoglobin
PAGE	Polyacrylamide gel electrophoresis
Pc	*Paramecium caudatum*
PDB	Protein data bank
Phe, F	Phenylalanine
ppm	Parts per million
Pro, P	Proline
rHb-DPIX	Recombinant hemoglobin reconstituted with 2,4-dimethyldeuteroheme

rHb-R	Recombinant heme reconstituted hemoglobin
rHb-A	Recombinant hemoglobin with a covalent heme attachment
S6803	*Synechocystis* sp. PCC 6803
S7002	*Synechococcus* sp. PCC 7002
SDS	Sodium dodecylsulfate
Ser, S	Serine
swMb	Sperm whale (*Physeter catodon*) myoglobin
T	Temperature
T_1	Spin-lattice relaxation time
Thr, T	Threonine
TOCSY	Totally correlated two-dimensional spectroscopy
TPPI	Time-proportional phase incrementation
trHb	Truncated hemoglobin
Tris	Tris(hydroxymethyl)aminomethane
Trp, W	Tryptophan
Tyr, Y	Tyrosine
UV	Ultra-violet
Val, V	Valine
WATERGATE	Water suppression by gradient-tailored excitation
WEFT	Water elimination Fourier transform
wt	Wild-type
ZnPPIX	Zinc protoporphyrin IX

ACKNOWLEDGEMENTS

The successful completion of my graduate career would not be possible without the support many people. First, I would like to express my gratitude to Dr. Juliette Lecomte for her invaluable guidance, infinite patience, and unwavering kindness during my time here. Without her, I could never dream to be the scientist I am today. I would like to thank Dr. Christopher Falzone and the members of the Lecomte Group for all the thought-provoking discussion, experimental assistance, personal support, and laughter-filled days which made every day a new adventure. I also would like to thank the members of my committee for reading the manuscript and helping me understand the broader implications of scientific research. Namaste and Dhanyavaad to Janell Schaak, Christina Kraemer-Pecore and Sue Mattingly for all the support and laughter over endless bowls of kheer. I thank Arti Patel and other friends from days gone by who listened and lifted me up, even if they didn't quite understand what I was talking about. Most importantly, I would like to thank my family, especially mom and dad, for believing in me, especially on days I didn't understand my own potential. I've walked a different path than originally planned, but I am fortunate and grateful for all the support of all those around me. I hope to be a reflection of all your goodness.

Chapter 1

Introduction

1.1 Hemoglobins

Hemoglobins (Hbs) form a large protein superfamily and can be found in all kingdoms of organisms (Hardison 1998). Members of this family are defined by a unique α-helical fold that includes a single iron-protoporphyin (heme, Figure 1.1) group per polypeptide chain (Antonini & Brunori 1971). Among the Hb superfamily, vertebrate Hbs and myoglobins (Mbs) are well known for their oxygen transport and storage properties. Hbs have been widely studied to understand how structure-function relationships vary in various organism groupings. Over the past decade, a number of new Hbs have been discovered in plants root nodules (Arrendondo-Peter et al. 1997), unicellular eukaryotes (Couture & Guertin 1996), pathogens (Couture et al. 1999b), cyanobacteria (Angeloni & Potts 1994, Kaneko et al. 1996), nerve tissue, (Burmester et al. 2000) and human tissue (Burmester et al. 2002). Cyanobacterial, protest, algal and certain bacterial Hbs have shortened primary structures and are called truncated hemoglobins (trHbs, Wittenberg et al. 2002). Finally, structural studies on several Hbs from plants, animals and cyanobacteria reveal a heme iron coordinated by two protein side chains. These hexacoordinate hemoglobins are able to bind exogenous ligands following displacement of one of the endogenous axial ligands (Dewilde et al. 2001, Hvitved et al. 2001, Kundu et al. 2003, Sawai et al. 2003, Trent et al. 2001a, Trent et al. 2001b). The remainder of this introduction expands on these key aspects of Hb chemistry.

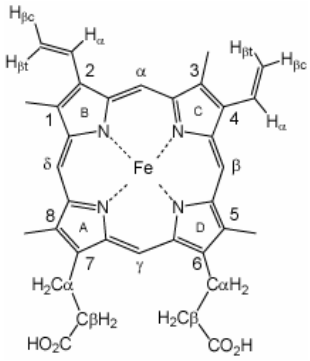

Figure 1.1 The structure of iron-protoporphyrin IX (heme) with substituent numbering as in the text.

1.1.1 The Globin Fold.

The typical β globin fold contains approximately 150 residues. The structure of sperm whale Mb, a well-studied representative, is shown in Figure 1.2. The chain folds to form eight helices (A-H, defined in Figure 1.3) in a unique three-on-three structure (Kendrew et al. 1960). The helices are arranged around the heme group to protect it from excessive water access (Liong et al. 2001) and to form a pocket suitable for oxygen binding. Helix F contains a strictly conserved histidine (HisF8) that coordinates the iron ion and defines the proximal side of the heme (Kendrew et al. 1960). The physiological oxidation state of the iron in Hb and Mb is Fe^{2+}. In the absence of oxygen, the heme is coordinated by five ligands, four from the porphyrin nitrogens and one from a nitrogen of HisF8 (Antonini & Brunori 1971, Kendrew et al. 1960). At the sixth coordination site, or distal site, water may be loosely associated with the iron ion (Antonini & Brunori 1971). Binding of oxygen to this "deoxy" state on the distal side produces a hexacoordinated heme. In the ferrous state, Hb and Mb bind not only O_2 but also CO. The composition

and structure of the heme cavity are essential to control the relative affinity for these two ligands (Gibson et al. 1992, Springer et al. 1989).

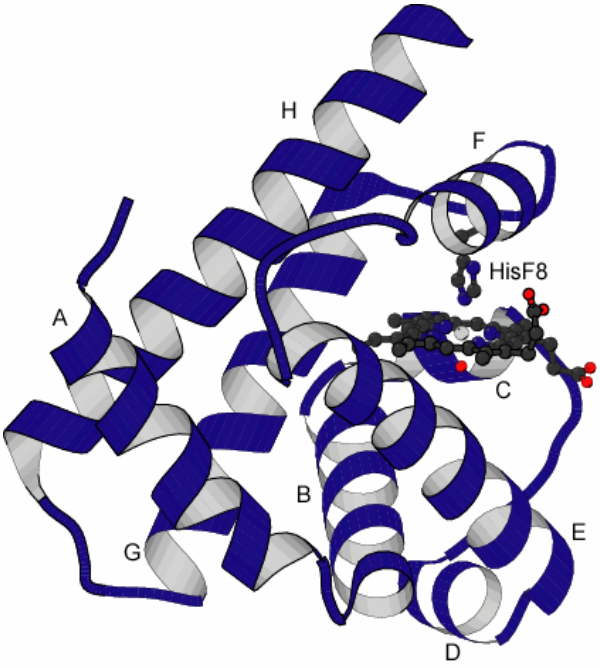

Figure 1.2 The crystal structure of sperm whale (*Physeter catodon*) Mb (swMb, PDB code 4mbn). The helices (A-H) have been labeled according to the Perutz notation (Perutz et al. 1965) as shown in Figure 1.3. The proximal ligand, His93(F8), is shown coordinating the heme iron.

Oxidation of the iron to the ferric state leads to a non-functional ("met") form of the protein. This met compound is capable of binding different ligands, such as water, hydroxide ion, cyanide ion and others, and has been useful for many structural studies, in particular when the reduced state of the protein is unstable. The spin state of the Fe(III) these various complexes, and therefore their spectral properties, depend on the strength of the sixth ligand. When water is bound, the iron is high spin (S = 5/2) but ligands such as cyanide and imidazole form low-spin complexes (S = 1/2). MetHb and metMb from

vertebrates are hexacoordinated species with water or hydroxide ion bound to the iron (Antonini & Brunori 1971).

1.1.2 Structure-Function Relationships in Globins

Besides HisF8, only one residue, PheCD1, appears strongly conserved across all globin sequences (Bashford et al. 1987, Burmester et al. 2002, Burmester et al. 2000). This residue is thought to be key in holding the heme in its binding pocket. Multiple sequence alignment also reveals a selective pressure to maintain the hydrophobic environment of the heme pocket (Bashford et al. 1987, Perutz et al. 1965, Ptitsyn & Ting 1999). One example of conservation of hydrophobic residues in vertebrate globins occurs at ValE11. Mutation of this valine to arginine in swMb results in increased oxygen affinity (Krzywda et al. 1998). Whereas incorporation of polar residues at E11 increases oxygen affinity, it greatly decreases the stability of apoMb (Hargrove et al. 1994). Residues controlling the differential affinity for O_2 and CO include those at positions E7 and B10. HisE7 is a notable exception to the conservation of hydrophobic residue in the heme pocket. This side chain, which is found in many vertebrate Mbs and Hbs, regulates ligand affinity and specificity through H-bonding with O_2 (Lukin et al. 2000). The size of the residue at E7 also plays a role; mutation of HisE7 to Tyr resulted in decreased CO affinity presumably because of steric hindrance (Springer et al. 1989). Conservation of LeuB10 in vertebrate Mb results from a selective pressure to optimize the relationship between auto-oxidation and oxygen dissociation (Carver et al. 1992). Substitution of smaller residues at B10 leads to increased water disorder in the pocket and indeed facilitates auto-oxidation of the reduced heme. At the same time, larger residues

such as phenylalanine at this position decrease the oxygen dissociation rate and decrease auto-oxidation of the protein. Although LeuB10 is highly conserved in mammalian Hbs and Mbs, isoleucine is occasionally tolerated in Hbs (Bashford et al. 1987, Ptitsyn & Ting 1999). Structural elements regulating ligand binding in nonvertebrate Hbs vary from those in their vertebrate partners. Instead of LeuB10 and HisE7, tyrosine and glutamine are typically found at B10 and E7, respectively (Bolognesi et al. 1997, Weber & Vinogradov 2001). These residues form a hydrogen bonding network that stabilizes the ligand bound at the distal site. When apolar residues are incorporated at position E7, the affinity for polar ligands (O_2, CN^-, N_3^-) diminishes (Bolognesi et al. 1997, Conti et al. 1993). In addition, the residues at B9, B14, CD1, E10 and E11 are especially important in nonvertebrate Hbs and have been shown to bring the B10 and E7 sidechains into the correct position to facilitate ligand binding (Bolognesi et al. 1997, Conti et al. 1993, Qin et al. 1993, Quillin et al. 1993, Quillin et al. 1995, Rizzi et al. 1996).

1.2 Truncated Hemoglobins

Truncated hemoglobins (trHbs) represent a distinct set of proteins within the Hb superfamily (Wittenberg et al. 2002). These proteins can be found in a variety of plants, unicellular eukaryotes and bacteria. Compared to other nonvertebrate Hbs, trHb sequences are shorter by 20-30 residues (Figure 1.3), with deletions and additions occurring in specific regions of the primary structure. Differences in trHb structure include shortened A helices and elimination of the D helix to form a compact CD loop. Sequence analysis indicates that trHbs can be separated into three groups: I (N), II (O), and III (P) (Wittenberg et al. 2002). Invariant among these groups is HisF8, the proximal

histidine ligand conserved across all Hbs (Dickerson & Geis 1983). A PheB9-TyrB10 pair is strongly conserved among trHb sequences with only a few exceptions (Wittenberg et al. 2002). Within these trHb groups, specific patterns of conservation are seen. Within group I and II trHbs, Gly-Gly motifs are found in the AB and EF interhelical regions. PheCD1 is strictly conserved in group I and III trHbs but His and Tyr residues are also observed at this position in group II members. An apolar region in the heme pocket is maintained by the predominance of phenylalanine at position E14.

Figure 1.3 (following 2 pages) TrHb primary structure alignment. The sequences of trHbs reviewed by Wittenberg et al. plus that from *Synechococcus* sp. PCC 7002 (S7002) are listed. They are compared to the primary structure of sperm whale (*Physeter catodon*) Mb (swMb). The sequences are arranged by group I (top), II (middle) and III (bottom) trHbs. The helical arrangement in Perutz notation (Perutz et al. 1965) is shown above the swMb sequence. Patterns of conservation among Hbs are shown in color. The positions in blue, B10, CD1, E7 and F8, are key in regulating ligand binding across all Hbs. HisF8 is the only residue strictly conserved among all Hb sequences. The AB and EF glycine motifs (shown in green) are characteristic of the trHb fold. In S6803 and S7002 trHbs, the distal ligand, His46(E10), and reactive residue, His117(H16), are highlighted in orange and red respectively. The organisms listed are: *Chlamydomonas eugametos* (*C. eugametos*), *Chlamydomonas reinhardtii* (*C. reinhardtii*), *Paramecium caudatum* (*P. caudatum*), *Mycobacterium tuberculosis* (*M. tuberculosis*), *Mycobacterium avium* (*M. avium*), *Mycobacterium smegmatis* (*M. smegmatis*), *Mycobacterium leprae* (*M. leprae*), *Tetrahymena pyriformis* (*T. pyriformis*), *Legionella pneumophila* (*L.*

pneumophila), *Synechocystis* sp. PCC 6803 (*Synechocystis* sp.), *Nostoc commune* (*N. commune*), *Pseudomonas syringae* (*P. syringae*), *Methylococcus capsulatus* (*M. capsulatus*), *Synechococcus* sp. PCC 7002 (*Synechococcus* sp.), *Corynebacterium diptherae* (*C. diptherae*), *Streptomyces coelicolor* (*S. coelicolor*), *Shewanella putrefaciens* (*S. putrefaciens*), *Bordetella pertussis* (*B. pertussis*), *Thiobacillus ferrooxidans* (*T. ferrooxidans*), *Sinorhizobium meliloti* (*S. meliloti*), *Burkholderia mallei* (*B. mallei*), *Deinococcus radiodurans* (*D. radiodurans*), *Bacillus subtilis* (*B. subtilis*), *Bacillus anthracis* (*B. anthracis*), *Staphylococcus aureus* (*S. aureus*), *Staphylococcus epidermis* (*S. epidermis*), *Arabidopsis thaliana* (*A. thaliana*), *Gossypium hisurtum* (*G. hisurtum*), *Hordeum vulgare*(*H. vulgare*), *Glycine max* (*G. max*), *Campylobacter jejuni* (*C. jejuni*), *Brucella suis* (*B. suis*), and *Caulobacter crescentus* (*C. crescentus*).

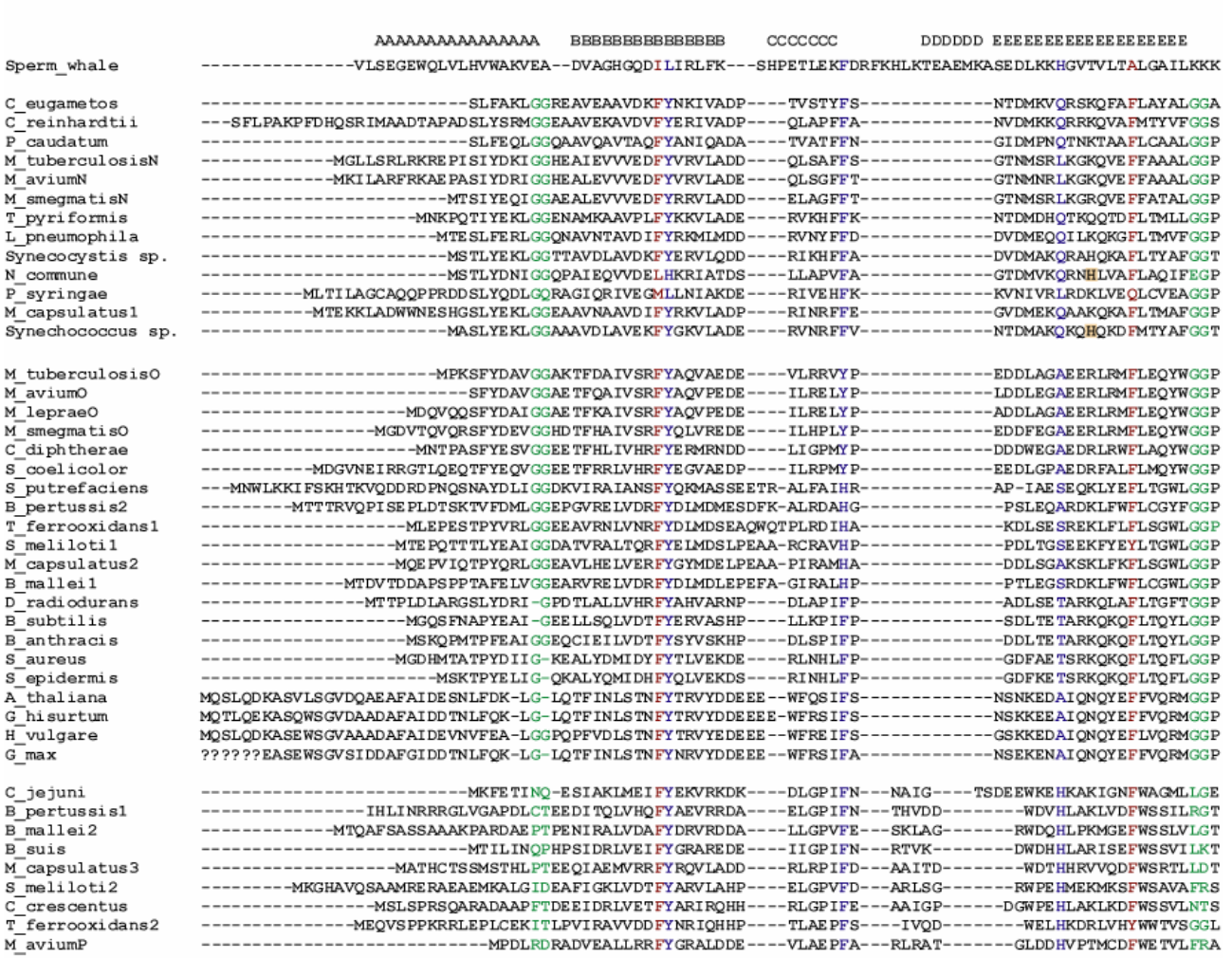
AAAAAAAAAAAAAAA BBBBBBBBBBBBBB CCCCCCC DDDDDD EEEEEEEEEEEEEEEEEE
Sperm_whale
C_eugametos
C_reinhardtii
P_caudatum
M_tuberculosisN
M_aviumN
M_smegmatisN
T_pyriformis
L_pneumophila
Synecocystis sp.
N_commune
P_syringae
M_capsulatus1
Synechococcus sp.
M_tuberculosisO
M_aviumO
M_lepraeO
M_smegmatisO
C_diphtherae
S_coelicolor
S_putrefaciens
B_pertussis2
T_ferrooxidans1
S_meliloti1
M_capsulatus2
B_mallei1
D_radiodurans
B_subtilis
B_anthracis
S_aureus
S_epidermis
A_thaliana
G_hisurtum
H_vulgare
G_max
C_jejuni
B_pertussis1
B_mallei2
B_suis
M_capsulatus3
S_meliloti2
C_crescentus
T_ferrooxidans2
M_aviumP


FFFFFFFF GGGGGGGGGGGGGGGGGG HHHHHHHHHHHHHHHHHHHHHHHH
Sperm_whale GHHEAE----LKPLAQSHATKHK------IPIKYLEFISEAIIHVLHSRHPG----DFGADAQ-GAMNKALELFRKDIAAKYKELGYQG----------
C_eugametos --SEWK---GKD-MRTAHK--DLVPH---LSDVHFQAVARHLSDTLTEL-------GVPPEDITDAMAVVASTRTEVLNMPQQ----------
C_reinhardtii --GAYE---GRDL-GASHR--RLIREQ-GMNHHHFDLVAAHLDSTLQEL-------GVAQELKAEAMAIVASARPLIFGTGEAGAAN----------
P_caudatum --NAWT---GRN-LKEVHA--NMGV-----SNAQFTTVIGHLRSALTGA-------GVAAALVEQTVAVAETVRGDVVTV----------
M_tuberculosisN --EPYT---GAP-MKQVHQ--GRGIT-----MHHFSLVAGHLADALTAA-------GVPSETITEILGVIAPLAVDVTSGESTTAPV----------
M_aviumN --HPYT---GAP-MKQVHQ--GRGIT-----MHHFGLVAGHLADALTAA-------GVPSETVSEILGAIAPLAPEIATGEA----------
M_smegmatisN --DEYT---GAP-MRQVHQ--GRGIT-----MHHFDLVAGHLGDALSAA-------GMPGATTSQIIAAIAPLAPEIATARTA----------
T_pyriformis --NHYK---GKN-MTEAHK--GMNLQ-----NLHFDAIIENLAATLKEL-------GVTDAVINEAAKVIEHTRKDMLGK----------
L_pneumophila --NQYT---GKS-MREGHQ--HLLARGLN--DSHVDIVIEHLGETLKEL-------GANEEDIQKVAAIANSVRGDVLGRSS----------
Synechocystis sp. --DKYD---GRY-MREAHK--ELVENHGLN-GEHFDAVAEDLLATLKEM-------GVPEDLIAEVAAVAGAPAHKRDVLNQ----------
N_commune --KQYG---GRP-MDKTHA--GLNLQ-----QPHFDAIAKHLGERMAVR-------GVSAENTKAALDRVTNMKGAILNK----------
P_syringae --CRYT---GDS-MAESHK--GQNLT-----PSDFNALVENLIAAMDTE-------NVPVPVQNRLIARLAPMRGEVLGK----------
M_capsulatus1 --HNYT---GMD-MRRGHA--HLVKQGLN--DAHFDAVMEHLGATMKEL-------NVPDELIAQAAAIAESTRNDVLGR----------
Synechococcus sp. --DRFP---GRS-MRAAHQ--DLVENAGLT-DVHFDAIAENLVLTLQEL-------NVSQDLIDEVVTIVGSVQHRNDVLNR
M_tuberculosisO --RTYSEQRGHPRLRMRHA--PFRIS-----LIERDAWLRCMHTAVASIDSETLDDEHRRELLDYLEMAAHSLVNSPF----------
M_aviumO --RTYSDRRGHPRLRMRHV--PFRIT-----PLARDAWLRCMHTAVASIDSKTLDDEHRRELLDYLEMAAHSLVNSP----------
M_lepraeO --RTYSSQRGHPRLRMRHA--PFRIT-----AIERDAWLRCMHTAVASIDSHTLDNEHRRELLDYLEMAAHSLVNSAS----------
M_smegmatisO --RTYSDQRGHPRLRMRHA--PFRIG-----FLERDAWLRCMHTAVAEIDSQTLDDAHRRALLDYLQMAADSMVNSAF----------
C_diphtherae --QTFSENRGHPRLRMRHA--HFPIG-----MNEAQRWLDIMSDTLDSIEATLPPAHRAAMWDHMQRVAQMLINQAP----------
S_coelicolor --TTYSDNRGHPRLRMRHA--PFAVD-----RAAHDAWLKHMRVALDELGLSEEHEQTLWKYLTYAAASMINTPG----------
S_putrefaciens --QLYQQKYGHPALRARHM--HFAVD-----EAMRDQWLFCMKFAIEKHIKKPEHRAAIYEAISTLADHMRNQ----------
B_pertussis2 --DHYIERFGHPRLRARHL--PFSIG-----EIERDQWVACMGRAMQDQQLPAALVDRLLQAFYGTADWMRNRAG----------
T_ferrooxidans1 --DLYVQRFGHPRLRARHA--SVPVD-----DQARDQWMACMLQAMHEVGIEPELYGHLQGAFQRTADFMRNR----------
S_melilotil --PIYVQKRGHPMLRRRHF--IAGIG-----PAERDEWLFCFTRALEETVSHPKLREIILEPITRLAHHMQNKE----------
M_capsulatus2 --DLFVQEFGHPRLRARHF--PFSIG-----VPERDQWLLCMRKALDDIPLDGPFREALYEALARTAHHMINRED----------
B_mallei1 --DHYIERFGHPRLRARHL--PFPIA-----SSERDQWLRCIAWAMQDVGLDEPLRERLMHSFHDTADWMRNRPG----------
D_radiodurans --PLYHELYGHPRLRARHL--PFPIT-----PGRARAWLACMNAALRETPGLAEADAHELYAALARVAVHMVNTEEAPDSDSSGEAANATPNAT--------
B_subtilis --PLYTEEHGHPMLRARHL--PFPIT-----NERADAWLSCMKDAMDHVGLEGEIREFLFGRLELTARHMVNQTEAEDRSS----------
B_anthracis --NLYTEEHGHPMLRARHL--PFEIT-----PKRAEAWLSCMEQAMDDTGVHGHIREFVFERLALTAQHMVNTPNETGEI----------
S_aureus --NIYTEEHGHPMLRKRHI--DFTIT-----EFERDAWLENMQTAINRAAFPQGVGDYLFERLRLTANHMVNS----------
S_epidermis --DLYTQEHGHPMLKRRHM--EFTIS-----EYERDAWLENMHTAIQHAELPAGVGDYLFERLRLTAHHMVNS----------
A_thaliana --PLYSQRKGHPALIGRHR--PFPVT-----HQAAERWLEHMQNALDDSVDIDQDSKIKMMKFFRHTAFFLVAGNELKNQNEKPKHKPQ----------
G_hisurtum --PLYSQRKGHPALIARHK--PFPVT-----HQAAERWLYHMEKALKSTPDIDADSRVKMMNFLRHTAFFLVAGDELKT----------
H_vulgare --PLFSQRRGHPALIGRHR--PFPVT-----HRAAERWLHHMQQALETTQSINPDTKTKMMNFFRHTAYFLVAGNEMTRQTQSVPPCKH----------
G_max --PLFSQRRGHPALIARHR--PFPVT-----HQAAERWLHHMQHALDSTTDIDDDSKTKMMNFFR----------
C_jejuni --GDYN---GQP--LKKHL--DLPPFP----QEFFEIWLKLFEESLNIVY-NEEMKNVILQRAQMIASHFQNMLYKYGGH----------
B_pertussis1 --GRFR---GTP--MPRHV--ALPGLH----AGLFERWLRLFRATAAAQPN-QAMAEQACLMAGRIAQSLWYGYQLHRSPDQAPTDLAHG----------
B_mallei2 --KSYR---GNV--QAAHQ--PLDGLE----PVHFSRWLALFLKTVEARYE-PAAAVRFMEPALRIAQSLQLSRFGWDYRIPAEQQVILDLIAPKRPDDAAH
B_suis --GGYD---GRP--MPPHL--ALN-LE----NEHFDRWLELFEQTAREIFP-PEAAIIFVDRARRIADSFEMAIATHSGRIRAPRHSRRPLIS---------
M_capsulatus3 --DRYR---GHP--YPVHA--QLP-LQ----PEHFDIWLELFRKAAREVLP-ADSAARAIARAEHMAESFKAGMFSFPRYEGPKLWKPAR----------
S_melilotil2 --GAYG---GKP--VQAHL--GVANMS----PELFPKWLGLFAATLDDIAPNEEAKAWFMATAERIARSLTLSLFYNPALDDPALKRS----------
C_crescentus --GRYK---GQP--VAAHQGVEGVTEG------LFTPWLGLFHMTCAELFD-APRAAIIGQKAERIAATLKLGLFHRP----------
T_ferrooxidans2 PYKDYR---YAL--GDKHA--PLGITH-----SLVDDWLALFHETMLDHMD-ADMARRWHGMAAGIGESLRLMFAPR----------
M_aviumP --GRYR---GSA--LQAHR--DIHRRAP-LSDRHFRRWLTLWHITVDEMYR-GPAADRAKIQAARIAWAMHRRLTGADSPELLVTQRVRDDRAPDRTGSDDR

Like other Hbs, trHbs are capable of binding oxygen. The rate constant of O_2 association is comparable for most globins (1.7×10^7 -2.4×10^8 M^{-1} s^{-1}) and is high, close to the diffusion limit (Hvitved et al. 2001, Springer et al. 1989 and references therein); as a result, dissociation rate constants are often used to indicate affinity. The truncated Hb from *Paramecium caudatum* has an oxygen dissociation rate constant of 25 s^{-1}, similar to that of Mb (Das et al. 2000), and the rate constant reported for *Nostoc commune* trHb is 79 s^{-1} (Thorsteinsson et al. 1999). These rates are comparable to the oxygen dissociation rate constants from mammalian Mb, which vary from 15 s^{-1} to 40 s^{-1} (Carver et al. 1992). In contrast, the rate constants for O_2 dissociation for *Mycobacterium tuberculosis* trHbO and *Chlamydomonas eugametos* trHb are 0.0014 s^{-1} and 0.0141 s^{-1}, respectively (Couture et al. 1999a, Ouellet et al. 2003). Differences in ligand binding are likely influenced by the heme pocket characteristics of each protein.

Crystal structures are available for a number of trHbs: *Chlamydomonas eugametos* trHb (*Ce* trHb, 1dly, Pesce et al. 2000), *Paramecium caudatum* trHb (*Pc* trHb, 1dlw, Pesce et al. 2000), *Mycobacterium tuberculosis* (*Mt*) trHbN (1idr, Milani et al. 2001) and *Mt* trHbO (1ngk, Milani et al. 2003b). The structures reveal that the three-on-three helical fold found in full-length Hbs has been reduced to a two-on-two helical sandwich (Pesce et al. 2000). At the distal site, hydrogen bonding is detected between the bound ligand (O_2, CO, CN^-) and TyrB10. The structures of *Ce* trHb, *Pc* trHb and *Mt* trHbN show that GlnE11 (Thr in *Pc* trHb) provides additional stabilization of the ligand through hydrogen bonding (Milani et al. 2001, Pesce et al. 2000). In the *Ce* trHb and *Pc* trHb structures, the hydrogen bonding network is expanded to include GlnE7 (Pesce et al.

2000). In contrast, the structure of *Mt* trHbO reveals an altered network. A covalent link is observed between the phenolic oxygen of TyrB10 to the ring of TyrCD1; instead of hydrogen bonding to TyrB10, the cyanide ligand is hydrogen bonded to the hydroxyl group of TyrCD1 (Milani et al. 2003b). In addition, a bifurcated hydrogen bond is observed from the ligand to TrpG8 $N\varepsilon_1$. The presence of TrpG8 as part of the network also serves to control ligand access to the distal site by maintaining hydrophobic contacts in the heme pocket (Milani et al. 2003b, Ouellet et al. 2003).

The *Ce* and *Pe* trHb structures reveal a long tunnel near the AB and GH corner of the distal pocket (Pesce et al. 2000). A shorter tunnel is found between the G and H helices. These tunnels are lined with hydrophobic residues. Ligand binding studies indicate that these tunnels facilitate ligand access to the heme iron (Milani et al. 2004b, Samuni et al. 2003).

The functions of trHbs are not well understood and appear to vary. Limited information is available for the purified members. In the cyanobacterium *N. commune*, cyanoglobin, a group I trHb, is believed to sequester oxygen for reaction by a terminal cytochrome oxidase complex under nitrogen fixing conditions (Thorsteinsson et al. 1996). Studies on *Mycobacterium bovis* trHbN show that the protein is able to convert nitric oxide to nitrate (Ouellet et al. 2002). Milani and co-workers have suggested that nitric oxide detoxification by *Mt* trHbN is a defense mechanism by the pathogen during infection (Milani et al. 2003a). In the case of *Ce* trHb, the protein is expressed as a response to photosynthesis, but additional action is unclear (Couture et al. 1994).

1.3 Hexacoordination in Hemoglobins

Within the Hb superfamily, a small group of proteins exhibits a non-classical coordination scheme in the absence of an exogenous ligand. These proteins contain two protein ligands to the heme iron, rather than the typical single histidine, and are thus termed hexacoordinate hemoglobins (hxHbs). Ligation is primarily bis-histidyl with the conserved HisF8 and a histidine at position E7. The members of this group can be found in plants (rice and barley non-symbiotic hemoglobins, nsHb) (Arrendondo-Peter et al. 1997, Duff et al. 1997) and in various animal tissue (neuroglobin, cytoglobin) (Burmester et al. 2002, Burmester et al. 2000, Trent & Hargrove 2002). Hexacoordination in the chloroplastic trHb from unicellular eukaryotes *C. eugametos* (*Ce* trHb) differs and involves HisF8 and TyrB10 (Couture et al. 1999a). The functions of hxHbs are unknown. Like their pentacoordinate counterparts, hxHbs bind oxygen, many with very low O_2 dissociation constants (Arrendondo-Peter et al. 1997, Burmester et al. 2000, Duff et al. 1997, Hargrove 2000). These low values suggest that oxygen transport and storage is unlikely. In a few cases, hxHb production is upregulated in organisms under hypoxic conditions (Hunt et al. 2001, Sun et al. 2001) suggesting a stress-response function. Binding studies on rice nsHb indicate that ligand binding involves competition between the endogenous and exogenous ligand at the distal site of the heme iron (Hargrove 2000, Trent et al. 2001a). This binding mechanism represents a new model for regulating ligand binding.

1.4 *Synechocystis* sp. PCC 6803 Hemoglobin

Synechocystis sp. PCC 6803 is a unicellular freshwater cyanobacterium; it is a light activated heterotroph incapable of nitrogen fixation (Anderson & McIntosh 1991). *Synechocystis* sp. PCC 6803 was the first cyanobacterium whose genome was entirely sequenced (Kaneko et al. 1996). Its gene organization suggests that it is an evolutionary intermediate between bacteria and plant chloroplasts (Lill & Nelson 1991). DNA sequence analysis reveals a gene that encodes a globin (slr2097) amidst genes coding for unrecognized proteins. The product of the *glbN* gene, *Synechocystis* sp. PCC 6803 hemoglobin (S6803 Hb), belongs to the trHb group. The function of this globin in *Synechocystis* sp. PCC 6803 is currently not known.

1.4.1 Early Characterization

Preliminary studies of the protein product suggest unique structural features for a globin as NMR and optical spectra of the oxidized form are consistent with a low-spin hexacoordinated heme under varying pH conditions (Scott & Lecomte 2000). Proton NMR data exhibit a relatively narrow chemical shift window and a limited extent of line broadening consistent with the low-spin assignment. The reduced holoprotein also appears hexacoordinated according to optical data but is capable of binding CO and O_2 (Scott & Lecomte 2000). NMR and resonance Raman data confirmed the proximal ligand as His70(F8) and identified His46(E10) as occupying the distal site (Couture et al. 2000, Lecomte et al. 2001) The helical position of the distal ligand differs from other hxHbs where E7 is usually the sixth protein ligand.

Couture and co-workers report an oxygen dissociation rate constant of 0.011 s^{-1} (Couture et al. 2000). In a separate study, Hargrove and co-workers examined the oxygen dissociation using a model which included a step for endogenous decoordination at the distal site. The study reported an apparent association rate constant of 2.4×10^8 M^{-1} s^{-1} for the distal ligand-dissociated state (Hvitved et al. 2001)[1]. The comparatively low value k_{off} for S6803 Hb suggests that the protein is not involved in oxygen transport. The value for S6803 Hb is similar to that for *Ascaris suum* Hb, a full-length oxygen-scavenging Hb with k_{off} equal to 0.0041 s^{-1} (Gibson & Smith 1965), and to that of the truncated Hb of *C. eugametos*, a chloroplastic Hb with k_{off} of 0.0141 s^{-1} (Couture et al. 1999a).

1.4.2 Structure of S6803 rHb-R and Comparison to Other trHbs and hxHbs

The structure of recombinant-reconstituted *Synechocystis* sp. PCC 6803 Hb (S6803 rHb-R) was solved in solution by NMR methods (Figure 1.4) (Falzone et al. 2002). As such, the solution structure of S6803 rHb-R was compared to the X-ray crystal structure of metcyano *Ce* trHb. This comparison revealed a predominantly helical structure reminiscent of other trHb structures, but with significant differences. Coordination of the heme iron in S6803 rHb-R versus *Ce* trHb emphasizes distinct changes in the overall arrangement of the helices. In S6803 rHb-R, coordination of His46 brings the E helix approximately parallel to the heme group. Given the high level of identity between *Ce* and S6803 trHbs (43%), it was expected that decoordination of His46 to allow exogenous ligand binding would cause the E-helix to rotate away from the

[1] Hargrove and co-workers also reported a distal ligand dissociation rate constant of 930 s^{-1} and association rate constant of 4200 s^{-1} (Hvited et al. 2002). These data suggested exogenous ligand binding is limited by the transition from endogenous hexacoordination to pentacoordination.

heme as is observed in the chlorplastic trHb (Pesce et al. 2000). On the other side of the heme group, the F-helix of S6803 rHb-R is longer than in other trHb structures by one turn. Inspection of the structure for ligand access tunnels reveals only a short tunnel between the G and H helix. Longer tunnels at the AB and GH regions of the protein are not apparent. However, accessibility to the heme pocket may be provided through the EF loop of S6803 rHb-R. NMR data indicate that this region of the protein is flexible and, in conjunction with endogenous hexacoordination, may modulate O_2 binding and heme reactivity.

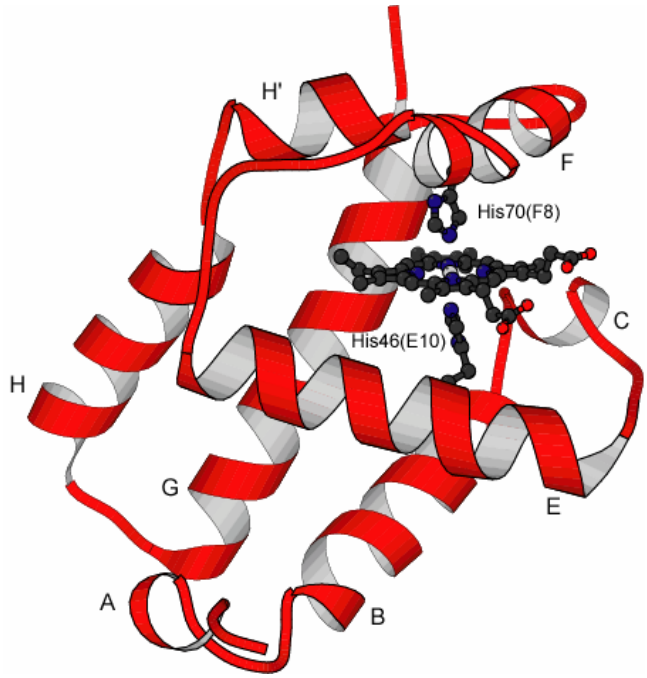

Figure 1.4 The structure of S6803 rHb-R (1mwb, Falzone et al. 2002). The helices are labeled as in Figure 1.2, but without the D helix. The axial histidine residues, His70(F8) and His46(E10) are shown ligated to the heme iron.

Interestingly, the structure that most closely resembles the structure of S6803 rHb-R in the hemichrome form (bis-histidyl coordination of the ferric iron) is that of the

hexacoordinate non-symbiotic Hb (nsHb) from rice (Figure 1.5). nsHb does not belong to the truncated family of globins but one of its proposed functions is as an oxygen sensor in a signal transduction mechanism (Hargrove et al. 2000). Hargrove and co-workers postulated that binding of oxygen and subsequent displacement of the distal histidine would cause a conformational change at the CD corner of rice Hb. Such changes may be detected by other signaling proteins.

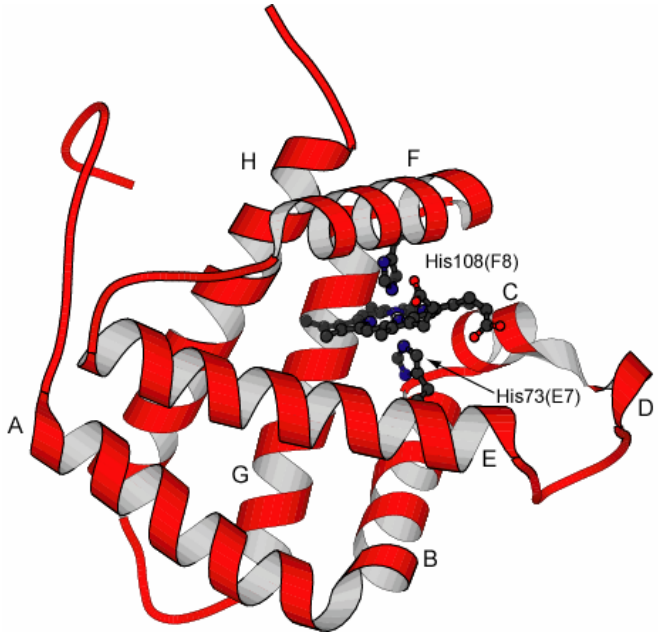

Figure 1.5 The crystal structure of rice (*Oryza sativa*) non-symbiotic Hb (1d8u, Hargrove et al. 2000). The helices are labeled as in Figure 1.2. The axial histidine residues, His73(E7) and His108(F8) are shown ligated to the heme iron.

This thesis details continued structural and biophysical investigations of the heme binding pocket of S6803 rHb-R. A number of issues are of interest to this work. Hb chemistry is typically focused on understanding the role of specific protein residues in regulating ligand affinity. Studies on S6803 and related trHb from the cyanobacterium

Synechococcus sp. PCC 7002 (S7002) have revealed that a vinyl group modification is found under certain circumstances (Scott et al. 2002). Modification of the heme group often observed in cytochromes (Barker & Ferguson 1999, LeBrun et al. 2002) or peroxidases (DePillis et al. 1997, Kooter et al. 1999, Leesch et al. 2000, Oxvig et al. 1999) but it is rare among Hbs (Reeder et al. 2002).. The observation of a heme modification in a Hb provides an opportunity to understand further the factors influencing chemistry in hemoproteins. Chapter 3 describes the characterization of the vinyl group modification and probes conditions that promote reactivity.

Hexacoordination in Hbs represents a new mechanism for regulating ligand binding if the rate limiting step is decoordination of the distal histidine ligand. Of particular interest to this work is the role of His46(E10) in ligand binding. Chapters 4 and 6 examine the structural changes occurring upon exogenous ligand binding to the distal site or the formation of a pentacoordinate state in S6803 rHb.

NMR methods can be used to characterize the electronic structure of the heme group and to discover how it is affected by various ligands. Bertini, Turner and others have employed paramagnetic shift analyses in cytochromes to determine the axial ligand orientation (Bertini et al. 1999, Shokhirev & Walker 1998a, Shokhirev & Walker 1998b, Turner 2000, Turner et al. 2000). Chapter 5 uses these methods to investigate the orientation of the axial histidines in S6803 rHb.

The overall goal of this work is to expand the structure-function relationships within the Hb family. The covalent linkage discussed in Chapter 3 may be a mechanism to modulate ligand binding effects through the environment of the heme 2-vinyl group.

Additionally, S6803 rHb structural changes upon ligand binding are compared to those occurring in other trHbs and hxHbs.

Chapter 2

Materials and Methods

2.1 Chemicals

Chemicals were purchased either from EMD Chemicals (Gibbstown, NJ) or Sigma-Aldrich (St. Louis, MO) unless otherwise noted. ^{2}H, ^{13}C, and ^{15}N isotope-enriched chemicals were purchased from Cambridge Isotope Laboratories (Andover, MA) or Isotec, Inc. (Miamisburg, OH). All chemicals were used without further purification except where noted.

2.2 Purification of Apo-S6803 rHb

S6803 Hb was prepared using recombinant methods (rHb). The gene for S6803Hb (slr2097, *glbN*, Kaneko et al. 1996) was contained in a pET3c vector with ampicillin resistance as the selection marker (Scott & Lecomte 2000). The plasmid was used to transform competent BL21(DE3) cells (Novagen, Madison, WI) using a modified version of the Hanahan method (Sambrook & Russell 2001); cells were plated onto M9-ampicillin medium plates, and incubated for 20-24 hours at 37 °C. A 60-mL starter culture of M9-ampicillin medium was inoculated with an isolated colony and incubated, shaking for 16-20 hours at 37 °C. 15 mL of the starter culture was used to inoculate 500 mL of M9-ampicillin medium and; the large culture was incubated, shaking at 37 °C until OD_{600}=0.8. Protein production was induced by adding IPTG to a final concentration of 0.5 mM. The cell culture was harvested 6 hours post-induction by centrifugation in a

Beckman J2-21M/E Centrifuge at 11,000 × *g*. Cell pellets frozen to facilitate cell lysis and stored at −20 °C overnight.

Previous studies indicated that little protein is available from soluble cell lysis products (Lecomte et al. 2001). Thus, the apoprotein was purified from inclusion bodies. Cell pellets were thawed and resuspended in 20 mL of 50 mM Tris, 5 mM EDTA, pH 8.0 per 5 g cells. The suspension was placed on ice and the cells disrupted by sonication for six 15 s burst at 70% power (Fisher Scientific Model 60 Dismembrator, Pittsburgh, PA). The mixture was separated by centrifugation at 16,000 × *g* for 15 minutes. The sonication-centrifugation step was repeated once. The resulting pellet was suspended in 30 mL of 0.5% Triton-X 100 (Boehringer Mannheim/Roche Diagnostics, Indianapolis, IN) detergent in 50 mM Tris, 5 mM EDTA, pH 8.0. The suspension was separated by centrifugation as above. Residual detergent was rinsed from the cell pellet by resuspension in 40 mL of 50 mM Tris, 5 mM EDTA, pH 8.0, followed by centrifugation at 16,000 × *g* for 10 minutes. The pellet, containing the inclusion bodies, was solubilized in 8 M urea in 50 mM Tris, 1 mM EDTA, pH 8.0 for 30 minutes while stirring. A concentrated urea stock was purified on a BioRad AG-501 mixed bed resin (Hercules, CA) column prior to preparation of the solubilization buffer. Insoluble cell matter was removed by centrifugation at 31,000 × *g* for 15 minutes. Purification and refolding of S6803 rHb was performed by applying the supernatant to a Sephadex G-50 fine (Pharmacia, Piscataway, NJ) column (2.5 cm × 100 cm) equilibrated in 50 mM Tris, 1 mM EDTA, pH 8.0, with a UV monitor in line. SDS-PAGE analysis was performed to identify the fractions free of contaminating proteins. Trace urea was removed by exchange or dialysis into ddH_2O or buffer, as necessary. Protein yield was determined by

UV spectroscopy on an Aviv (Lakewood, NJ) model 14 DS spectrophotometer, using the extinction coefficient at 278 nm (ε_{278} = 7.36 cm^{-1} mM^{-1}, Lecomte et al. 2001). The protein was lyophilized from ddH_2O and stored at −20 °C.

When necessary, the apoprotein was uniformly labeled with ^{15}N using established methods (Lecomte et al. 2001). Transformed BL21(DE3) cells were cultured in M9 medium containing $^{15}NH_4Cl$ (Isotec, Inc.,Miamisburg, OH). Protein expression and purification was carried out as above.

2.3 Preparation of Holoprotein Solutions

2.3.1 Reconstitution using Fe(III) Protoporphyrin IX (heme)

To prepare the holoprotein, the apoprotein was reconstituted with hemin chloride. To a 30 mL solution of apoprotein in 50 mM Tris, 1 mM EDTA, pH 8.0 2-3 equivalents of 50 mg/mL hemin chloride (dissolved in 0.1 M cold NaOH) was added. The resulting solution was stirred overnight to allow complete incorporation of the heme group. Excess hemin was removed from the reconstituted holoprotein (rHb-R) solution by centrifugation at 31,000 × *g* for 45 minutes. The solution was further clarified by filtration through a 0.45 μ filter and applied to a DEAE Sephacel (Pharmacia) anion exchange column (2.5 cm × 10 cm). The holoprotein solution was eluted from the column with 0.2 M NaCl in 50 mM Tris, 1 mM EDTA, pH 8.0 or a 0-0.5 M NaCl gradient in 50 mM Tris, 1 mM EDTA, pH 8.0 as necessary. Exchange or dialysis against ddH_2O or buffer was used to remove NaCl from the solution. Holoprotein concentration and yield were determined by inspection of the Soret band maximum, at 410 nm, by UV

spectroscopy (ε_{410} = 100 cm^{-1} mM^{-1}, Scott & Lecomte 2000). The protein was lyophilized from ddH_2O and stored at −20 °C.

2.3.2 Reconstitution using Fe(III) 2,4-dimethyldeuteroheme

Apo S6803 rHb was reconstituted with Fe(III) 2,4-dimethyldeuteroheme (2,4-DPIX, a modified heme with methyl groups replacing the vinyl substituents). In such cases, the holoprotein (rHb-DPIX) was purified as in section 2.3.1.

2.3.3 Reconstitution using Zn(II) protoporphyin IX

Zn-substituted S6803 rHb was prepared as S6803rHb. However, because of high light sensitivity, all steps were performed in the dark or under red-light conditions. Here, the apoprotein was reconstituted with 2 equivalents of Zn(II)-protoporphyrin IX (Mid-Century Chemicals, Posen, IL, 50 mg/mL dissolved in 0.1 M cold NaOH). The resulting solution was stirred overnight and the excess Zn(II) porphyrin removed by gel filtration using a short G25 Sephadex column equilibrated in 20 mM phosphate buffer, pH 7.2. Final NMR sample concentrations were 1 mM in 20 mM phosphate, pH 7.2.

2.4 NMR Spectroscopy of S6803 Hb Samples

The purity of all protein preparations was assessed by SDS-PAGE and mass spectrometry analysis. The protein content of each sample was verified by ^{1}H NMR spectroscopy. Protein samples were either prepared by concentration in an Amicon ultrafiltration device equipped with a YM3 membrane (Millipore, Billerica, MA) or directly from lyophilized protein. Experimental concentrations ranged from 1-4 mM.

Solvent conditions were 20 mM phosphate buffer, pH 7.2, in 95% $^{1}H_2O$/5% $^{2}H_2O$ or 100% $^{2}H_2O$. NMR spectra were collected on a Bruker DRX-600 (or AMX2-500) spectrometer operating at ^{1}H frequency of 600.13 (or 500.13) MHz, ^{13}C frequency of 150 (or 125.76) MHz, and ^{15}N frequency of 60.81 (or 50.68) MHz. The probe temperature was maintained 298 K, unless otherwise noted. Temperature was calibrated using ethylene glycol or methanol (Cavanagh et al. 1996). Proton chemical shifts were referenced through the water line (Wishart et al. 1995). Data were processed using XWIN-NMR (Bruker BioSpin, Rheinstatten, Germany) or FELIX (Accelerys, San Diego, CA).

2.4.1 One-Dimensional NMR Experiments

1D proton data were collected with a 1.2 presaturation of the water signal. A total of 256 (to 1024) transients were collected using 8192 points over 24 kHz for holoprotein samples and 9 kHz for zinc-substituted rHb and apoprotein samples. The raw data were zero-filled to twice the number of points and the FID filtered with a squared-cosine bell function.

2.4.2. Two-Dimensional Homonuclear Experiments

Homonuclear NOESY (Kumar et al. 1980), DQF-COSY (Rance et al. 1983), and TOCSY (Cavanagh & Rance 1992) data were collected using 2048 transients in the direct dimension over a range of 9 to 24 kHz. In the indirect dimension 512 points were collected over 9 kHz. When the NOE effect to hyperfine shifted protons were on interest, the data were folded in the indirect dimension. Mixing times for NOESY and TOCSY

data were 100 ms and 45 ms, respectively. TOCSY data were collected using a relaxation compensated DIPSI mixing scheme (Cavanagh & Rance 1992). Suppression of the water signal was achieved by presaturation of the water line or a WATERGATE scheme (Piotto et al. 1992). Quadrature detection was achieved either by the TPPI (Marion & Wüthrich 1983) or STATES method (States et al. 1982). Homonuclear data were zero-filled in the indirect dimension. A squared-sine bell window shifted by either 45° or 90° was applied in both dimensions.

2.4.3 Two Dimensional Heteronuclear Experiments

Natural abundance ^{1}H-^{13}C HMQC (Mueller 1979) spectra were acquired over 20 kHz in the direct (^{1}H) and 32 kHz in the indirect (^{13}C) dimensions. The spectra were centered at 150 ppm in the ^{13}C dimension. A total of 800 transients were collected with 2048 points in the direct and 256 points in the indirect dimension. A $1/2J_{CH}$ delay of 2 ms was used to detect couplings without excessive loss of magnetization. A squared-cosine bell window was applied in both dimensions. Data were collected at 298 K and 308 K.

^{1}H-^{15}N HMQC spectra (Bodenhausen & Ruben 1980, Mueller 1979), optimized for detection of long range couplings in histidine rings (Pelton et al. 1993), were collected at 305 K or 298 K, in 20 mM phosphate buffer (pH 7.2), using uniformly ^{15}N-labeled protein. A delay of 15 ms corresponding to $^{2}J_{NH}$ of 6-12 Hz optimized for long-range ^{1}H-^{15}N couplings in the histidine imidazole ring (Pelton et al. 1993) was used. The spectra were collected over a range of 7-9 kHz in the ^{1}H dimension. A spectral width of 9 kHz was used in the ^{15}N dimension and the spectra centered at 210 ppm.

^{1}H-^{15}N HSQC spectra (Kay et al. 1992) were acquired using a WATERGATE water suppression scheme (Piotto et al. 1992). Spectra were collected over 7-9 kHz in the direct dimension. Quadrature detection was achieved using TPPI with 4k complex pairs in the direct dimension. In the indirect dimension 128-256 t_1 increments were collected over 2 kHz. The carrier in the indirect dimension was placed at 115 ppm.

2.5 Protein Structures

Representations of the structures in this work were created using MOLSCRIPT (Kraulis 1991).

Chapter 3

Characterization of the Covalently Modified *Synechocystis sp.* PCC 6803 Hemoglobin

Material in this chapter has been presented in the following publications:

"Novel histidine-heme covalent linkage in a hemoglobin." Vu, B.C, Jones, A.D., and Lecomte, J.T.J (2002) *J. Am. Chem. Soc.*, **124,** 8544-8545.

"Characterization of the heme-histidine cross-link in cyanobacterial hemoglobins from *Synechocystis* sp. PCC 6803 and *Synechococcus* sp. PCC 7002." Vu, B.C., Vuletich, D.A., Kuriakose, S.A., Falzone, C.J., and Lecomte, J.T.J. (2004) *J. Biol. Inorg. Chem.* **9**, 183-194.

"Cyanide binding to hexacoordinate cyanobacterial hemoglobins: Hydrogen bonding network and heme pocket rearrangement in ferric H117A *Synechocystis* Hb." Vu, B.C., Nothnagel, H.J., Vuletich, D.A., Falzone, C.J., and Lecomte, J.T.J *Biochemistry*, *in press*.

Mass Spectrometry data were collected by Dr. A. Daniel Jones.

Acid Denaturation of S6803 proteins, monitored by optical spectroscopy, was performed by Syna Kuriakose.

NMR data for *Synechococcus* sp. PCC 7002 rHb-R and rHb-A were provided by David Vuletich.

3.1 Introduction

Preparations of holo S6803 rHb reconstituted from soluble portions of cells grown in M-9 medium resulted in heterogeneous protein solutions after extensive purification

(Scott & Lecomte 2000). These protein preparations contained two forms, one that was identical to protein purified via inclusion bodies (rHb-R), and a second, rHb-A, which yielded distinct paramagnetic signals in NMR spectra. Unlike rHb-R, rHb-A was found to be resistant to acid-butanone extraction of the heme. Mass spectrometry of samples containing rHb-A indicated a tightly associated heme-protein species not observed for rHb-R. Hemochromogen assays indicated modification of a vinyl substituent on the porphyrin ring (Scott et al. 2002). The conversion of rHb-R to rHb-A was found to occur spontaneously via an unknown mechanism. During experiments aimed at characterizing ferrous S6803 rHb-R, the ferric protein was treated with sodium dithionite, a common hemoprotein reducing agent. When performed under aerobic conditions, reduction of the iron took place and the sample returned to the ferric form. However, examination of these samples revealed that they contained exclusively rHb-A. NMR spectra of the related trHb from *Synechococcus* sp. PCC 7002 (S7002 rHb-R) also contain a second species with an altered vinyl group (Scott et al. 2002). Modifications of the heme group are rarely observed in Hbs. Covalent bond formation between the heme prosthetic group and the protein matrix is commonly associated with c-type cytochromes (Allen et al. 2003, Barker & Ferguson 1999 and references therein). In these proteins, cysteine thiol groups react with heme vinyl β-carbons to form two thioether linkages (Barker & Ferguson 1999). Formation of the thioether bonds is believed to stabilize the protein and regulate the protein reduction potential *in vivo* (Allen et al. 2003). Studies on variants of cytochrome c_{552} have demonstrated that only a single linkage is necessary to impart the stability and reduction potential characteristics of cytochromes c (Cowley et al. 2004, Tomlinson & Ferguson 2000a, Tomlinson & Ferguson 2000b). Cysteine residues are not

found in the primary structures of S6803 and S7002 rHbs precluding thioether bond formation. However, the linkage found in c-type cytochromes may provide useful insight to vinyl group modification in S6803 and S7002 rHb-A. The observation of the unusual chemistry in proteins from two different sources supported that the reaction was not an experimental artifact, or at least, one interesting to investigate. Thus, studies were initiated to characterize fully adduct formation on S6803 rHb. Mutagenesis was performed to test simple hypotheses of reactivity. In addition, methods to inhibit and rescue reactivity were explored.

3.2 Materials and Methods

3.2.1 Preparation of S6803 rHb-A

S6803 rHb-R was purified as described in Chapter 2. rHb-A samples were prepared by treating rHb-R in 20 mM phosphate, pH 7.2, with 1.5 equivalents of phosphate-buffered sodium dithionite (pH 7.2). Following reduction of the ferric iron and its subsequent re-oxidation, excess sodium dithionite was removed on a short G-25 desalting column equilibrated in phosphate buffer or water. Samples were either concentrated in an Amicon ultrafiltration cell or lyophilized. The reaction was also carried out at pH 8.5 and 5.5.

3.2.2 Mass Spectrometry

To probe for a site of covalent linkage between the heme and the protein matrix, mass spectrometry of proteolytic fragments was performed. Digestion of rHb-A and rHb-R samples was carried out by adding 8 μL porcine gastric pepsin in 1% formic acid

(1 mg/mL) to 10 µL of a 10 µM protein sample (final pH = 2.5) followed by incubation at 37 ºC for 24 hours. Another 20 µL of 0.15 % formic acid was added to each sample before analysis by mass spectrometry. The Protein Prospector analysis program (UCSF) was used to predict peptide mass fragments resulting from pepsin digestion.

Mass spectrometry of rHb-R and rHb-A samples was performed by Dr. A. D. Jones of the Penn State University Mass Spectrometry Facility. Protein samples were analyzed on a Perseptive Biosystems Mariner mass spectrometer (Framingham, MA), using electrospray ionization in positive ion mode, equipped with a Hewlett-Packard model 1100 HPLC (Palo Alto, CA). Prior to ionization, peptide fragments were separated by reversed phase chromatography with a BetaBasic C-4 column (1.0 mm I.D. × 50 mm length, 3 µm packing, Keystone Scientific, Bellefonte, PA) at 25 ºC using a multi-step gradient over 45 minutes (solvent A, H_2O + 0.15% formic acid; solvent B, acetonitrile + 0.15% formic acid; solvent C, 2-propanol + 0.15% formic acid). The gradient was applied as follows: 0-30 minutes 95% A-5% B (0.5 mL/min), then changed to 5%A- 95%B (0.5 mL/min) from 30-35 minutes and held from 35-40 minutes, then changed to 10%A-90%C (0.3 mL/min) from 40-45 minutes. HPLC-UV was achieved by coupling a Hewlett Packard 1100 series diode array detector to the HPLC instrument. Tandem mass spectrometry analyses were performed on a Quattro-II mass spectrometer (Micromass, Manchester, UK) interfaced to a LC-10ADvp HPLC (Shimadzu Instruments, Columbia, MD) using electrospray ionization, with collision induced dissociation effected using argon as collision gas (2×10^{-3} mbar) and 30 V offset of the collision cell.

3.2.3 NMR Spectroscopy.

NMR spectroscopy was carried out as in Chapter 2 or as in Lecomte et al. (2001), and Vu et al. (2002 and 2004b). The program DmFit (Massiot et al. 2002) was used where spectral simulations were necessary.

3.2.4 pH Titration by NMR spectroscopy

The protonation state of the reactive histidine versus other histidines in S6803 rHb-R and rHb-A was determined via pH titrations monitored by ^{1}H NMR spectroscopy. A 1 mM sample of rHb-R (or rHb-A) was prepared in D_2O at pH 7.2. The pH was either raised with $NaO^{2}H$ or lowered with ^{2}HCl. Chemical shift values of the CεH and CδH of the histidines as well as those for heme substituents were plotted versus pH and fitted to a modified Henderson-Hasselbalch equation assuming the simplest case of fast exchange on the chemical shift time scale:

$$\delta_{obs} = \delta_{His^o} + (\delta_{His^+} - \delta_{His^o}) \frac{10^{n(pK_a - pH)}}{1 + 10^{n(pK_a - pH)}} \qquad (1)$$

In this equation, δ_{His^o} (chemical shift of the neutral histidine), δ_{His^+} (chemical shift of the protonated histidine), n (Hill coefficient), and pK_a (apparent ionization constant, pH at which 50% of the given histidine population is protonated) are adjustable parameters and δ_{obs} is the measured chemical shift at any pH.

3.2.5 Thermal Denaturation Monitored by Optical Spectroscopy

The absorbance of the holoprotein between 260 and 700 nm was monitored as a function of temperature between 25 °C and 95 °C. Typically, the holoprotein solution was 8 μM in 20 mM phosphate buffer at pH 7.2 and absorbance data were collected at 2 °C intervals, allowing for a three-minute equilibration period. Reversibility was verified by refolding the protein from 95 °C to 24 °C, collecting data points at 3 °C intervals, with a seven-minute equilibration time. The data were fit with NFIT (University of Texas, Galveston, Texas) using the van't Hoff equation as detailed in Equations 2 and 3.

$$\Delta G°(T) = \Delta S°_{Tm}(T_m - T) + \Delta C_p°[(T - T_m) - T \ln(T/T_m)] \quad (2)$$

$$\Delta G°(T) = - RT \ln [(y_F - y)/(y - y_U)] \quad (3)$$

In Equation 2, ΔCp° is assumed to be independent of temperature and T_m the melting temperature determined at the midpoint of the unfolding transition (Dill 1990). In Equation 3, y is the observable quantity (for example the absorbance at the wavelength of interest), y_F corresponds to this quantity in the folded state, and y_U to the quantity in the unfolded state (Schmid 1989). These two values are themselves dependent on temperature and are expressed as linear functions to represent the baselines of the denaturation curve. These equations were used to obtain thermodynamic quantities and T_m, the temperature at which the equilibrium constant is equal to 1.

3.2.6 pH Titration by Optical Spectroscopy

The investigation of protein resistance to acid denaturation was performed by Syna Kuriakose and published in Vu et al. (2004b). The absorbance of a 10 μM rHb-R or

rHb-A sample was colleted between 260 and 700 nm at pH values ranging from 1.5 to 7.2. The data were processed using an equation similar to (1), where absorbance was substituted for chemical shift and an additional transition was included, as required by the data (see Results).

3.2.7 Mutagenesis of His117 and Asp120

Primers were obtained from IDT DNA Technologies (Coralville, IA). The primers for mutagenesis were as follows, with the mutation codon in bold:

H117A 5'- GCTCCAGCC**GCT**AAACGGGACGTGC-3' and

5'-GCACGTCCCGTTT**AGC**GGCTGGAGC-3';

H117F 5'-GGCTCCAGCC**TTC**AAACGGGACGTGC-3' and

5' GCACGTCCCGTTT**GAA**GGCTGGAGCC-3';

D120A 5'-CCATAAACGG**GCC**GTGCTTAATCAG-3' and

5'- CTGATTAAGCAC**GGC**CCGTTTATGG-3'.

Mutagenesis was carried out using the Stratagene QuikChange® Site-Directed Mutagenesis method. Mutations were verified by DNA sequencing carried out at the Pennsylvania State University Nucleic Acid Facility. For each mutant protein, test growths were performed to verify that mutagenesis did not affect protein expression levels or inclusion body formation. The protein purification and NMR spectroscopy was performed as in Chapter 2.

3.2.8. Ligand Binding to H117A S6803 rHb-R

In preparation for imidazole rescue of the H117A site, imidazole was titrated into the sample. To a 1 mM protein sample, a solution of imidazole (800 mM, 20 mM phosphate, pH 7.2) was added to a final imidazole concentration of 200 mM. Cross-linking was probed by reaction of the sample with 1.5 equivalents of sodium dithionite as above.

3.3 Results and Discussion

3.3.1 One Dimensional NMR Spectroscopy of S6803 rHb-A

In an attempt to prepare and study the holoprotein in the ferrous state, rHb-R was treated with sodium dithionite. Samples of rHb-R that were reduced with 1.5 equivalent of sodium dithionite and re-oxidized to ferric iron in the presence of air were found to be rHb-A (Figure 3.1). This conversion was performed quantitatively and reproducibly to obtain pure ferric rHb-A samples. NMR data indicated that rHb-A had a low-spin iron coordinated by the same axial ligands as rHb-R.

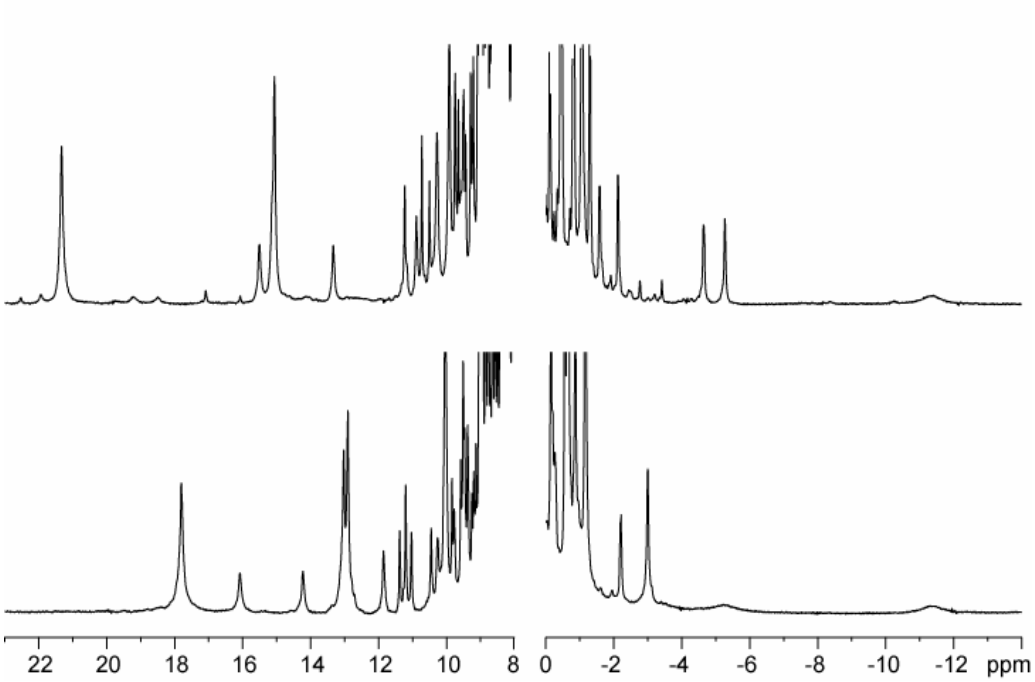

Figure 3.1 ^{1}H NMR spectra of S6803 (A) rHb-R and (B) rHb-A collected in 20 mM phosphate, pH 7.2 (95% $^{1}H_2O$: 5% $^{2}H_2O$) at 298 K. The differences in appearance of the two spectra demonstrated changes in the structure near heme molecule.

Reduction of the heme iron using electrochemical methods did not result in direct formation of rHb-A (Lecomte et al. 2001). The conversion of rHb-R to rHb-A is efficient when using sodium dithionite. In the reduction of hemoproteins, this reagent sequesters oxygen and decomposes to sulfites and sulfates. Additionally, covalent attachment was not observed upon incorporation of either Zn(II) protoporphyrin IX or 2,4 dimethyldeuteroheme in S6803 rHb followed by treatment with sodium dithionite. This confirmed the requirement of the 2-vinyl group and the presence of the iron metal center. The requirement of the iron and involvement of oxygen suggested that radical-mediated mechanisms may be responsible for cross-link formation. Radical inhibitors were sought out to probe the role of sodium dithionite mediated radicals in rHb-A formation.

Traditional "radical-sponges" utilize electron transfer properties of various large heme-proteins, such as catalase, to capture radicals in solution. Utilizing such agents to quench radical processes is potentially complicated by efficient purification of rHb-A for NMR methods. Alternately, methanol has been shown to quench radical reactions in various systems (Arnao et al. 1996, Polyakov et al. 2001, Wink et al. 1994). The reagent was utilized to probe radical involvement in rHb-A formation. A rHb-R sample containing methanol was prepared and treated with 1.5 equivalents of dithionite. The sample was examined by NMR spectroscopy and found to be pure S6803 rHb-A. This indicated that the cross-link formation did not involve a radical accessible by methanol under these reaction conditions. However, it remained possible that the radical was confined to the heme cavity and could not come into contact with the quenching agent. The experiment was therefore inconclusive.

3.3.2 Mass Spectrometry of S6803 rHb-A

Mass spectrometry applying MALDI methods confirmed that the heme in rHb-A remained associated with the protein, unlike that in rHb-R, which is released during the ionization. rHb-A was digested using pepsin for further analysis. LC-UV detection at 394 nm was used to identify the chromatographic peak containing heme-bound peptide. LC-ESI mass spectrometry on this fragment returned a mass of 1848.8 Da (Figure 3.2), corresponding to the sequence, ^{111}VAGAPAHKRDVL, with heme attached. The sequence of the heme containing peptide was verified by MS/MS. In this sequence, there were four likely candidates for reactivity, His117, Lys118, Arg119 and Asp120. Comparison to the same region in S7002 rHb-A showed His117 and Asp120 to be

conserved. His117 was favored as the likely reactive candidate for attachment to the heme (Vu et al. 2002).

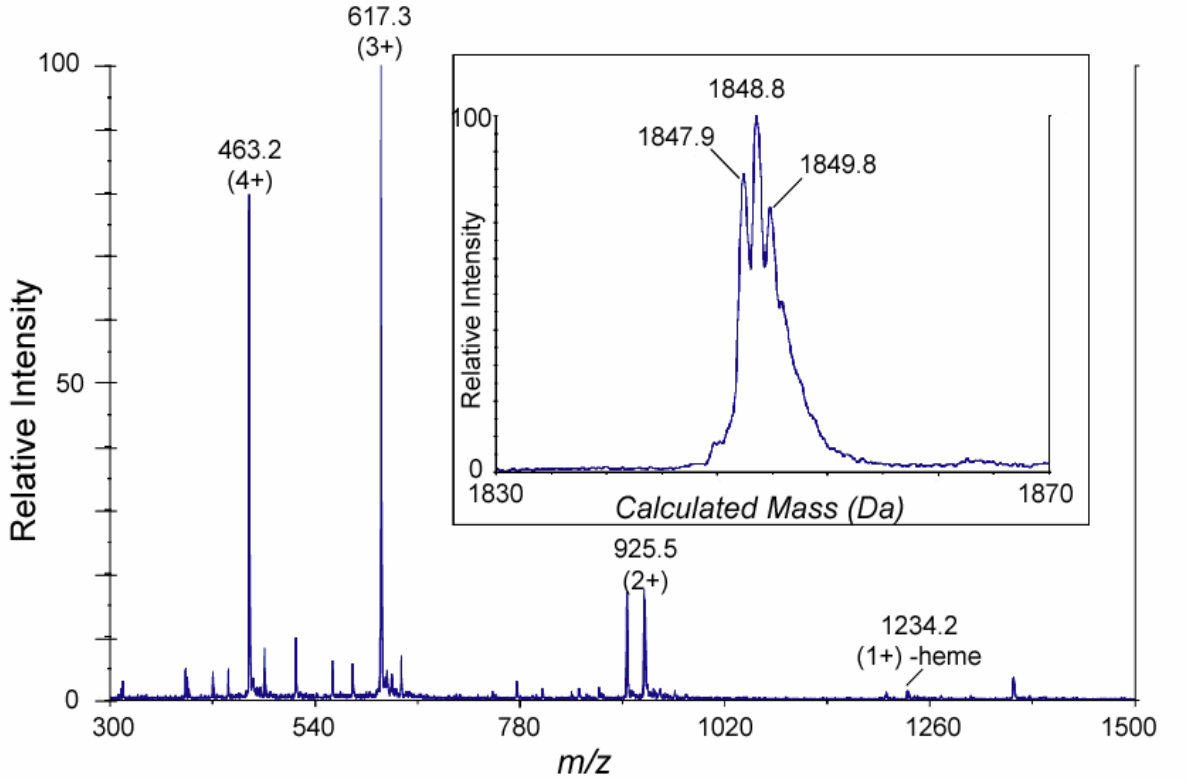

Figure 3.2 Mass-to-charge ratio of the peptide fragment eluted during LC-MS and absorbing at 394 nm. The mass to charge ratio of 1234.2 is the only peptide fragment without the heme group. The inset shows the mass resulting from deconvolution of the triply charged peak of 617 m/z units.

3.3.3 Two-Dimensional NMR Spectroscopy of S6803 rHb-A

2D ^{1}H NMR data on rHb-A indicated that the magnetic properties of the heme are moderately altered compared to rHb-R. WEFT-NOESY and ^{1}H-^{13}C HMQC data were used to assign signals arising from the heme group unambiguously (Figure 3.3 and 3.4, Table 3.1). The WEFT-NOESY data readily identified all four meso ^{1}H signals. The δ-meso proton has connectivities to the 1- and 8-CH_3 and the α-meso to the 3-CH_3; unlike

in rHb-R, no spin system consistent with the 2-α-vinyl appears in contact with this meso proton. The data are in agreement with reaction at that site as originally proposed (Scott et al. 2002). A NOE was observed between the 1-CH_3 and a set of protons resonating at 0.57 ppm (Figure 3.3). The NOE is weak under WEFT conditions, but is stronger in the standard NOESY data. The signal at 0.57 ppm was scalarly coupled to a signal at 2.24 ppm. No other *J*-coupled protons were found from this pair, and suggested they belonged to a modified 2-vinyl group.

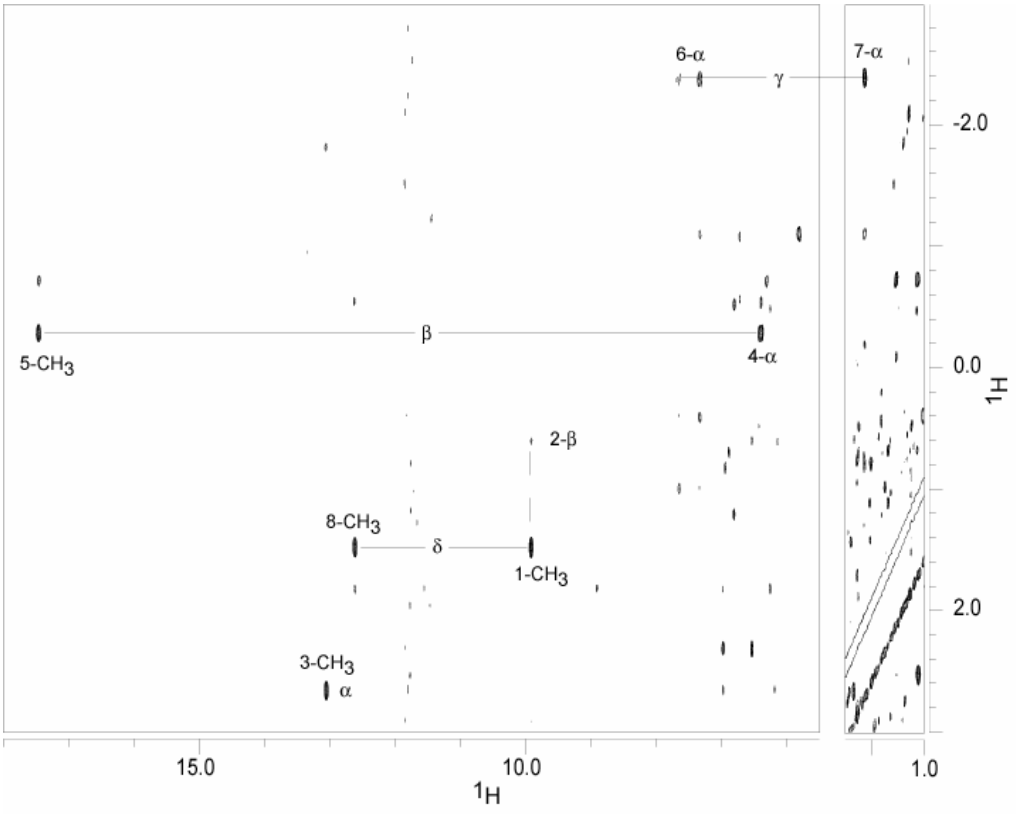

Figure 3.3 A portion of WEFT-NOESY data collected on S6803 rHb-A at 308 K (20 mM phosphate buffer, pH 7.2, 100% ^2H_2O), showing dipolar connectivities from heme substituents to meso protons. The 1-CH_3 was identified by a NOE to modified 2-vinyl group.

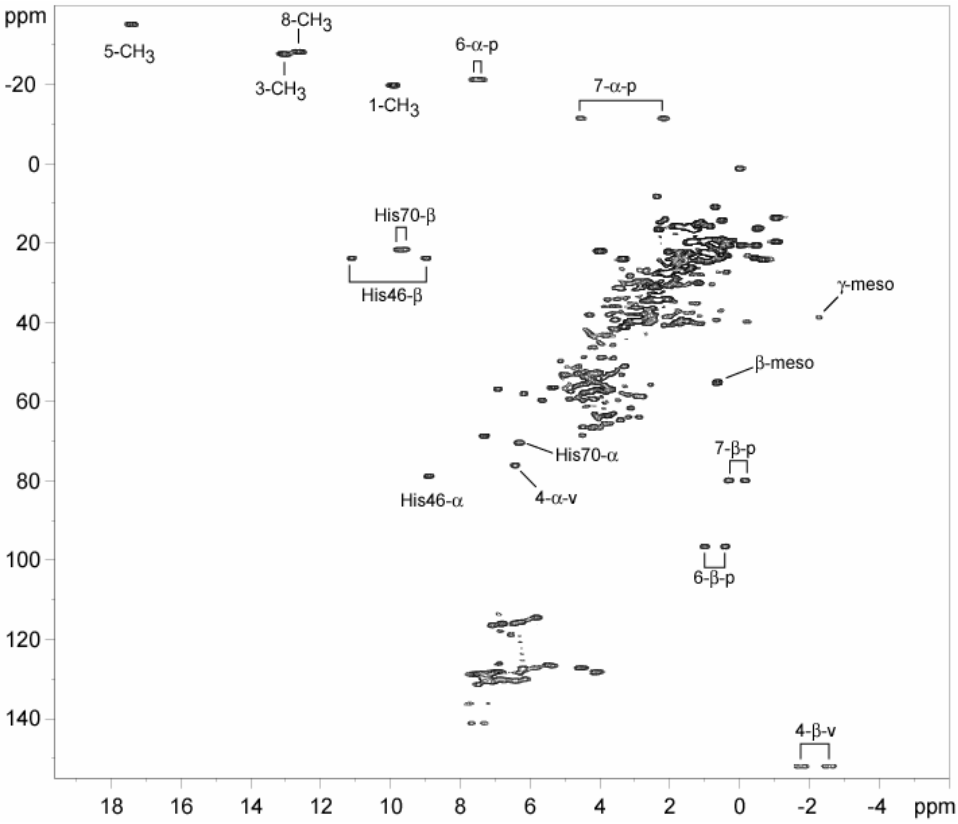

Figure 3.4 The ^{1}H-^{13}C natural abundance HMQC spectrum for S6803 rHb-A used to assign heme protons and identify axial histidine residues. Sample conditions were 20 mM phosphate buffer, pH 7.2, 100% $^{2}H_2O$ at 308 K. Only one set of β-vinyl protons, assigned to the 4-vinyl group, were observed at their usual shift.

Table 3.1 ^{1}H and ^{13}C chemical shifts for the heme resonances in S6803 rHb-R and rHb-A at 298 K[a]

	rHb-R (ppm)		rHb-A (ppm)	
	^{1}H	^{13}C	^{1}H	^{13}C
1-CH_3	15.03	-30.2	10.6	-20.4
2-α-v	15.56	49.1[b]	2.35[c]	9.0[c]
2-β-v *cis*	-4.57	189.8		
2-β-v *trans*	-5.22		0.55[d]	57.1[d]
3-CH_3	9.99	-24.3	13.14	-28.2
4-α-v	6.80	80.5	6.09	74.9
4-β-v *cis*	-1.53	149.0	-2.96	153.6
4-β-v *trans*	-2.05		-2.10	
5-CH_3	21.28	-40.4	17.84	-36.2
6-α-prop	8.32	-24.0	7.61	-22.0
6-α'-prop	9.67		7.23	
6-β-prop	1.41	106.4	0.98	99.3
6-β'-prop	0.67		0.31	
7-α-prop	3.76	-11.3	4.42	-11.9
7-α'-prop	1.74		1.77	
7-β-prop	-0.44	79.6	0.16	81.4
7-β'-prop	-0.81		-0.37	
8-CH_3	10.33	-26.2	12.66	-28.7
α-meso	1.74		2.36	
β-meso	0.30		-0.79	38.2
δ-meso	-1.10	-29.3	-3.02	36.8
γ-meso	0.35		1.15	

[a] Collected in $^{2}H_2O$; [b] At 308 K; [c] 2-α-CH; [d] 2-β-CH_3

Reaction of the vinyl with a histidine side chain was expected to result in altered spectral properties of the latter. The nature of the covalent linkage was elucidated in S6803 rHb-A in part via experiments monitoring histidine spectral properties (Vu et al. 2002). ^{1}H-^{15}N heteronuclear data are conveniently used to establish the tautomeric state of neutral histidines (Pelton et al. 1993). Residues near the heme iron undergo rapid relaxation. The HMQC sequence has a shorter recycling time versus the HSQC and was optimal for detecting rapidly relaxing resonances. In the HMQC experiment, ^{1}H-^{15}N cross-peaks are obtained between the C-bound imidazole protons and the imidazole nitrogens. Typically, in $^{2}H_2O$, a maximum of four cross-peaks is obtained per imidazole, illustrating the CδH and CεH connectivities to $^{15}N\delta$ and $^{15}N\varepsilon$. Although the data collected on rHb-R revealed normal histidine patterns, the data obtained on rHb-A were unusual. Three of the patterns were consistent with normal non-axial histidine residues: His33, 83 and 77. In the fourth histidine pattern, additional *J*-correlated connectivity to the 2 vinyl at 0.57 ppm, at 32 °C, for the histidine assigned as His117 (Figure 3.5, Vu et al. 2002) was observed. Thus, the identity of the protein residue responsible for the modification was established. Similar spectral properties were observed for S7002 rHb-A (David Vuletich, Vu et al. 2004b).

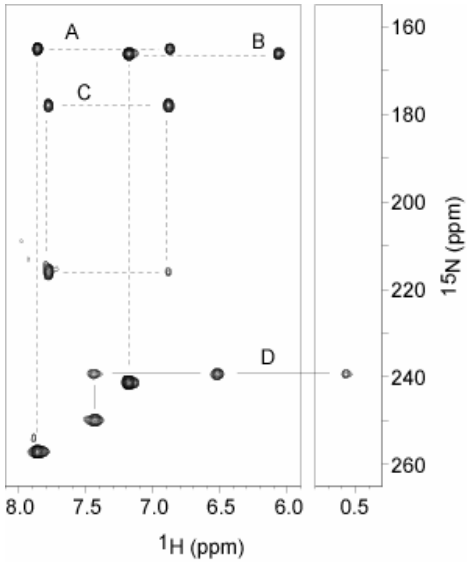

Figure 3.5 ^{1}H-^{15}N HMQC collected on S6803 rHb-A in 20 mM phosphate, pH 7.2, at 305 K. His A, B and C correspond to His83, 33 and 77 respectively. His D, His117, shows an additional scalarly coupled signal at 0.57 ppm.

Because of the paramagnetism of ferric rHb-A and the change in covalent structure, it was necessary to verify the histidine ring assignments of His117 after formation of the linkage. The identity of the CδH and CεH signals was confirmed in a uniformly ^{13}C/^{15}N labeled sample with a ^{1}H-^{13}C HMQC spectrum centered on the aromatic region. In these data, the ^{13}C-^{13}C coupling is active during evolution; His ^{13}Cδ appears as a doublet because of coupling to the adjacent Cγ with a relatively large ^{1}J (~ 75 Hz at low pH, Tran-Dinh et al. 1975), whereas ^{13}Cε is a singlet. It followed that the CδH and CεH assignments were as usual for His117 and other histidines of rHb-A as well as rHb-R. The ^{1}H-^{15}N HMQC data supported the reaction of the Nε atom of His117 and a neutral imidazole at neutral pH.

The observation of a coupling between His117 Nε and 2-β-CH_3 in rHb-A implied that $|^3J_{NH}| > |^2J_{NH}| \sim 0$. In general, $^2J_{NH}$ for a pyrrole-like nitrogen across a saturated carbon is small (0-2 Hz). For example, in 1-methylimidazole, $|^2J_{N\text{-}CH3}|$ is below 2 Hz, whether or not the ring is protonated (Alei et al. 1980). The three-bond coupling may be larger (reaching 7 Hz when following a Karplus-type relationship), and such was the case here with a freely rotating CH_3 group. Several contributions are expected to the ^{15}N chemical shifts of the modified histidine compared to a normal histidine in a diamagnetic protein: contact and pseudocontact, ring current, and for Nε, directly bonded carbon substituent effects. Thus, the origin of the shift experienced by the $^{15}N\varepsilon$ nucleus was not readily interpreted. The ^{13}C shifts for the ring carbons were also downfield with respect to the unreacted species, whereas the ^1H shifts were practically unchanged. The data indicate a cross-link structure as in Figure 3.6, with covalent bond formation between the histidyl ring Nε and the α carbon of the former 2-vinyl position.

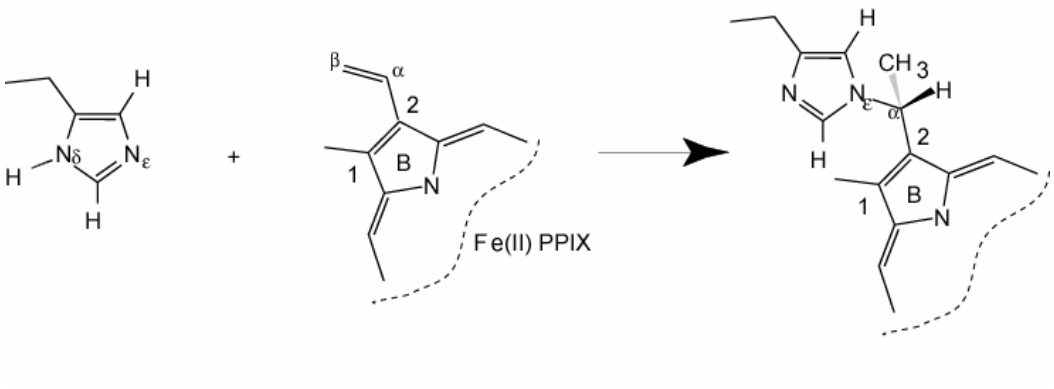

Figure 3.6 The reaction of His117 and the heme molecule in the presence of sodium dithionite produces the adduct pictured. A covalent link is formed between the Nε of His117 and the α carbon of the former 2-vinyl position.

3.3.4 Heme Environment and Stereochemistry of the Linkage

Nearly complete protein assignments were obtained in S6803 rHb-R via uniform $^{15}N/^{13}C$ labeling and a series of two- and three-dimensional experiments (Falzone & Lecomte 2002). Partial assignments were also obtained for S6803 rHb-A. Comparison of rHb-A and rHb-R data from each source showed that the consequences of the cross-link on the chemical shifts are modest and localized, in support of minor global structural rearrangement.

Cross-link formation generated a new stereo center at the 2-α-C of the porphyrin (Figure 3.6). rHb-A gave rise to only one set of NMR lines and supported the formation of a pure enantiomeric form. In the case of rHb-R (and other b-type hemoproteins), two distinct sets of signals were observed by NMR spectroscopy. The different signals correspond to protein structures in which the orientation of the heme group differs by a rotation of 180° about the α-γ meso axis (La Mar et al. 1999). The relative proportion of each heme isomer can vary depending on heme pocket structure. S6803 rHb-R has a heme isomer ratio of 95:5. In the majority of molecules, the heme group is oriented such that the 2-vinyl group is on the His117 side of the protein (Falzone et al. 2002, Lecomte et al. 2001). Structural data on rHb-R indicated that the 2-β-CH_2 points toward the 1-CH_3, rather than the α meso H. The constraints of the starting rHb-R structure favored an attack by His117 on the proximal face of the heme group. These restrictions and the steric clashes limited the reorientation of the modified imidazole, and there are two possible classes of environment for the new CH-CH_3 moiety. In the R enantiomer, the 2-β-methyl group points toward the heme 1-CH_3; in the S enantiomer, it points toward the α-meso hydrogen, and the methine proton is directed toward the heme 1-CH_3.

Stereochemistry of rHb-A was tentatively determined by NOE data. A medium size NOE was observed between the heme 1-CH_3 and the CεH of the reacted histidine and none between the same methyl group and the CδH. NOEs were also observed from His117 CδH to Phe84. These effects positioned the imidazole ring with the CεH toward the heme iron ion and CδH toward the periphery of the porphyrin ring. A medium size dipolar contact between the 1-CH_3 and the 2-β-CH_3 and no dipolar contact between the 1CH_3 and the 2-α-CH were consistent with the R enantiomeric form. The same set of NOEs was observed in both S6803 and S7002 rHb-A. In addition to these, the α proton of Val121 was found in dipolar contact with one of the β protons of the proximal histidine. This observation was expected for helical structure near Val121 and limited the structural possibilities for the covalent linkage.

Recently, the crystal structure of rHb-A was solved by Hargrove and co-workers (Hoy et al. 2004). The covalent modification did not change the overall topology of the fold as reported in Falzone et al. (2002). As expected, formation of the bond between His117 and the heme 2-vinyl group resulted in a slight modification of the heme pocket. The structure showed a tighter packing of the H-helix and the heme group resulting from the covalent linkage. In the crystal structure a tilt of the proximal (His70) and distal (His46) histidine is observed with respect to the heme plane. The NMR structure of S6803 rHb-R shows a short tunnel near the G and H helices (Falzone et al. 2002). Tunnels such as this and extended tunnels observed in other trHbs are proposed ligand access points (Wittenberg et al. 2002). The crystal structure of rHb-A reveals that Tyr53 prevented access to the distal heme pocket through the short G-H tunnel (Hoy et al.

2004). The differences in ligand access tunnels are likely related to structural rearrangements due to covalent bond formation.

The ready reaction of the heme with His117 (H16) in S6803 and S7002 Hb suggested that other heme proteins may undergo the same modification. Inspection of Hb structures identified few sequences with a histidine at or within a few residues of position H16. An instance is provided by *Mt* trHbO. The three-dimensional structure shows that the H helix in this protein is regular and directs HisH16 away from the heme group (Milani et al. 2003b). Positioning the ring near the 2-vinyl group would require a rearrangement of the backbone. The three-dimensional structures of other candidates (as possibly in several *Bacillus* subspecies Hbs and the trHb from *Xanthomonas campestris*) have not been determined yet. Beyond the Hb family, a histidine–heme vinyl linkage is formed transiently in CcmE, a protein of the cytochrome c maturation system (Schulz et al. 1998, Stevens et al. 2003, Thöny-Meyer 2003) In this case, the linkage is formed between the histidine residue and the β position of the 2-vinyl group (Linda Thöny-Meyer, personal communication). The different linkage may suggest that the exact structure of the linkage is modulated by protein function.

3.3.5 Examination of pH Effects by NMR Spectroscopy

The environment of the 2-vinyl group was inspected for unusual features in the structure of S6803 rHb-R. The group is protected from solvent and surrounded by aromatic and aliphatic residues, namely Phe50, Tyr53, Phe84, and Val121. The NMR model of the wild-type protein also reveals that His117 is not packed against the heme but is likely to sample different conformations at neutral pH. In rHb-R His117 is in the

NεH tautomer, (where the Nε position is protonated). The protonation state of this site may influence the reaction if acid-base chemistry is involved. To this end, pH titrations were performed on wild-type rHb-R and rHb-A to determine the pK_a of His117 as well as other non-coordinated histidine residues. The chemical shifts of non-axial histidine CδH and CεH and heme protons were examined as a function of pH and shown in Figure 3.7 (panel B). A resolved transition was observed for His33. Fitting of the chemical shift versus pH data to Equation 1 indicated an apparent pK_a of 5.6 for this residue. The pH response of rHb-R His83 is small in the investigated titration range (4.5-8.3) and indicated a low pK_a value (<4). Examination of the structure of S6803 rHb-R revealed a hydrogen bond between His83 Nδ and Asn80 NH (Figure 3.8). Low histidine pK_a values due to hydrogen bonding have been observed for His24 (hydrogen-bonded to His119) in Mb (Cocco et al. 1992) and His80 (hydrogen-bonded to Asp82 NH) in cytochrome b_5 (Altman et al. 1989). The proton signals for His77 and His117 broadened in the neutral pH region and were undetectable by 1D NMR spectroscopy. At high pH the signals were observed in ^{1}H-^{15}N HMQC experiments. Curves with a Hill coefficient of n = 1 were used to simulate the fragmented titration curves defined by the data. The results suggested that the pK_a of His77 is approximately 7.4 and His117 is near 6.9, i.e., minimally perturbed from an exposed histidine value (Figure 3.7, panel B). Examination of rHb-R heme methyl and vinyl chemical shift versus pH indicated titration events near the 1-CH_3 and 2-vinyl positions with inflection points similar to rHb-R His117 (Panels A and C). The pH response of the NMR signal suggested sensitivity to the protonation state of this residue, either directly, or through conformational changes associated with proton

loading. Formation of the histidine-heme linkage lowers the pK_a value for His117 by more than 2 units. All other pK_a values in rHb-A appear unaffected.

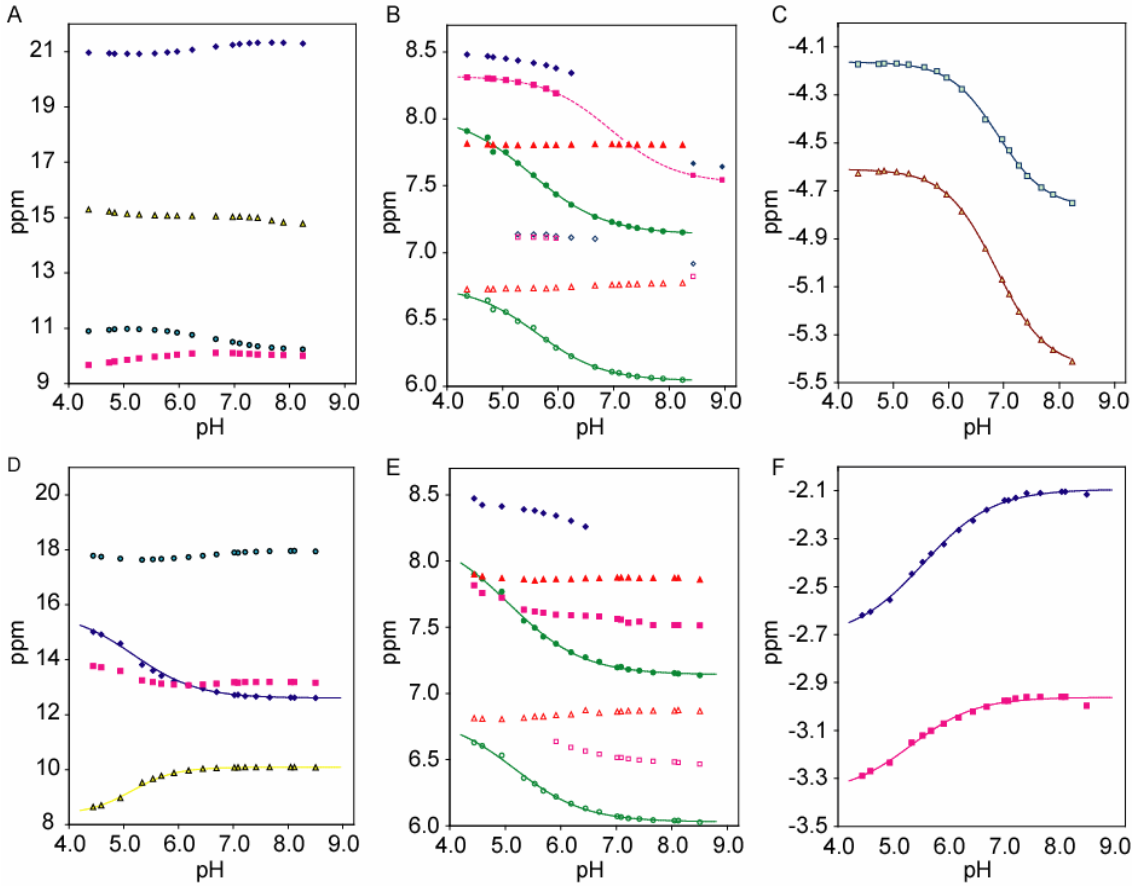

Figure 3.7 pH titration of S6803 rHb-R (panels A-C) and rHb-A (panels D-F) monitored by ^{1}H NMR spectroscopy. Panels (A) and (D) show the pH response of the heme methyl protons. The methyl group labels are as follows: 1-CH_3, open yellow triangles with yellow line; 3-CH_3, blue diamonds; 5-CH_3, open circles; and 8-CH_3, pink squares. Panels (B) and (E) show the non-axial histidines and are labeled: His33, green circles; His77, blue diamonds; His83, red triangles, and His117, pink squares. CεH protons are represented by filled symbols, and CδH protons with open symbols. Panel (C) shows the pH response of the 2-β-vinyl protons in rHb-R, while panel (F) represents

the 4-β-vinyl protons of rHb-A. Data for the 4-β-vinyl protons of rHb-R are not shown but follow a similar transition as observed for rHb-A. The chemical shift range in each column of panels has been adjusted for effect. pK_a values were obtained by fitting data where possible. The dotted line for His117 in panel (B) represents a simulated fit. Near neutral pH, the signals are not observed owing to broadening and thus only an estimated pK_a value is provided.

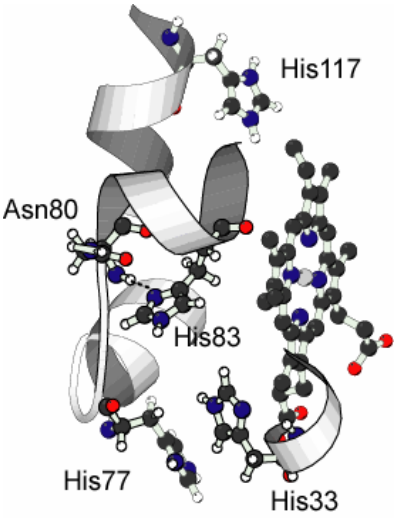

Figure 3.8 Region of the S6803 rHb-R structure showing non-axial histidine residues with respect to the heme molecule. The selected structure shows His117 facing the 2-vinyl position. The hydrogen bond between the backbone NH of Asn80 and His83 Nε is shown.

Once modified, the imidazole ring of His117 remains available for protonation (Figure 3.6). The pH titration curves for S6803 rHb-A are shown in Figure 3.7 (panel E). In this species, His33 had a pK_a of 5.2 and His83 was pH-invariant. These pH profiles were similar to those in rHb-R and in agreement with a limited effect of the cross-linking on the structure. In contrast, the modified His117 displayed an incomplete titration

curve, with an apparent transition onset below pH 6.5. This behavior indicated a lower pK_a value than in rHb-R as a result of covalent and non-covalent contributions, the net effect being an energetic penalty for the introduction of a positive charge in the heme pocket. Panels D and F (Figure 3.7) illustrate that some of the resonances from the modified heme exhibited enhanced sensitivity to pH ($\Delta\delta > 2$ ppm). A transition was observed near pH 5.4, which affected strongly the 4-β-vinyl but was not accompanied with a spin-state change.

pH titration data on rHb-R suggested the protonation state of His117 may affect cross-link reactivity. To test this possibility, rHb-R was subjected to treatment with sodium dithionite at lower (5.5) and higher (8.5) pH values. Covalent bond formation was observed under both conditions. It is possible that the pH affected the rate of rHb-A formation, but that the reaction remained too rapid for the effect to be detected with the manual method applied here. NOE data collected at the same pH values did not support a change in His117 environment upon protonation or deprotonation.

3.3.6 Optical Characterization of S6803 rHb-A

Ferric rHb-A has an optical spectrum exhibiting a Soret maximum at 409 nm (Figure 3.9). This represents a 1-nm blue-shift compared to rHb-R. Additional comparison of the two protein forms reveals that the spectrum of rHb-A has a broader band below the Soret down to 300 nm, and a less pronounced shoulder around 460 nm.

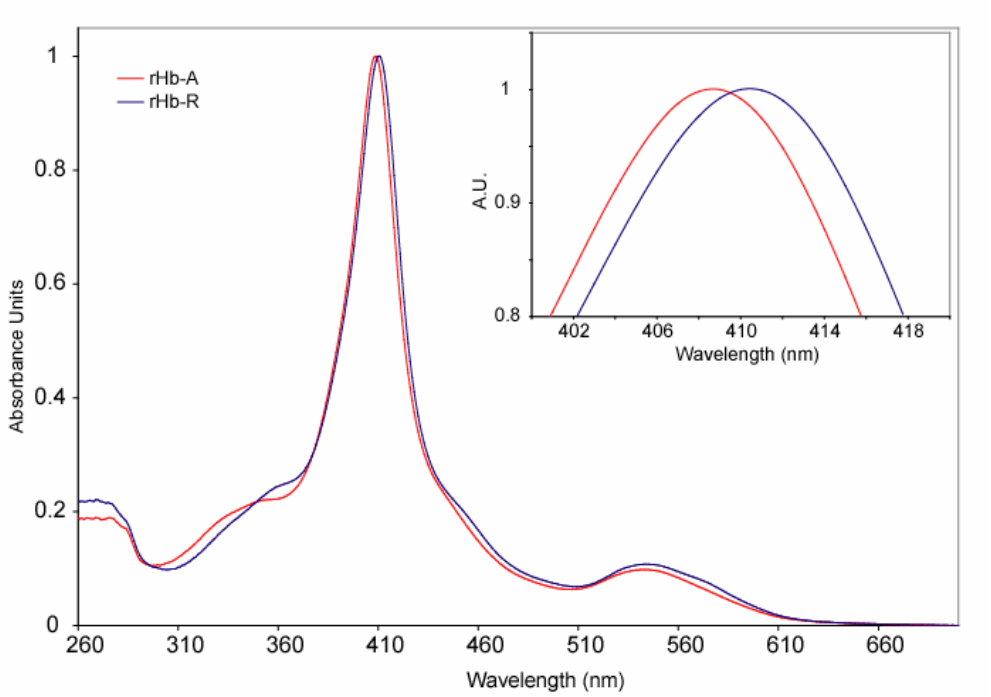

Figure 3.9 The optical spectra of S6803 rHb-R (blue) and rHb-A (red) at 25 °C in 20 mM phosphate buffer, pH 7.2, collected with a 0.5-nm bandwidth. The inset shows the region at the Soret band maximum where a blue-shift is observed from rHb-R to rHb-A. Changes in extinction coefficient were not determined and are not shown.

To examine the consequences of heme attachment on protein stability, the thermal denaturation of rHb-A was monitored by optical spectroscopy between 260 nm to 700 nm. The data were compared with those for rHb-R, which displays an apparent T_m of 74 °C (Lecomte et al. 2001). The lack of an unfolded baseline at 95 ºC in the melting of rHb-A revealed that the protein was not fully denatured at the upper temperature limits of the experiment and indicated a higher apparent T_m, and therefore stability, than rHb-R (Figure 3.10). Three clear isosbestic points were observed and were consistent with a two-state unfolding process. Covalent attachment of the heme to the polypeptide prevented dissociation of the heme into the bulk solution during denaturation and, unlike

rHb-R, thermal denaturation of rHb-A samples regained full absorbance when returned to room temperature.

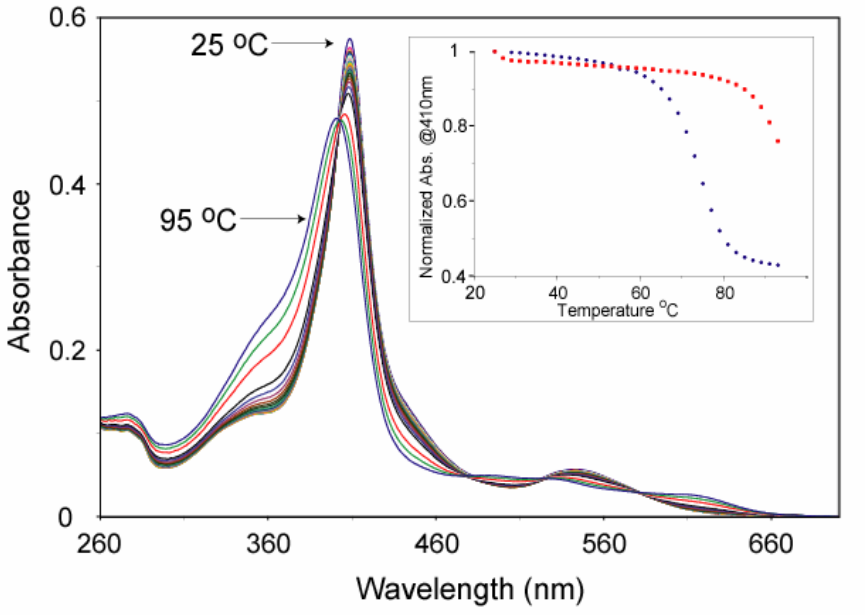

Figure 3.10 Optical spectra of S6803 rHb-A from 260 nm and 700 nm between 25 °C and 95 °C. The inset shows the normalized absorbance at 410 nm for S6803 rHb-R (blue) and rHb-A. The covalent linkage increases the apparent T_m by S6802 rHb by greater than 20 °C.

Hbs and Mbs lose the heme group when subjected to acid pH. This effect is due to unfolding of the protein and protonation of the proximal histidine (Acampora & Hermans 1967, Hermans & Acampora 1967). rHb-R and rHb-A stabilities were also probed using acid-induced unfolding, monitored by optical spectroscopy (experiments performed by Syna Kuriakose). Figure 3.11 shows the absorbance at 410 nm as a solution of rHb-R or rHb-A was acidified. For rHb-R, a transition of small amplitude was observed near pH 4, indicating a protonation event detected by the heme group, but

not corresponding to heme release Below pH 4, a larger transition is observed. Inspection of the absorbance spectra in this pH region revealed change from a low-spin (α and β bands at 546 and 578 nm) to a high spin (a charge transfer band at 645 nm) heme. This event reflects the release of free heme in an acidic environment. The main transition is well fit using a two-state titration model with a midpoint pH of 3.6. Similar changes were observed for the acid denaturation of rHb-A, but with a lower midpoint of pH 2.5. In the main transition range, isosbestic points are observed for rHb-R (pH 3-4.5) and rHb-A (pH 2-3.5) unfolding and are consistent with simultaneous decoordination of the axial histidine ligands. In this region, there was no evidence for intermediate ligation schemes (i.e metaquo Hb).

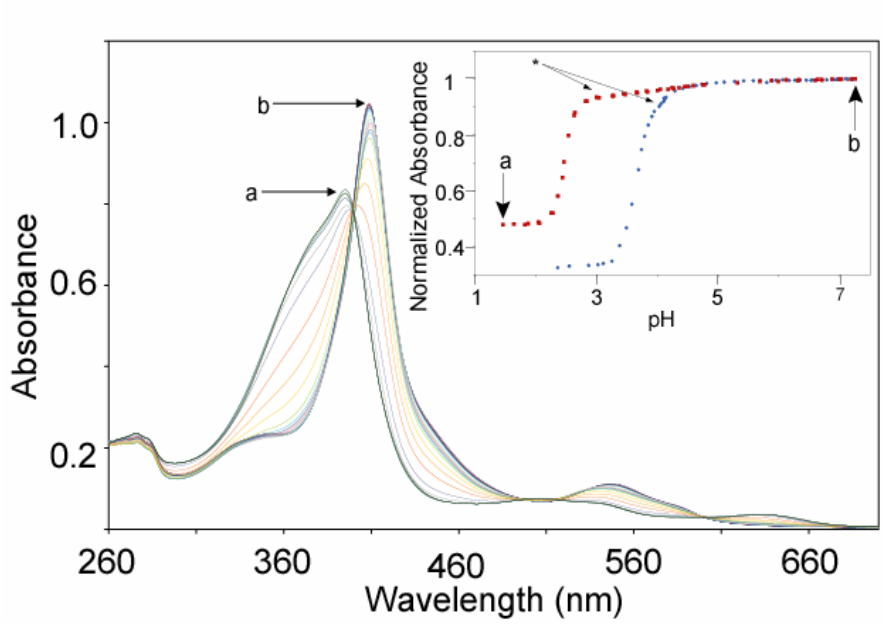

Figure 3.11 Optical absorbance of S6803 rHb-A from 260 nm and 700 nm between pH (a) 1.5 and (b) 7.2. The inset shows the normalized absorbance at 410 nm for S6803 rHb-R (blue) and rHb-A (red). The asterisk indicates the minor transition observed for rHb-R and rHb-A. Acid denaturation midpoint in rHb-A is lowered by 1.1 pH units versus rHb-R.

The Hill coefficient (Equation 1) can provide an estimate of the number of protons involved in the transition. The best fits of the absorbance versus pH returned n values of 3.4 ± 0.1 for rHb-R and 4.9 ± 0.1 for rHb-A; these values were subject to variations depending on how the minor transition occurring at higher pH was taken into account. In both proteins, the masked histidines (His46, His70, and His83) could account for three protons. In rHb-A, a fourth may be from His117.

3.3.7 Mutagenesis Studies (H117A, H117F, D120A)

The rHb-R NMR pH titration results raised the possibility that a residue at H16 is capable of influencing the heme site. To confirm reactivity of His117 in forming the cross-link, and to generate a form of the protein that certainly will not react, Ala and Phe mutants of His117 were generated. The first was intended to open a cavity near the reactive heme vinyl and the second as an isosteric mimic of the histidine residue. Asp120, which is common to S6803 and S7002 Hbs, was also modified to inspect its influence on the reaction, if any. The ^{1}H NMR spectra of the H117F, H117A and D120A variants are shown in Figure 3.12. The H117F rHb-R spectrum yielded broad signals and was distinct from the spectrum of wild-type S6803 rHb-R. In addition, the H117F replacement resulted in perturbation of the heme rotational isomer equilibrium from 95:5 (major: minor isomer) to approximately 1:1. Thus, the spectroscopic properties of the Phe replacement were unsuitable wild-type mimic. In contrast, the spectra of H117A and D120A rHb-R have similar hyperfine shifts to the wild-type protein. Two-dimensional homonuclear data (not shown) demonstrated widespread chemical shift perturbations,

overall smaller in magnitude than observed upon formation of rHb-A ($|\Delta\delta| < 0.5$ ppm), but nevertheless indicative of repercussions throughout the heme environment.

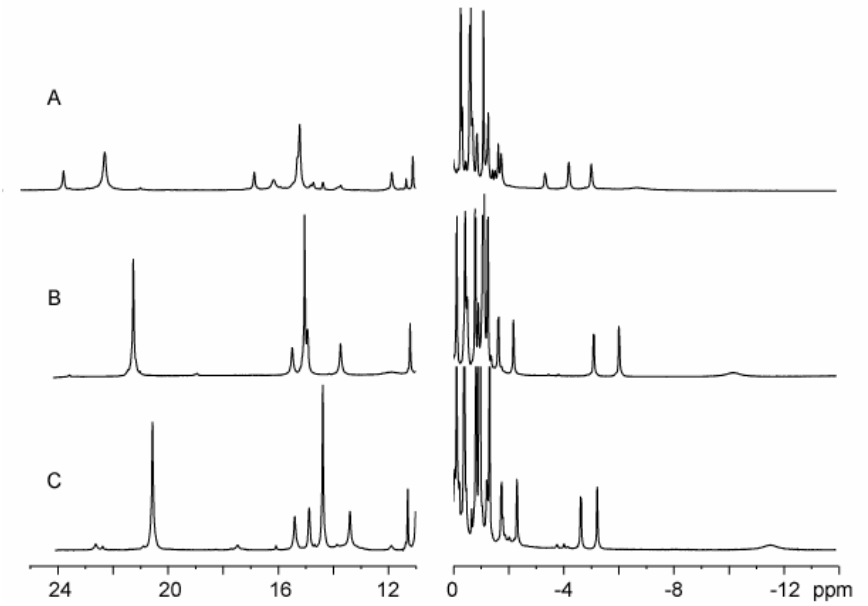

Figure 3.12 Hyperfine shifted regions from the ^{1}H NMR spectra of S6803 (A) H117F, (B) H117A, and (C) D120A rHb-R. Traces (B) and (C) are similar in appearance to the wild-type hemichrome. The spectrum of H117F is broadened versus the wild-type protein and a larger number of lines are observed.

H117A and D120A rHb-Rs were examined for cross-link formation. Upon addition of sodium dithionite, both samples changed color to a cherry-red consistent with reduction of the ferric heme iron to Fe(II). These samples remained reduced until applied onto the desalting column. ^{1}H NMR spectroscopy revealed H117A rHb-R did not form the cross-linked protein and confirmed the role of His117 in covalent bond formation. As expected, D120A rHb-R converted to cross-linked protein. Mass spectroscopy on the dithionite-treated mutants confirmed these results. However, any possible effects of the

D120A mutant on reactivity were not observed by method used here and cannot be ruled out.

In an additional control experiment (performed by Henry Nothnagel), H117A S6803 rHb was studied for its resistance to thermal denaturation using the methods described above. The apparent midpoint for heme loss obtained from two-state fitting of the data was 74.8 °C, within error of the wild-type number (Lecomte et al. 2001). From the point of view of structure and stability, H117A S6803 rHb was therefore an acceptable candidate for exogenous ligand binding studies.

3.3.8 Imidazole Binding to H117A S6803 rHb-R

Crystal structures of sperm whale Mb showed that xenon atoms are capable of occupying distinct cavities near the heme group (Tilton et al. 1984). These cavities provide docking sites for small ligand access to the distal binding site (Bourgeois et al. 2003, Teeter 2004). More recently, these cavities have been observed in the crystal structures of *Mycobacterium tuberculosis* trHbO, *Ce* trHb, and *Pc* trHb obtained in the presence of xenon (Milani et al. 2004b). The NMR structures of S6803 rHb-R showed His117 is primarily outside of, but occasionally occupies, the heme binding pocket (Falzone et al. 2002). The region between His117 and the 2-vinyl group corresponds to the Xe2 site observed in swMb and other trHbs. The H117A mutant may maintain a cavity in which imidazole can be titrated to form the covalent bond via a trans rescue process. A H117A rHb-R NMR sample was prepared in 20 mM phosphate, 10 mM imidazole. Examination by ^{1}H NMR revealed changes to H117A rHb-R related to imidazole addition. A number of new hyperfine shifted peaks with low intensity relative

to the original protein were observed (Figure 3.13). These signals were not present after gel filtration and indicated the binding of imidazole to the protein but absence of covalent chemistry. The proportion of imidazole bound species increased as the imidazole concentration was raised. At 200 mM imidazole, only a fraction of the sample contained free H117A rHb-R. Intermediate concentration data indicated a slow exchange process on the chemical shift time scale. Integration of resolved imidazole-free and bound signals provided an estimated dissociation constant of 20 mM. To attempt covalent bond formation, the imidazole-bound H117A protein was treated with 1.5 equivalents of sodium dithionite as above. No reaction was observed over days and the imidazole-free H117A spectrum was obtained after gel-filtration of the reacted sample. Unlike for the H117A mutant, the appearance of the wild-type rHb-R spectrum in the presence of imidazole was like that of the imidazole-free spectrum but also contained many small broad peaks. Heme methyl shifts in H117A S6803 rHb-R suggested that imidazole was binding to the heme iron. Under conditions where the imidazole concentration largely exceeds the protein concentration, displacement of one or more axial ligands should be expected. In *b*-hemoproteins, intramolecular heme reorientation is observed and requires dissociation of the axial ligand bond (La Mar et al. 1999, La Mar et al. 1984). By increasing the concentration of imidazole in solution, the equilibrium favors dissociation of an endogenous ligand followed by recombination with the strong imidazole ligand in solution. It should be noted that imidazole may also bind in the Xe2 site. This possibility cannot be discarded with the available NMR data. The lack of reactivity may simply indicate that the orientation of the bound imidazole is not adequate for the reaction to proceed.

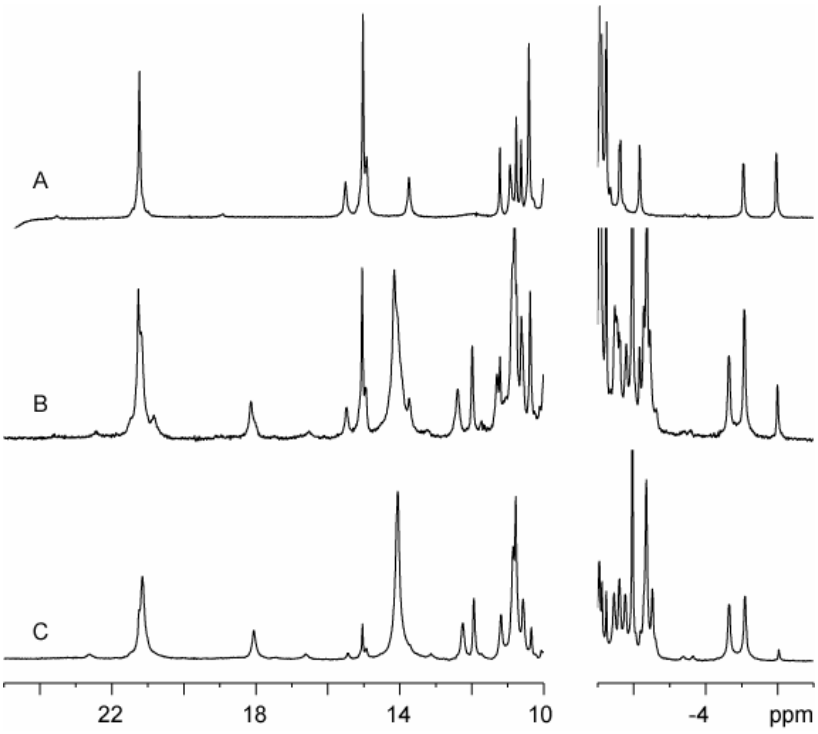

Figure 3.13 Hyperfine shifted regions from the ^{1}H NMR spectra of H117A S6803 rHb-R with (A) 0 mM (B) 50 mM , and (C) 200 mM imidazole. Other sample conditions were 20 mM phosphate, pH 7.2 at 298 K. At 50 mM total imidazole concentration, the spectrum clearly reflects a combination of imidazole bound and imidazole free protein. At higher concentrations, the spectra reflect mainly imidazole-bound sample.

3.4 Conclusions

This chapter detailed the structural properties of a novel histidine-heme linkage by NMR and optical methods. The characterization described here is expected to provide a basis for the identification of the same cross-link in other heme proteins. The selectivity for a single 2-α attachment point with pure stereochemistry in two different protein sequences favors a reaction initiated at the porphyrin ring. The environment of the reactive histidine had no extraordinary feature, except for flexibility allowing

occasional dipolar contact with the heme. In addition, position H16 appeared to be a sensitive site for the modulation of the electronic properties of and access to the heme group. These observations will contribute to an understanding of the determinants of reactivity of the heme vinyl so that cross-link formation can be predicted, engineered, or avoided, into other structures.

Covalent bond formation in rHb-A resulted in increased resistance to thermal and acid denaturation. The stabilizing effect of heme-protein linkages has been observed in other systems such as cytochrome c, where thioether linkages to the heme vinyl group are observed . The functional relevance of protein stabilization by thioether bond formation has not been clearly established. Another proposed function of the thioether linkage in cytochrome c is to modulate the protein reduction potential (Cowley et al. 2004, Tomlinson & Ferguson 2000a, Tomlinson & Ferguson 2000b).

Further studies are required to establish the functional relevance of the covalent linkage in S6803 and S7002 rHb-A. Conditions that promote protein production in *Synechocystis* sp. PCC 6803 and *Synechococcus* sp. PCC 7002 are still unknown. If both rHb-R and rHb-A are found *in vivo*, understanding the determinants of reactivity is key. To this end, *in vitro* studies are currently under investigation to explore the conditions of covalent link formation. One possible function for this histidine-heme bond may be to modulate protein reactivity. Electrochemical data are needed on S6803 and S7002 rHb-A as well as S7002 rHb-R to determine any changes in reduction potential resulting from covalent heme modification. Mutagenesis of His117 provides the opportunity to characterize the heme pocket structure and ligand binding in a non-reactive environment. NMR data indicate the spectral characteristics of the H117A variant are similar to those

of wild-type rHb-R. Imidazole binding was not able to initiate a *trans* rescue process. However, the data suggest the imidazole is able to displace the distal histidine ligand. Chapter 4 investigates the structural changes that accompany displacement of the distal histidine upon ligand binding.

Chapter 4

Ligand Binding to *Synechocystis* sp. PCC 6803 H117A Hemoglobin

Material in this chapter was published as part of "Cyanide binding to hexacoordinate cyanobacterial hemoglobins: Hydrogen bonding network and heme pocket rearrangement in ferric H117A *Synechocystis* Hb" Vu, B.C., Vuletich, D.A., Nothnagel, H.J., Falzone, C.J., and Lecomte, J.T.J. (2004) *Biochemistry*, *in press*.

Data on H117A S7002 rHbCN were collected by David Vuletich.

Experiments measuring cyanide binding kinetics monitored by optical spectroscopy were performed by Henry Nothnagel.

4.1 Introduction

The discovery of hexacoordinate hemoglobins (hxHbs) (Arrendondo-Peter et al. 1997, Burmester et al. 2002, Burmester et al. 2000, Couture et al. 1999a, Duff et al. 1997, Scott & Lecomte 2000) has expanded structure-function relationships in the Hb family. In the case of pentacoordinate Hbs, there is no ligand at the distal heme iron site in the reduced deoxy state (Antonini & Brunori 1971). However, in hxHbs a protein residue occupies the sixth iron coordination site (distal site); this residue must be displaced to allow for exogenous ligand binding. Among the small number of hxHbs examined thus far, the distal ligand appears to regulate ligand binding (Du et al. 2003, Herold et al. 2004, Kundu et al. 2003). The kinetic analysis of O_2 and CO binding to rice nsHb and S6803 Hb indicates decoordination of endogenous ligand as the rate limiting step (Hargrove 2000, Trent et al. 2001a) in the simple mechanism of Figure 4.1. Comparison

of the rice nsHb to other plant Hbs and Mb also suggests distinct changes in the orientation of the E- helix and structure of the C-D region of the protein (Hargrove et al. 2000).

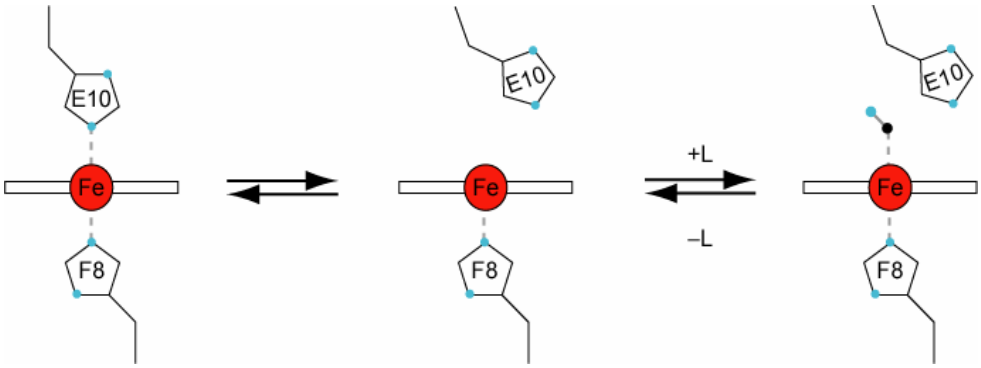

Figure 4.1 The model for exogenous ligand binding in hxHbs showing decoordination at the distal site. The proximal histidine (F8), His70 in S6803 rHb, is shown below the heme. The distal histidine is shown here as E10, and reflects this identity of the residue in S6803 and S7002 rHbs. In other hxHbs, HisE7 is the distal ligand.

Ligand binding data on trHbs that are not hexacoordinate Hbs also point to a role for hydrogen bonding networks in stabilizing exogenous complexes. The distal region of trHbs is characterized by a tyrosine residue at position B10; this residue is strongly conserved among known sequences (Wittenberg et al. 2002 , David Vuletich, personal communication). TyrB10 is part of a hydrogen bond network observed to stabilize the exogenous ligand at the distal site (Das et al. 2000, Milani et al. 2001, Pesce et al. 2000). In the case of oxygen binding, this network involves interactions between the phenolic oxygen of TyrB10 and Gln/ThrE11. Structures of cyanide-bound trHbs show GlnE7 is also recruited as a hydrogen bonding partner (Pesce et al. 2000). Binding studies indicate these residues regulate ligand binding in concert with apolar tunnels (Couture et al.

1999a, Couture et al. 1999b, Das et al. 2001, Milani et al. 2004a, Ouellet et al. 2003, Samuni et al. 2003, Yeh et al. 2000).

To our knowledge, no structural data are available for ligand-bound S6803 rHb-R.[2] Crystal structures for other trHbs in the ligand bound have been published (Milani et al. 2001, Milani et al. 2003b, Pesce et al. 2000) and provide potential models for changes resulting from exogenous ligand binding to S6803 rHb-R. According to sequence alignment data, *Ce* trHb (group I) is the closest relative of S6803 rHb (43% identity). In the cyanide-bound form the former protein will be used to predict changes due to ligand binding in the latter (Falzone et al. 2002). In S6803 rHb-R, His46(E10) is ligated to the heme iron and the side chains of Tyr22(B10), Gln43(E7) and Gln47(E11) are approximately parallel to the heme group, outside of the pocket (Figure 4.2). The corresponding residues in metcyano *Ce* trHb, Tyr20(B10), Gln41(E7) and Gln45(E11), point towards the heme iron and are located within hydrogen bonding distance of the cyanide ligand (Figure 4.2). In this structure, LysE10 points away from the heme binding pocket. The E-helix of S6803 rHb-R would need to rotate outward 45° about the helical axis to adopt a *Ce* trHb like conformation (Falzone et al. 2002). Formation of hydrogen bonds between B10, E7, E11 and the cyanide ligand in *Ce* trHb brings the B-helix in closer proximity to the heme group than is observed in the S6803 rHb-R structure.

[2] During preparation of this chapter, a paper describing the structure of the ligand bound form of rHb-A was published on-line (Trent et al. 2004) and will be addressed later in the chapter. The RCSB Protein Data Bank indicates that coordinates for S6803 rHb-A-CN (1S69) and rHb-A-N_3 (1S6A) have been deposited; they are to be released at a later date.

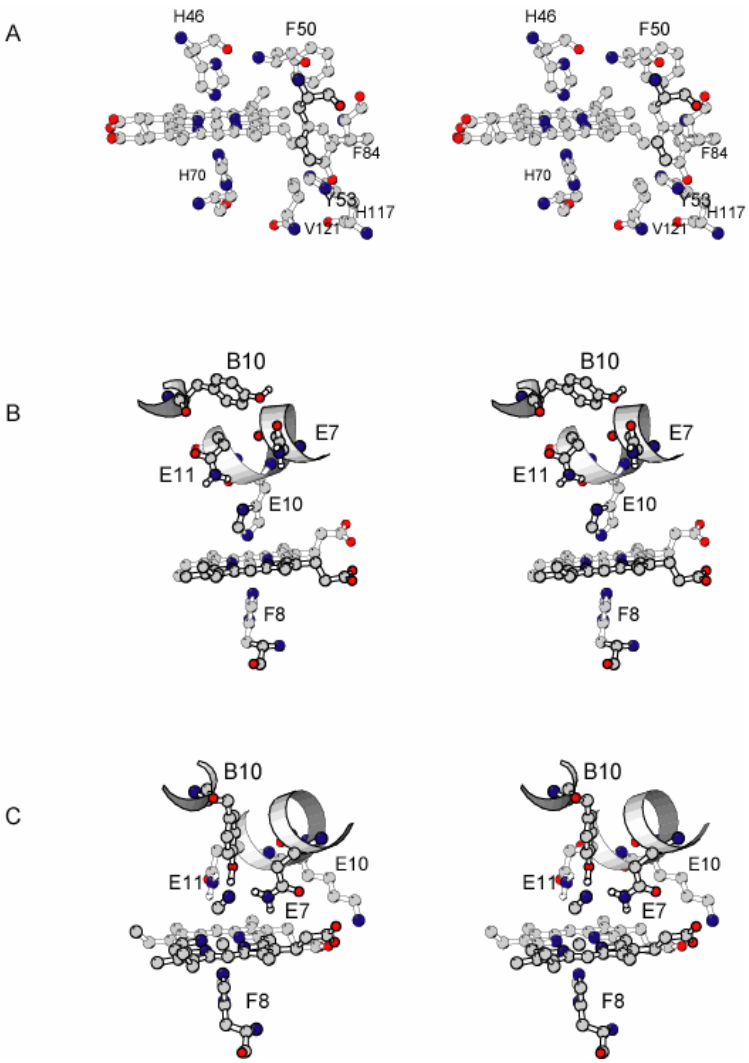

Figure 4.2 (A) Stereo view of the solution structure of wild-type S6803 rHb-R (1mwb, one representative structure, with His117 near the heme group), showing the environment of the heme 2-vinyl and the heme axial ligands His70 (F8) and His46 (E10); the 2-vinyl group should appear front and right. (B) Stereo view of the same structure, showing residues on the distal side of the heme: Tyr22 (B10), Gln43 (E7), and Gln47 (E11); (C) Stereo view of the X-ray structure of *Ce* trHbN (1dly) in the metcyano complex, showing the proximal heme axial ligand His68 (F8) and the distal side of the heme, including Tyr20 (B10), Gln41 (E7), Lys44 (E10) and Gln45 (E11).

Given the unpredictable reactivity of His117 S6803 rHb-R, the H117A mutant was used to avoid the complications due to the occurrence of the cross-link; the properties of the mutant were comparable to those of wild-type rHb-R. This chapter characterizes ligand binding to H117A rHb-R and examines structural rearrangement resulting from displacement of the distal histidine.

4.2. Materials and Methods

4.2.1 Preparation of H117A S6803 rHbCN

The mutant protein was prepared as described in Chapters 2 and 3. Uniformly ^{15}N-labeled H117A S6803 rHb was obtained with established protocols (Lecomte et al. 2001) using M9 minimal medium containing $^{15}NH_4Cl$ (Cambridge Isotopes, Andover, MA). The cyanide complex of the various proteins was prepared by addition of an excess of KCN (or $KC^{15}N$, Cambridge Isotopes, Andover, MA), adjusting the pH to the value of interest, and incubating at room temperature as necessary.

4.2.2 NMR Spectroscopy

One-dimensional ^1H spectra and 2QF-COSY, TOCSY, NOESY, and natural abundance ^1H-^{13}C HMQC data were collected as described in Chapter 2. Variable temperature data were collected on H117A S6803 rHbCN in 90% ^1H_2O, 10% ^2H_2O in the range 7 °C to 41 °C at pH 7.25. The chemical shift was plotted versus inverse absolute temperature to determine the Curie intercept (La Mar et al. 1999). Non-selective T_1 values were obtained by inversion recovery with recovery times varying between 1 ms

and 3 s. Peak intensities were analyzed with a single exponential return to equilibrium. The data were fit to the following equation:

$$I_t = I_\circ + P \times \exp(-t / T_1) \qquad (1)$$

where I_o is the equilibrium intensity, and P is the fractional intensity after non-selective inversion. Fits were limited to recovery time below one T_1, where they adhered to a single exponential function. Steady state NOE difference spectra were obtained with presaturation of the line of interest (or a signal-free reference position) with a 75 ms low-power pulse. WEFT-NOESY data were collected with 50-ms solvent presaturation, 150-ms inversion recovery time, 20-ms mixing time and 68-ms acquisition time.

^{1}H-^{15}N HMQC spectra were collected on uniformly ^{15}N labeled protein with a 15 ms delay to detect long range couplings in histidine residues. ^{1}H-^{15}N HSQC spectra and ^{15}N-separated NOESY and TOCSY data sets for assignment purposes were collected on uniformly ^{15}N labeled samples of H117A S6803 rHbCN as described for S6803 rHb-R (Falzone & Lecomte 2002, Lecomte et al. 2001).

4.3 Results and Discussion

4.3.1 Examination of Cyanide Binding to H117A S6803 rHb-R

Cyanide was incubated with wild-type rHb-R, wild-type rHb-A and H117A rHb-R. Optical spectra of the resulting solutions (Figure 4.3) showed a shift of the Soret band consistent with cyanide-bound hemoglobin (Antonini & Brunori 1971).

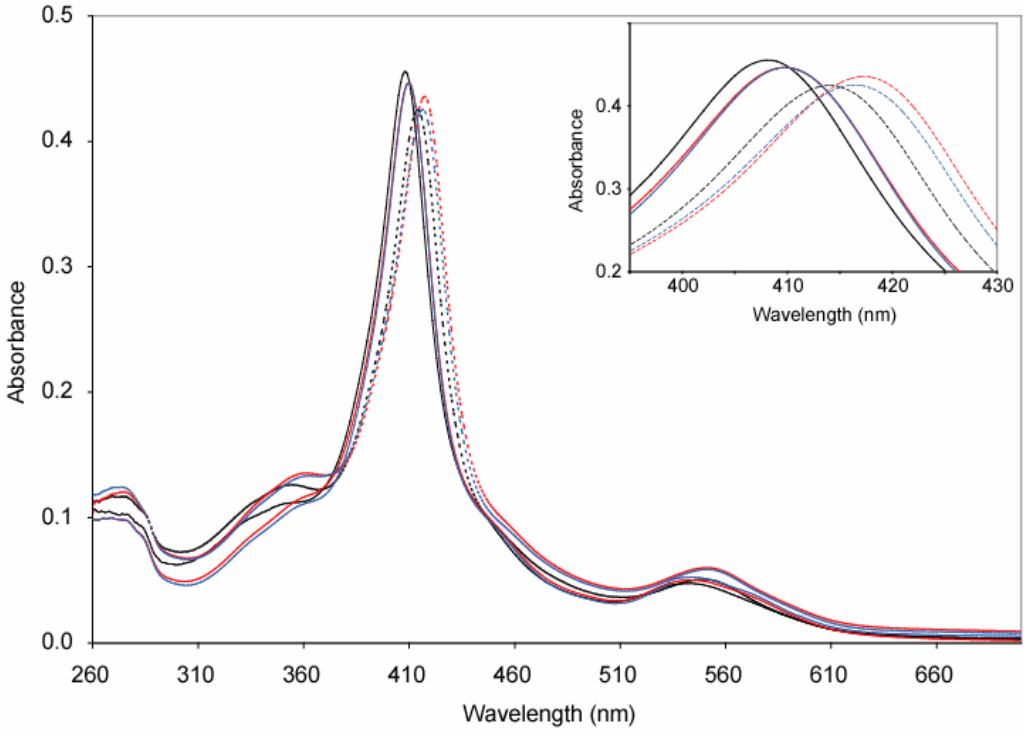

Figure 4.3 The optical spectra of wild type S6803 rHb-R (blue), rHb-A (black) and H117A S6803 rHb-R (red) in the presence (dotted lines) and absence (solid lines) of bound cyanide. All spectra were recorded in 100 mM phosphate buffer, pH 7.2.

^{1}H NMR spectra of the metcyano proteins are shown in Figure 4.4. The complex of wild-type (wt) rHb-R yielded a spectrum with broad lines, whereas the similar spectrum for rHb-A was sharp with a number of shifted signals in a small shift window. In contrast, H117A rHbCN spectra contained sharp, well-dispersed lines comparable to those of wt rHb-R. Closer inspection of the H117A rHbCN spectra revealed a change in major to minor heme isomerization ratios from 95:5 in the hemichrome to 85:15 in the metcyano protein. Spectra of ^{15}N labeled H117A rHbCN showed an additional increase apparently independent of cyanide concentration (Figure 4.4). H117A S7002 rHbCN also illustrated an increase in minor heme isomer, up to 30% (work performed by David

Vuletich). A similar observation has been reported for neuroglobin (Du et al. 2003). For vertebrate globins, it is generally assumed that the rate of association of heme and apoprotein to form the holoprotein is independent of the protein (Hargrove et al. 1996) and heme orientation (Jue et al. 1983). This implied that the affinity for the heme group, and therefore the equilibrium ratio of isomer concentrations, are dictated by the rate of heme release from the protein matrix. Vertebrate globins, however, tend to experience a relatively modest conformational change upon small exogenous ligand binding.

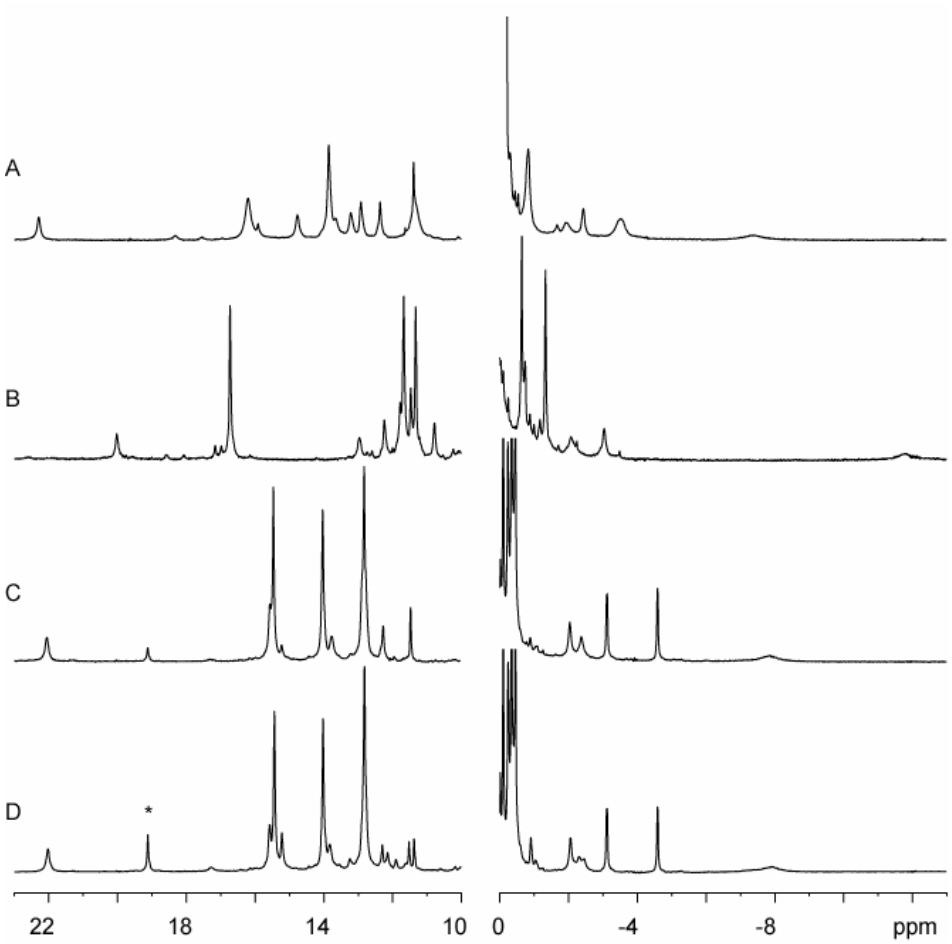

Figure 4.4 Hyperfine-shifted resonances in the ^{1}H NMR spectrum of cyanide-bound(A) wt S6803 rHb-R, (B) wt S6803 rHb-A, and (C) H117A S6803 rHb and (D) uniformly ^{15}N-labeled H117A S6803 rHb. Samples were incubated with a 10-fold excess of KCN.

Conditions were 20 mM phosphate, pH 7.2, 95:5 $^{1}H_2O$:$^{2}H_2O$, 25 °C. In spectrum (D), $^{1}J_{NH}$ coupling is clearly visible for an upfield resonance at –2.3 ppm (Q-2 in Table 4.1). Spectra A, C, and D were scaled using the intensity of the signal at 22 ppm. The * indicates an increase in the minor heme isomer concentration.

4.3.2 Assignment of Heme Substituents and Identification of the Axial Ligand

Heme substituents of H117A rHbCN were assigned through homonuclear correlated and NOE data (Figure 4.5) and heteronuclear ^{1}H-^{13}C HMQC data (Figure 4.6). The chemical shifts are listed in Table 4.1. Further inspection of the ^{1}H-^{13}C HMQC data revealed only one set of signals consistent with axial histidine shifts; α-CH ($\delta(^{13}C)$ ~66 ppm; $\delta(^{1}H)$ ~ 6.3 ppm) and β-CH_2 ($\delta(^{13}C)$ ~ 23 ppm; $\delta(^{1}H)$ ~ 6.4 and 6.6 ppm). These shifts are typical of low-spin heme proteins (La Mar et al. 1999).

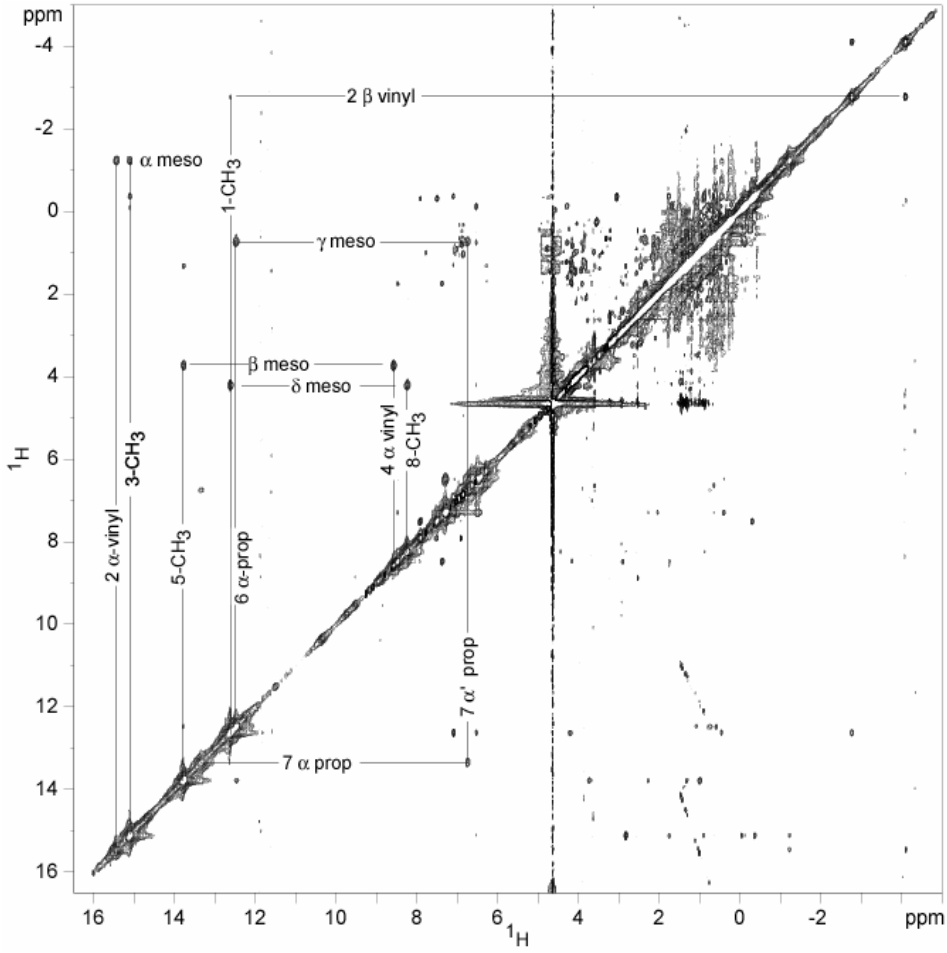

Figure 4.5 WEFT-NOESY spectrum of H117A S6803 rHbCN collected in 20 mM phosphate, pH 7.2 (100% ^2H_2O), at 308 K. Other experimental conditions were as follows: 50-ms presaturation, 150-ms inversion recovery, 20-ms mixing, and 68-ms acquisition times. The connectivities between heme substituents were used for assignments listed in Table 4.1.

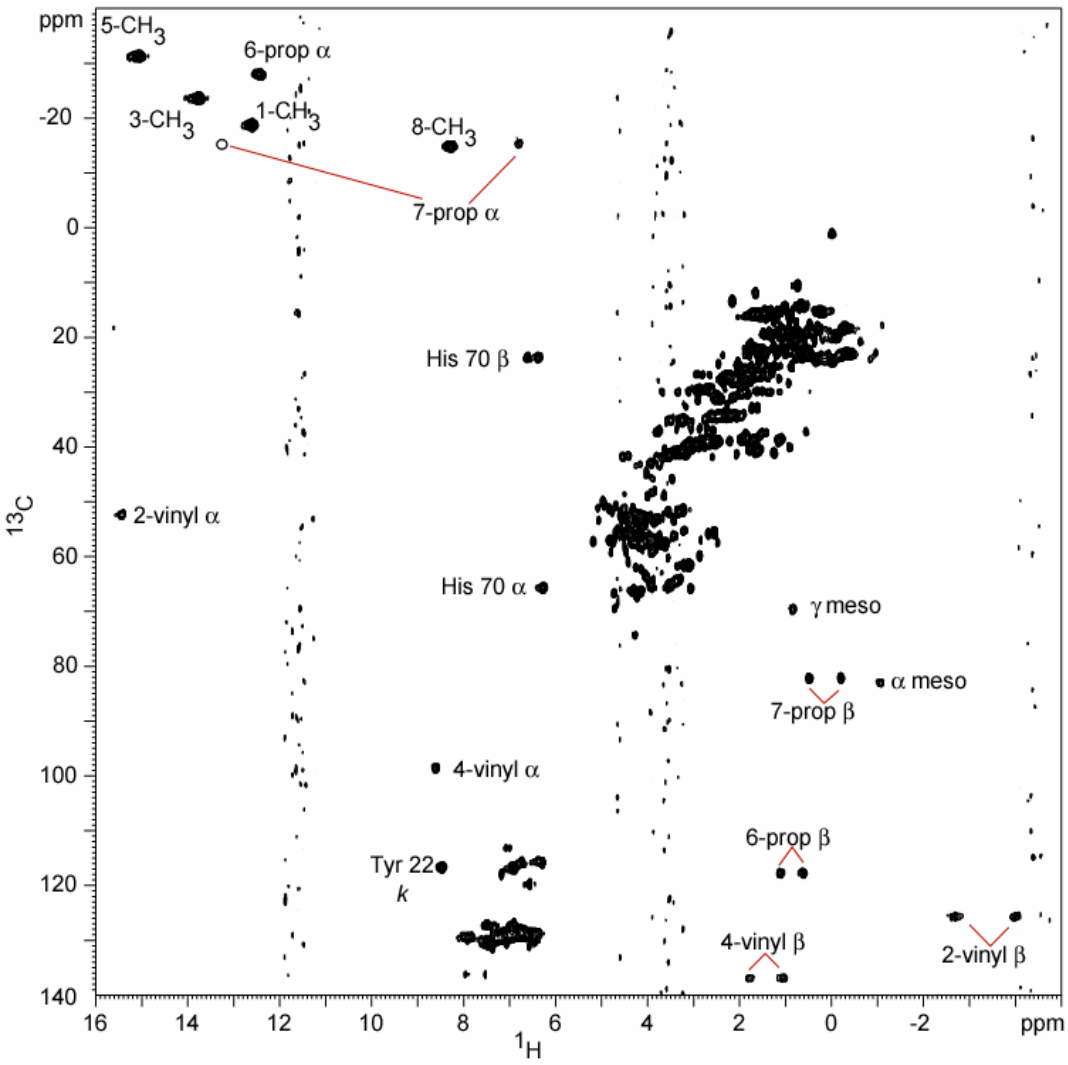

Figure 4.6 ^{1}H-^{13}C natural abundance HMQC spectrum of H117A S6803 rHbCN (20 mM phosphate buffer, pH 7.2, 100% $^{2}H_2O$) recorded at 308 K. Heme substituents and shifted residues have been labeled. Note that only one proton of the 7-α-propionate is observed under these conditions. Both protons are observed in ^{1}H data.

TOCSY data correlated the axial histidine α and β signals to a backbone NH at 8.45 ppm. One of the β protons and the NH were in NOE contact with an exchangeable proton at 12.2 ppm, a good candidate for the NδH of the ring because of its 90 ms T_1, placing it at

5.2 Å away from the iron center (Figure 4.8, Equation 1). The 12.2 ppm proton was connected via one-dimensional steady state NOE to the fast relaxing and broad peak at −8 ppm (Figure 4.9), assigned as the adjacent CεH. The signals were assigned to NδH and CεH ring protons respectively. Three-dimensional data (^{1}H-^{15}N HSQC-based experiments, analysis in progress) provided the ^{15}N shift of the peptide (110.3 ppm) and dipolar connectivities typical of helices were identified to Ala69 and Lys71 and their neighbors in the sequence. The data were in agreement with the F-helix pattern of *J* and NOE connectivities reported for the wild-type protein (Falzone & Lecomte 2002, Falzone et al. 2002) and the H117A rHb-R hemichrome. ^{1}H-^{15}N HSQC data correlated the 12.2 ppm ^{1}H signal to a ^{15}N signal at ~148 ppm, a plausible shift for the <u>Nδ</u>H moiety of an axial histidine (Figure 4.7). Uniformly ^{15}N-labeled protein confirmed the His70 NH assignment and therefore the rest of the side chain. Saturation transfer was not observed between the bulk water and the NδH at neutral pH. This is expected for axial histidines (La Mar et al. 1981, Lecomte & La Mar 1985), which are generally not exposed to solvent, and being committed to iron coordination via their Nε atom, experience only base-catalyzed exchange. His70 NδH was also poised for the formation of a hydrogen-bond to the backbone carbonyl of Met66.

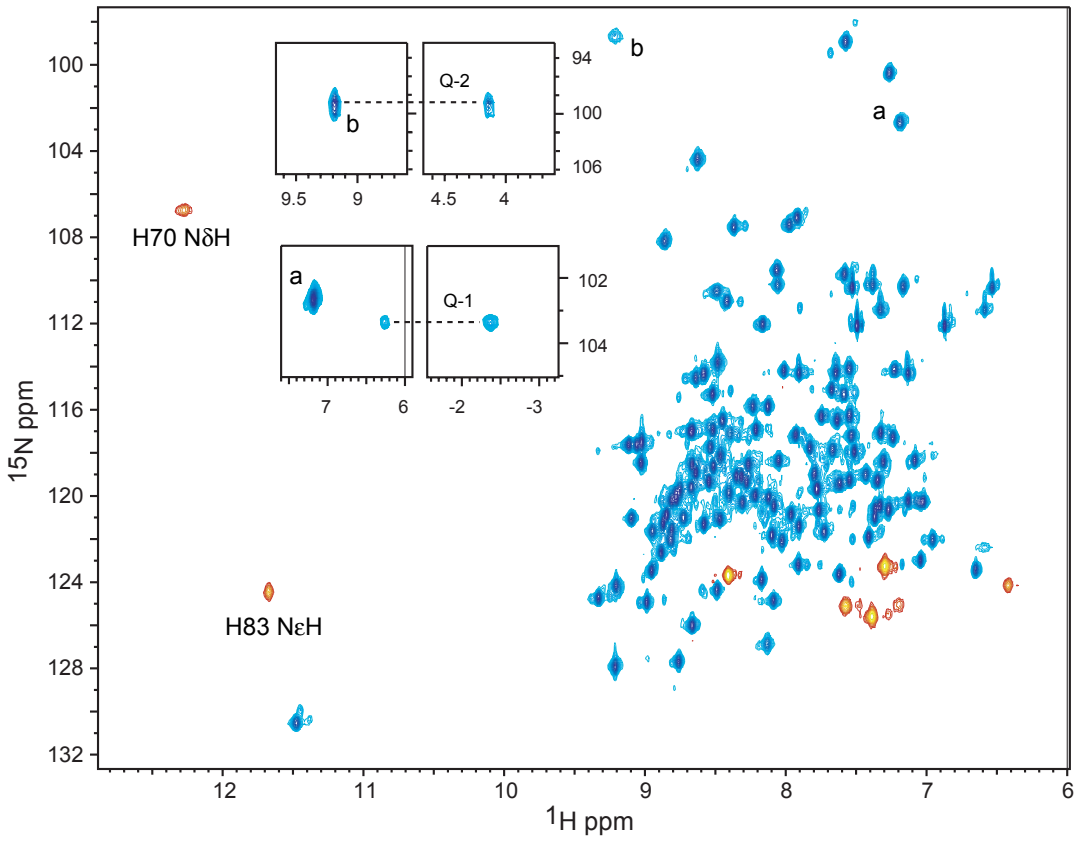

Figure 4.7 ^{1}H-^{15}N HSQC of H117A rHbCN collected at 298 K (20 mM phosphate, pH 7.3). Orange cross peaks represent folded arginine NεH's, His83 NεH, and His70 NδH. Shifted glutamine side chains are shown in the inset. Tentatively, Q-1 is assigned to Gln43 and Q-2 to Gln47.

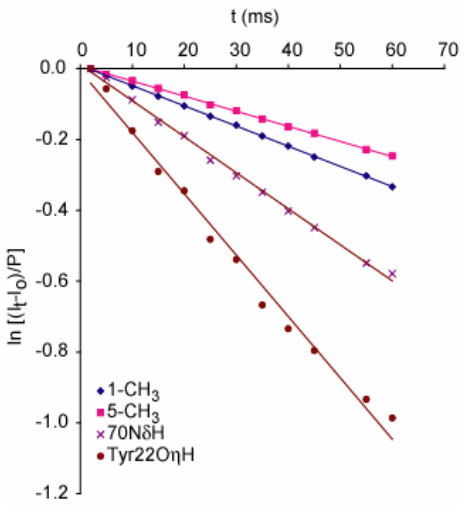

Figure 4.8 Semilogarithmic plot of recovered intensity fraction versus relaxation delay for non-selective inversion recovery. Two downfield shifted signals, which relax faster than heme methyl (1-CH_3 and 5-CH_3 selected) groups, are shown.

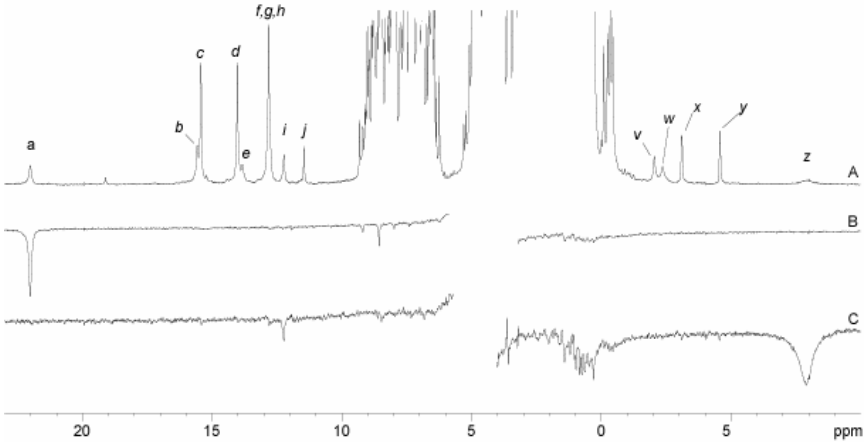

Figure 4.9 Steady-state NOE effects observed in H117A S6803 rHbCN (95:5 ^1H_2O:^2H_2O, pH 7.3, 25 °C). (A) Reference spectrum with peaks labeled as per Table 4.1. Difference spectrum obtained after saturation (75 ms) of (B) peak a, and (C) peak z.

Table 4.1 Selected ^{1}H NMR chemical shifts, T_1 and Curie intercepts for H117A S6803 rHbCN

	Assignment	Signal [a]	δ (ppm) [b]	T_1 (ms) [c]	Intercept (ppm)
heme	1-methyl	f	12.60	190	7.7
	3-methyl	c	15.06	290	5.2
	5-methyl	d	13.76	230	8.2
	8-methyl		8.28		
	2-α-vinyl	b	15.44		12.5
	trans-2-β-vinyl	x	–2.70		6.2
	cis-2-β-vinyl	y	–3.99		8.9
	4-α-vinyl		8.59		
	trans-4-β-vinyl		1.07		
	cis-4-β-vinyl		1.80		
	6-α-propionate	g	12.44		4.6
	6-α'-propionate	h	12.57		4.5
	6-β-propionate		1.11		
	6-β'-propionate		0.61		
	7-α-propionate	e	13.33	233	
	7-α'-propionate		6.79		
	7-β-propionate		0.49		
	7-β'-propionate		–0.20		
	α-meso	v	–1.23		20.3
	β-meso		3.72		
	γ-meso		0.74		
	δ-meso		4.21		

His70 (F8)	NH		8.30		
	CαH		6.24		
	CβH		6.57		
	CβH’		6.36		
	NδH	i	12.18	90	10.6
	CεH	z	–7.6		–0.5
	CδH		5.3		
Tyr22 (B10)	OηH	a	21.4	52	3.6
	CεH	k	8.41		
	CδH		7.32		
Q-2	Nε2H	w	–1.92	60	12.1

[a] Refer to Figures 4.9 for peak labeling [b] In 95:5 $^{1}H_2O$: $^{2}H_2O$, at 35 °C and pH 7.3, from WEFT, WEFT-NOESY, TOCSY, and 1D NOE data. [c] Measured in 95:5 $^{1}H_2O$:$^{2}H_2O$, pH 7.3, 25 °C.

4.3.3 Identification of Histidine Resonances in H117A rHbCN

Cyanide binding to the hemichrome must displace one of the axial histidines. The data presented above demonstrated that the proximal histidine (His70) remained coordinated and His46 was therefore the ligand replaced by cyanide. In addition, H117A S6803 rHb-R contains histidines at position 33, 77 and 83. The TOCSY data of the metcyano complex revealed four sharp signals characteristic of histidine CδH-CεH coupling (Figure 4.10) These signals ere sharp, which was consistent with residues greater than 6 Å of the heme iron center (La Mar et al. 1999). Thus, once displaced by cyanide, His46 moved out of the heme pocket. The four histidines were assigned by comparison of NOEs to the wild-type hemichrome. His83 Nδ was hydrogen bonded to

the backbone NH of Asn80. Other NOEs included His83 CδH to His33 CεH, His83 CεH and His33 CεH to Phe34 CεH, and His77 CδH to Leu 73. The remaining histidine was assigned to His46.

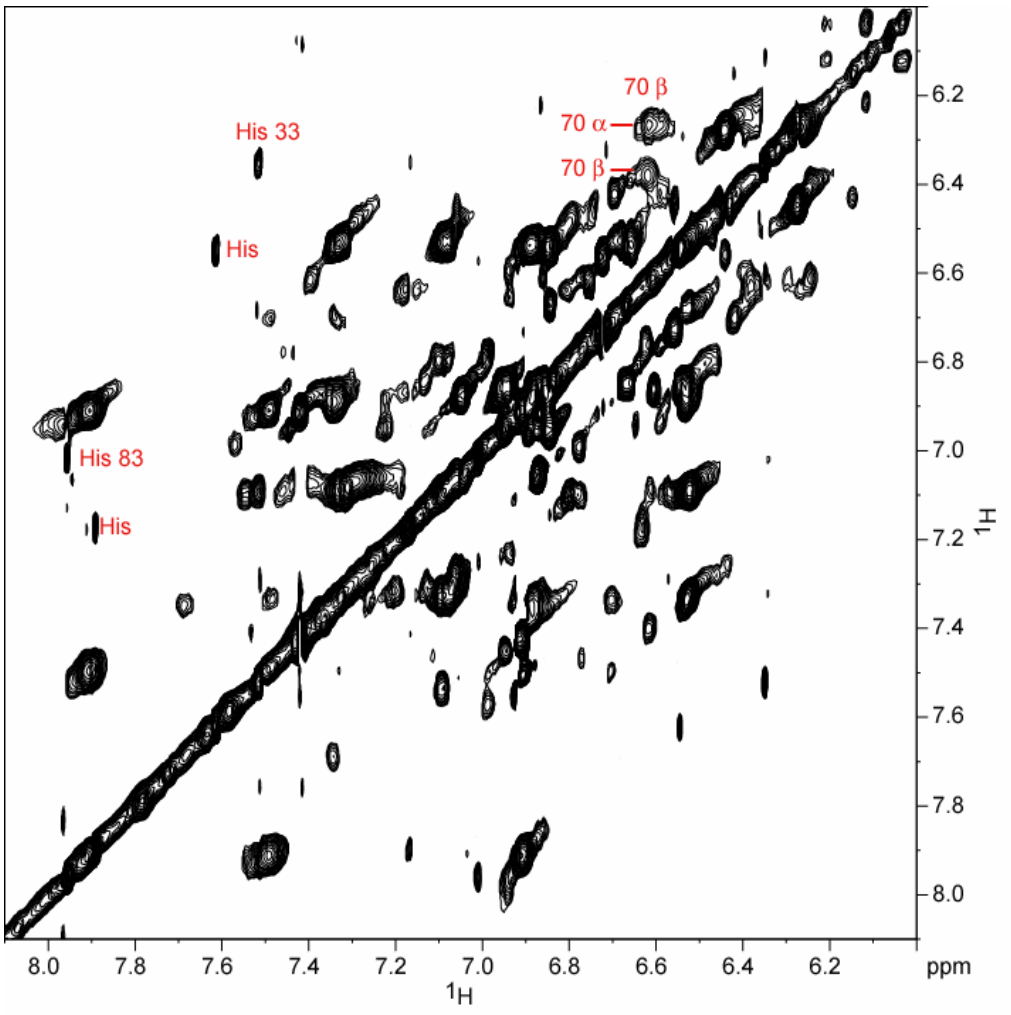

Figure 4.10 The aromatic region of the H117A rHbCN TOCSY (100% ^2H_2O, 20 mM phosphate, pH 7.2) at 308 K.

The ^{1}H-^{15}N HMQC spectrum collected to obtain long range ^{1}H-^{15}N *J*-coupling information for the imidazole rings (Pelton et al. 1993) returned patterns typical of the

NεH tautomeric state for His33 and His83 (Figure 4.11). At neutral pH, the signals from His77 and His46 were not detected, likely because of exchange between the protonated and unprotonated states on a time scale resulting in broadening of the ^{15}N signals. The similarity of the HMQC data to those collected on wild-type S6803 rHb-R (Chapter 3) suggested that His83, His33, and His77 had unchanged pK_a values.

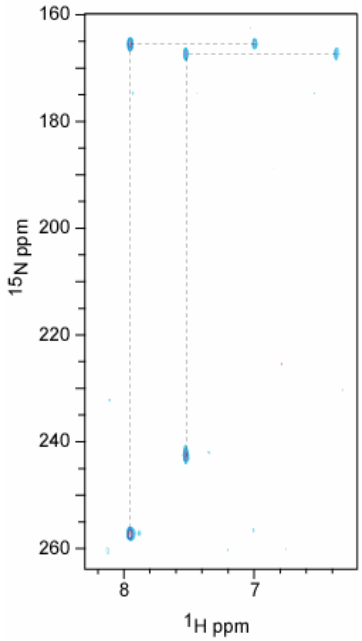

Figure 4.11 ^{1}H-^{15}N HMQC of H117A S6803 rHbCN (20 mM phosphate, pH 7.2, 95% $^{1}H_2O$: 5% $^{2}H_2O$) at 298 K.

The NMR spectra collected on the metcyano complex of H117A S6803 rHb supported the replacement of the distal-side histidine by the exogenous ligand. This behavior was consistent with that of other hxHbs (Couture et al. 1999a, Hargrove et al. 2000) and published data on His46 mutants of S6803 rHb (Couture et al. 2000). Furthermore, the reorientation of His46 outside of the influence of the paramagnetic center was in agreement with structural features of *Ce* trHbCN, which has Lys44(E10)

(equivalent to His46) pointing to the solvent (Pesce et al. 2000). The reason for the disparity in the behavior of His70 (kinetically stable) and His46 (replaceable) in S6803 rHb is not clear and is in contrast with other hexacoordinate hemoproteins such as cytochrome b_5, which does not bind exogenous ligands. Hargrove and co-workers compared iron-histidine bond lengths between cytochromes (1.8 – 2.1 Å) and various Hbs (2.0 – 2.2 Å, including rHb-A) and suggested the longer iron-histidine bonds found in hxHbs decreases the overall bond strength (Hoy et al. 2004).

4.3.4 Assignment of Heme Pocket Residues

The displacement of His46 from the heme pocket resulted in changed contacts between the protein and the heme. Based on the structure of the distal site in *Ce* trHb, Tyr22(B10), Gln43(E7), and Gln47(E11) in S6803 rHb were expected to point toward the heme and its cyanide ligand (Figure 4.2). These residues would be in close proximity to the bound-cyanide and are expected to be under the influence of the paramagnetic heme iron center. Most of the hyperfine shifted signals of H117A S6803 rHbCN were assigned to the heme group or axial ligand, except for an exchangeable peak at 22 ppm. This proton had a strong temperature dependence (Curie intercept of 3.6 ppm) consistent with a proton in close proximity to the heme iron. It had a short T_1 value placing it about 4.7 Å from the heme iron, closer than the observed values for NδH of His70. The ^{1}H spectrum of ^{15}N-labeled protein showed this signal remained a singlet and therefore was not bound to nitrogen (Figure 4.4). The 22 ppm signal showed a strong NOE to a signal at 8.53 ppm which was *J*-correlated to a ^{13}C at 113 ppm, consistent with the Cε of a tyrosine residue. Inspection of the *Ce* trHb and S6803 rHb-R structures indicated Tyr22

as the only likely candidate for this residue. In addition, NOE's were observed between the ring protons of Tyr22 and Phe21, consistent with a distal pocket geometry found in *Ce* trHb. The data indicated this residue to be Tyr22 and the proton at 22 ppm was the OηH. Saturation transfer from the bulk water line to this signal was not observed and provided further evidence hydrogen bonding. Proximity to the heme iron accounted for the large chemical shift value of Tyr22 OηH.

The heme environment of *Ce* trHb showed Gln41(E7)and Gln45(E11) pointed inward at the distal side of the heme pocket (Figure 4.2). In S6803 rHb these residues corresponded to Gln43 and Gln47. To search for glutamine residues in close proximity to the heme iron, a ^{1}H-^{15}N HSQC was collected on uniformly ^{15}N-labeled H117A S6803 rHbCN (Figure 4.7). Two NH_2 groups displayed chemical outside the region typical of glutamines and asparagines. The first pair (Q-1) occurred at an ^{15}N shift of 99 ppm with protons at 9.17 ppm and 4.14 ppm. A strong NOE between Tyr22 OηH and 9.17 ppm was observed. The second NH_2 pair (Q-2) were observed at a ^{15}N shift of 105 ppm with protons at 6.27 ppm and −2.35 ppm. The latter proton signal relaxed with a non-selective T_1 of 60 ms, corresponding to a distance 4.8 Å from the heme iron. Weak NOEs between these signals and Tyr22 OηH were also observed. Proximity to the heme iron and NOEs to Tyr22 located these glutamines in the distal pocket. Comparison to *Ce* trHb led to the assignment of Q-1 as Gln45 and Q-2 as Gln47.

Several other residues were assigned in the heme pocket. On the proximal side, the same network of dipolar contacts as in the hemichrome state was observed: His83 to Leu79; Leu79 to 4-vinyl; Leu73 to 5-CH_3, Leu79, and His77; Phe34 to 4-vinyl, Phe50 to 1-CH_3 and 8-CH_3; Val121 to His70 and Phe84; Ala117 to 2-vinyl. Among the side

chains affected by cyanide binding was Phe50, which in the hemichrome had NOEs to the 2-vinyl group, but in rHbCN shifted toward the heme δ meso position. A117 also appeared to be farther from the 2-vinyl. The lines from Phe34 remained sharp, and those from Phe35 broad. Phe35 was in contact with Tyr22 and, with Phe21 and Val25, defined a hydrophobic niche for this residue.

Cyanide binding to H117A S6803 rHb resulted in significant structural rearrangements. Consequently a number of heme pocket residues, such as Phe50, were repositioned. Studies on other *b*-hemoproteins, such as cytochrome b_5, have shown altered interactions near the heme result in changed heme orientation ratios (Cowley et al. 2002, Silchenko et al. 2000). The heme isomerization change observed in H117A S6803 rHbCN may be influenced by altered structural interactions resulting from cyanide binding. The differences between the metcyano and hemichrome proteins at the distal site also suggested that ligation of His46 (hemichrome) may impose steric constraints that are partially relaxed when the cyanide ion occupies the distal position and forms a H-bond with Tyr22.

4.3.5 Isotope Effect on Hydrogen Bonding Network in H117A rHbCN

In favorable circumstances, hydrogen bonds to the heme ligand can be identified through $^{1}H/^{2}H$ isotope effects (Lecomte & La Mar 1987). When spectra of H117A S6803 rHbCN were recorded in mixtures of $^{1}H_2O$ and $^{2}H_2O$, two resolved heme methyl signals were found to split into two components, weighted in proportion to the isotopic composition of the solvent (Figure 4.12). Data collected on H117A S7002 rHbCN (by David Vuletich) showed a more pronounced isotope effect. The two transitions are

attributed to distinct electronic structures of the heme caused by hydrogen bonding to either ^{1}H or ^{2}H. As observed in metcyanoMb, the downfield component was associated with the presence of ^{1}H and the upfield component with that of ^{2}H. Also as in metcyano Mb, the chemical shift difference between the two lines (~30 Hz) indicated a time scale for the $^{1}H/^{2}H$ exchange process slower than 10^{-2} s^{-1}. The isotope splitting confirmed hydrogen bonding to the ligand, but only two sets of lines were observed, each corresponding to the pure isotope shifts.

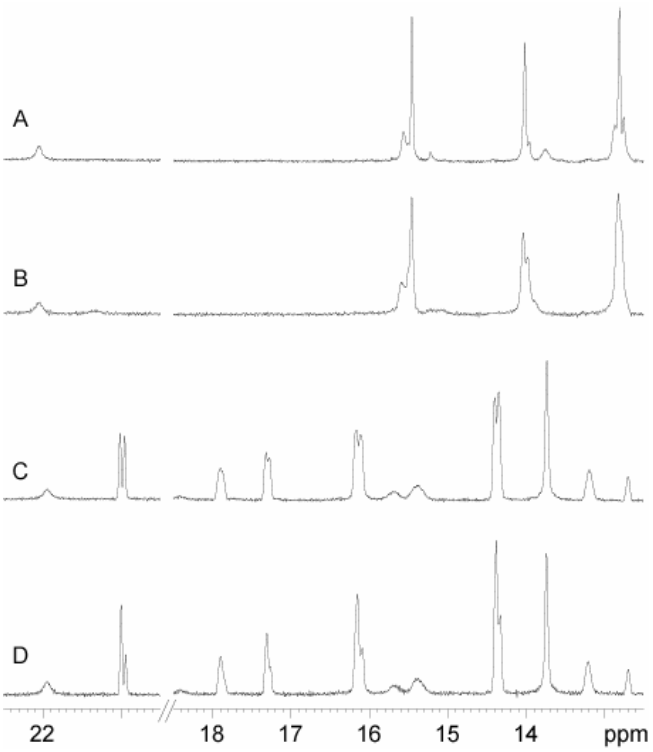

Figure 4.12 Downfield hyperfine-shifted portion of the ^{1}H NMR spectrum of H117A S6803 rHbCN in (A) 95:5 $^{1}H_2O$:$^{2}H_2O$, and (B) 1:1 $^{1}H_2O$:$^{2}H_2O$; and H117A S7002 rHb-CN (collected by David Vuletich) in (C) 1:1 $^{1}H_2O$:$^{2}H_2O$, and (D) in 7:3 $^{1}H_2O$:$^{2}H_2O$. Other conditions were 20 mM phosphate, pH 7.3, 25 °C and 10-fold excess of cyanide. Assignments for H117A S7002 rHb-R are as in (Vu et al. 2004a).

4.3.6 Kinetics of Cyanide Binding

Kinetics of cyanide binding to the H117A mutant appeared to differ from wild-type S6803 rHb-R and rHb-A. Figure 4.13 shows NMR spectra collected before cyanide addition, and 1.5 and 12 hours after cyanide addition at 10 fold excess. The intermediate spectrum clearly illustrated a mixture of the hemichrome and metcyano complex. After overnight incubation the metcyano complex was the only species present. In contrast, equilibrated metcyano spectra were obtained for wild-type rHb-R and rHb-A within one hour of cyanide addition under the same concentration conditions (not shown). Inspection of the H117A rHbCN spectra over time also indicated that the comparatively rapid binding of the minor heme orientational isomer.

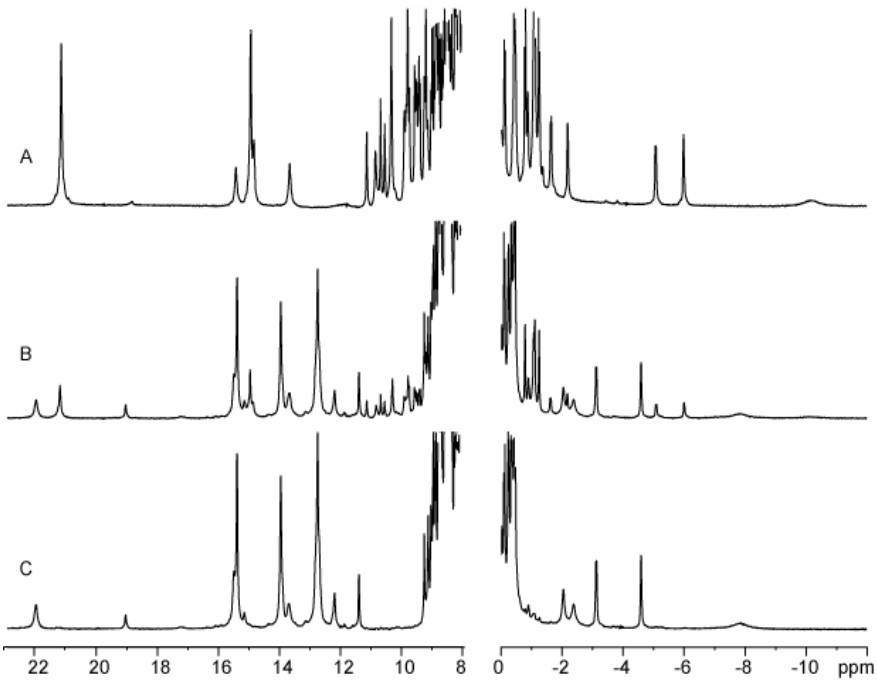

Figure 4.13 ^{1}H NMR spectra of H117A S6803 (A) Before cyanide addition, (B) 1.5 hours after addition, and (C) 12 hours after addition. Samples contained 20 mM phosphate buffer, pH 7.2 (95% $^{1}H_2O$; 5% $^{2}H_2O$) and spectra were collected at 25 °C

The kinetics of cyanide binding were examined quantitatively by Henry Nothnagel (Vu et al. 2004a). Data were collected at varying molar excesses of cyanide and monitored by optical spectroscopy. Unlike the NMR data, which report on the concentration of individual species if the signals are resolved, the absorbance reading has contributions from both heme isomers in both forms at all times. Multiple exponential decays were required to fit the data. Log plots at the three concentrations were used to determine an apparent second order rate constant of 3.0×10^{-2} $M^{-1}s^{-1}$ for the phase with the largest amplitude. Compared to wild-type rHb-R, cyanide binding to the H117A variant was slower by an apparent factor of 8. In kinetic studies on ferrous S6803 rHb (likely rHb-A), Hargrove and co-workers estimated the rate of His46 decoordination at 930 s^{-1} and a recoordination rate of 4200 s^{-1} (Hvitved et al. 2001). The apparent second order rate constant for cyanide binding given above assumed a simple bimolecular mechanism that did not include any such competing equilibria.

A recent study of the kinetics of cyanide association with pentacoordinate trHbs reported $k_{on} = 4.6 \times 10^2$ M^{-1} s^{-1} at pH 7.0 and 20 °C for *Ce* trHb (Milani et al. 2004a). Binding was found to be slower by decades in H117A S6803 rHb. Ikeda-Saito and coworkers have studied cyanide binding kinetics in mammalian metMb and identified the major factors controlling the association rate: acid dissociation constant of HCN in the heme pocket, steric hindrance and electrostatic interactions at the distal site, and strength of water coordination (Dou et al. 1996). For hxHbs such as S6803 rHb, the latter effect is replaced by the kinetic lability of the distal histidine; a large scale conformational change coupled to binding may also play a role. Cyanide binding as slow as reported here is rare

(Mintorovitch & Satterlee 1988); in the hexacoordinate neuroglobin (Du et al. 2003), it was attributed to the rupture of the Fe–His(E7) bond. This was not the case for H117A S6803 rHb since a first order dependence on cyanide concentration was observed at high cyanide concentrations. The rate constants for ligation and deligation of His46 were fast compared to the observed rate of cyanide binding. Assuming these rate constants were not affected to an extreme extent by the H117A replacement (and possibly the cross-link in the wild-type protein), they also supported a rate-limiting step different from decoordination.

The barrier to cyanide binding could arise from a cyanide-dependent heme pocket rearrangement leading to the final state, which contains displaced and rotated E and B helices. This rearrangement would be conditioned by the nature of the residue at position 117, perhaps through a repositioning of the heme group in its site. Alternative interpretations for the slower rate exhibited by H117A S6803 rHb call for a decrease in the efficiency of HCN dissociation caused by a modified electrostatic environment and possibly hindered access to the heme pocket. The structural and dynamic properties of the H117F and H117A variants (Chapter 3) and a recent study of cavities in *Mt* trHbN and *Ce* trHb identifying a Xe-binding site near the 2-vinyl group (site 2) (Milani et al. 2004b) supported to this interpretation. The observation that the minor heme orientational isomer, which had the 3-CH_3 in place of the 2-vinyl, reacted faster than the major isomer also suggested that the conformation near position 117 was critical. It is noteworthy that the replacement was on the proximal side, and that it resulted in ligand access to the distal side.

4.4 Conclusions

The large structural changes triggered by the binding of cyanide supported the stability of the H-bonding network reported for other trHbs. Solutions of the H117A S6803 rHbCN in mixtures of $^{1}H_2O$ and $^{2}H_2O$ established the predominance of one hydrogen bond to the cyanide ligand, likely with Tyr22 OηH as the donor because of the unusually slow exchange exhibited by this hydroxyl proton and its chemical shift strongly affected by the paramagnetic center. The distance between the H-bonded phenolic OH and the cyanide nitrogen in *Ce* trHbCN was calculated to be 4.4 Å based on the X-ray structure, shorter than obtained by T_1 measurements in H117A S6803 rHbCN. This may suggest that the tilt of the cyanide is not as pronounced in the latter protein. Evidence was found for a close interaction between Tyr22 and a glutamine amide, likely Gln43. Interactions were also observed to a second glutamine, Gln47. Overall, these interactions support a network similar to that observed in *Ce* trHbCN. During the preparation of this chapter, Hargrove and co-workers published the crystal structures of S6803 cyanide-bound and azide-bound forms of rHb-A (Trent et al. 2004). As expected for S6803 rHb, cyanide binding to rHb-A resulted in movement of the E helix, in particular His46, away from the heme iron. The B helix rotated inward toward the heme group positioning Tyr22 near the heme iron. Subsequently, Tyr22, Gln43 and Gln47 formed a hydrogen bonding network with the cyanide ligand similar to that observed for *Ce* trHbCN. Furthermore, the tilt of the cyanide ligand was diminished in comparison to the *C. eugametos* protein(Trent et al. 2004). This observation may be influenced by the nature of the histidine-heme linkage of rHb-A.

A recent study of NO-bound *Mt* trHbN, a protein that also contains Tyr B10 and Gln E11, established a role for Tyr B10 in positioning the exogenous ligand (Mukai et al. 2004) through H-bonding interactions. Interestingly, the NO binding appeared to have long-range structural effects extending to the loop leading into the F helix. A similar effect may be propagated to site 117 in the cyanobacterial trHb. However, these interpretations must be considered with caution since the network established by Tyr B10 in conjunction with Gln E7 can be perturbed, as illustrated by the minihemoglobin from *Cerebratulus lacteus* (containing Thr E11) and the Hb from *Ascaris suum* (containing Ile E11) (Pesce et al. 2004).

The kinetic data indicate the H16(His117) position in S6803 rHb-R is well suited to regulate ligand binding. Mutation of His117 to alanine and the changes in structure near the 2-vinyl group resulted in 8 fold slower cyanide binding. Interestingly, the region of His117 and the 2-vinyl group corresponds to the Xe2 cavity; a site observed in crystal structures of swMb, *Ce* trHb, and *Mt* trHbN (Milani et al. 2004b, Nienhaus et al. 2003, Tilton et al. 1984, Tilton et al. 1988) and shown to shown to facilitate ligand diffusion (Bourgeois et al. 2003, Schotte et al. 2003). The covalent attachment observed in rHb-A may further attenuate ligand binding by altering the properties of the Xe2 site. Kinetic data on S6803 rHb-A are needed to completely for comparison to wild type and H117A S6803 rHb-R.

Other influences of ligand binding at the Hb distal site include the orientation of the axial histidines with respect to the heme plane and HisF8-iron bond length (Hoy et al. 2004, Perutz et al. 1998, Samuni et al. 2003). The former case will be evaluated with respect to the heme electronic structure in the following chapter.

Chapter 5

Electronic Structure of the Heme: Effect of Axial Ligand Orientation

Material in this chapter has been presented in the following publications:

"The solution structure of the recombinant hemoglobin from the cyanobacterium *Synechocystis* sp. PCC 6803 in its hemichrome state." Falzone, C.J., Vu, B.C., Scott, N.L., and Lecomte J.T.J. (2002) *J. Mol. Biol.* **324**, 1015-1029.

"Characterization of the heme-histidine cross-link in cyanobacterial hemoglobins from *Synechocystis* sp. PCC 6803 and *Synechococcus* sp. PCC 7002." Vu, B. C., Vuletich, D.A., Kuriakose, S.A., Falzone, C.J., and Lecomte, J.T.J. (2004) *J. Biol. Inorg. Chem.* **9**, 183-194.

"Cyanide binding to hexacoordinate cyanobacterial hemoglobins: Hydrogen bonding network and heme pocket rearrangement in ferric H117A *Synechocystis* Hb." Vu, B.C., Nothnagel, H.J., Vuletich, D.A., Falzone, C.J., Lecomte, J.T.J. *Biochemistry*, *in press*.

5.1 Introduction

For bis-histidyl Hbs, the observation that the distal histidine is displaced (Arrendondo-Peter et al. 1997, Burmester et al. 2002, Hargrove 2000, Pesce et al. 2002, Sawai et al. 2003, Trent et al. 2001a, Trent et al. 2001b, this work) suggests that the strength of each iron-histidine ligation bond varies. In pentacoordinate Hbs, ligation to the distal site is influenced by the orientation of the proximal histidine with respect to the heme plane. In the absence of a distal ligand, the heme iron is observed out of the heme plane in a tensed (T) or puckered state (Perutz 1970, Perutz et al. 1998). The out of plane distortion results from the high energetic penalty to maintain the heme iron within the

heme plane (Warshel 1977). The out-of-plane distortion results in tilting of the proximal histidine imidazole ring with respect to the heme normal (Figure 5.1). Upon ligand binding, this energy penalty is relieved and the resting (R) state is observed with the iron in the heme plane. The energetic barrier between the T and R states is dependent upon the ability to form the ligand binding transition state. In multimeric Hbs, the iron-histidine bond regulates the cooperativity of ligand binding (Barrick et al. 1997, Perutz et al. 1998) and is influenced by the histidine tilt. Large tilts decrease the ligation bond strength and increase ligand affinity at the distal site by decreasing the tension of the T state (Das et al. 2000, Neya & Morishima 1981, Perutz et al. 1998). Hargrove and co-workers suggest that longer bond lengths influence decoordination at the distal site in Hbs (Hoy et al. 2004).

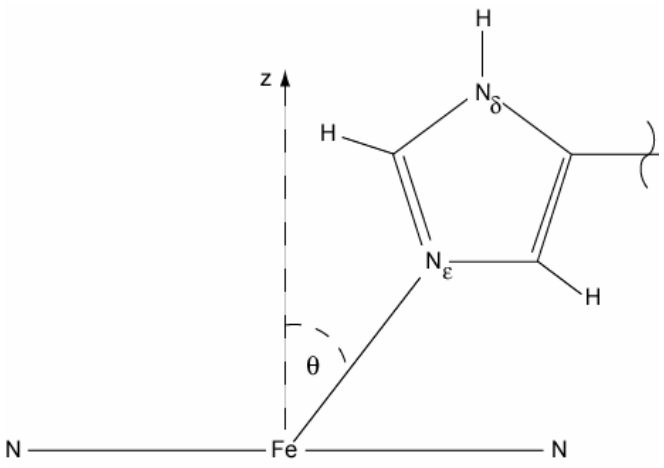

Figure 5.1 Description of the axial ligand tilt. The view of the heme group (on edge) has been simplified to two of the pyrrole nitrogens and the heme iron. The vector normal to the heme iron is shown as the z-axis. An axial histidine residue is shown coordinated to the heme iron. The tilt angle is defined by the z-axis and the iron-histidne coordination bond.

The orientation of the proximal histidine can be determined by either x-ray crystallography or a combination of NMR and EPR methods. In NMR of hemoproteins, precise structural information on ligating residues is complicated by two main factors: the small number of porphyrin protons resulting in few heme-ligand NOEs as well as strong relaxation effects in the ferric state (La Mar et al. 1999). The linear dependence of the chemical shift with inverse temperature supports that ferric *Synechocystis* sp. PCC 6803 rHb-R near room temperature has low-spin characteristics (Scott & Lecomte 2000). Under those conditions, it is possible to interpret the heme chemical shifts in terms of its electronic structure and protein structural properties. In general, the observed chemical shift (δ_{obs}) can be written as the sum of a diamagnetic (δ_{dia}) and a paramagnetic contribution. The paramagnetic contribution has two components, contact, δ_{con}, and pseudocontact or dipolar, δ_{dip}, as expressed in Equation 1:

$$\delta_{obs} = \delta_{dia} + \delta_{con} + \delta_{dip} \qquad (1)$$

Several (semi-)quantitative approaches are used to interpret the paramagnetic contribution; these call for the ^{13}C shifts at the heme α positions, and the ^{1}H shifts at the heme methyl, heme meso, axial histidine β and axial histidine Cδ and Cε positions.

Using data from a number of hemoproteins, Bertini and co-workers proposed equations relating heme methyl chemical shift to axial ligand orientation (Bertini et al. 1999). In the case of the heme methyl ^{13}C shift, the contact term in Equation 1 is dominant (La Mar et al. 1999, Shokhirev & Walker 1998b) and can be estimated by subtracting the diamagnetic term (obtained either from an isostructural diamagnetic complex or reference compound) and ignoring the relatively small dipolar term. The contact contribution is proportional to the π electron density, ρ_{π}, at the nucleus of interest.

In a low-spin ferric heme derivative with 4-fold symmetry the unpaired spin occupies degenerate d_{xz} and d_{yz} orbitals, giving rise to equal delocalization over the four pyrrole rings and identical shifts at the α positions. Orbital degeneracy is lifted by asymmetrical axial ligands, unequal porphyrin substituents, and the anisotropic protein environment. Distinct contact shifts then result from the perturbed electronic distribution (Shulman et al. 1971). The orbital ground state is determined principally by the orientation of the axial histidine imidazole planes relative to the heme group and to each other. If the orientation of the major magnetic axis is perpendicular to the heme group, this rhombic distortion of the D_{4h} symmetry predicts inversion symmetry through the iron (Hu et al. 2001).

Simple empirical calculations have been applied by Turner and co-workers to determine the orientation of the mean axial imidazole plane using the ^{13}C contact shift (Turner 2000). The procedure evaluates ρ_π with a rhombic perturbation of the D_{4h} symmetry and uses an orbital mixing parameter, an energy gap for the linear combination of orbitals, and unperturbed orbital coefficients derived from Hückel theory (Louro et al. 1998, Turner 1995). The method has met with success in certain cases of bis-histidyl coordination but it requires assumptions, for example that the major magnetic axis be perpendicular to the heme plane, that the two axial imidazoles exert equal influence in determining the in-plane magnetic axes, and that other influences are negligible. These studies do not include information from hxHbs for which the assumptions may not be valid.

Methyl ^1H chemical shift data are available for wild-type S6803 rHb-R, rHb-A, rHb-DPIX and H117A S6803 rHbCN proteins and are used to calculate the orientation of

the axial ligands. This chapter explores the relationship between methyl shift and calculated axial ligand orientation and compares the results to the available structure of rHb-A and rHb-R. In addition, the ^{13}C contact shifts of wild type S6803 rHb-R and rHb-A are qualitatively examined with respect to understanding the tilt of the axial ligands.

5.2 Materials and Methods

5.2.1 Calculation of Axial Ligand Orientation Using Heme Methyl ^{1}H Chemical Shifts

Heme methyl chemical shifts for wild-type rHb-R and rHb-A, wild-type rHb-DPIX, and H117A rHbCN were used to determine the orientation of the axial histidine plane(s) with respect to the porphyrin macrocycle. The shifts were corrected for diamagnetic contribution (3.3 ppm). A value of 2.4 ppm was added for groups immediately adjacent to vinyl groups (Bertini et al. 1999). Data for rHb-DPIX were only corrected for diamagnetic contributions. In addition to diamagnetic contributions the vinyl adjustment was only applied to the 3-methyl group for rHb-A. The adjusted chemical shift values were used to fit heuristic equations established by Bertini and co-workers (1999). For the bis-histidyl case, the following heuristic equation was applied:

$$\delta_{ppm} = \cos\beta\,[a\sin^2(\theta-\varphi) + b\cos^2(\theta+\varphi) + c] + d\sin\beta \qquad (2)$$

where β is the acute angle between the histidine imidazole plane, θ represents the angle defined by the Fe-NC vector and the Fe-CH_3 vector, and φ the angle defined by the Fe-NC vector and the bisector of β (Figure 5.1). The constants *a*, *b* and *c* were limited to values reported in (Bertini et al. 1999), *i.e.,* $a = 38.8 \pm 1.4$, $b = -10.5 \pm 1.0$, $c = -1.1 \pm 1.9$, $d = 9.4 \pm 0.6$.

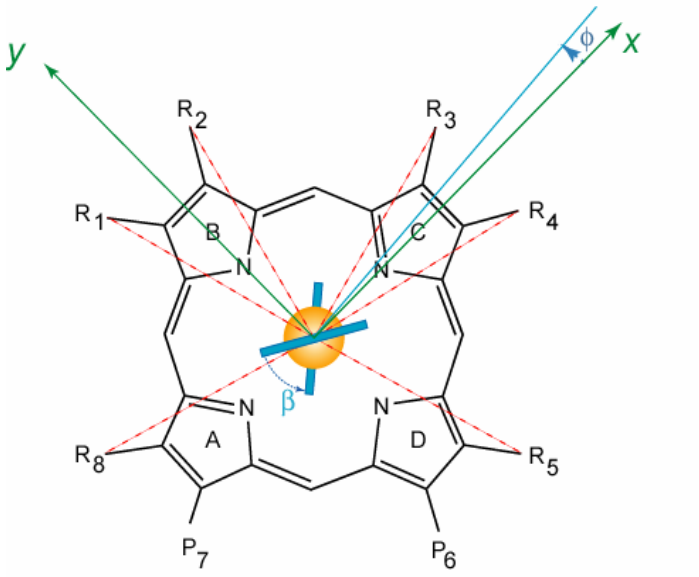

Figure 5.2 Definition of heme macrocycle geometry used in methyl chemical shift calculations. P_6 and P_7 represent the propionate groups of the porphyrin molecules used in this chapter. In Fe-protoporphyrin IX R_1, R_3, R_5 and R_8 are methyl groups, and R_2 and R_4 are vinyls. In 2,4-dimethyldeuteroheme, all R positions are occupied by methyl groups. The *X* axis goes through the nitrogen atoms of pyrroles A and C, and the *Y* axis intersects the nitrogen atoms of pyrroles B and D. Each methyl is at a specific angular displacement (counter-clockwise) θ from the *X* axis. The planes of the axial imidazoles are shown as blue bars. The angle between the two planes is β and the bisector of this angle forms an angle φ with the *X* axis.

In the bis-cyano complex, the equation used was:

$$\delta_{ppm} = a \sin^2(\theta - \varphi) + b \cos^2(\theta + \varphi) + c \qquad (3)$$

In this case, φ is the angle defined by the Fe-NC vector and the projection of the axial histidine plane onto the heme. The constants *a*, *b* and *c* were limited to, $a = 18.4 \pm 2.4$, $b = -0.8 \pm 2.0$, $c = 6.1 \pm 1.9$.

5.2.2. Contact Shift of ^{13}C Nuclei

The contact shift of the ^{13}C nuclei at the α position of the porphyrin ring was calculated from the observed values by subtracting 12.1 ppm (CH_3), 22.8 ppm (α-propionates) and 132.9 + 4.2 $\delta_{(\beta\text{-vinyl})}$ (α-vinyl) (Pierattelli et al. 1996). The modified 2-vinyl group was ignored in rHb-A.

5.3 Results

5.3.1 Heme Methyl ^{1}H Chemical Shifts

^{1}H chemical shift data the heme methyl groups of S6803 wild-type rHb-R, rHb-A, H117A rHb-R, and H117A HbCN were reported in Chapters 3 and 4. They are listed in Table 5.1 for comparison.

Table 5.1 Heme methyl ^{1}H chemical shifts for S6803 proteins, collected in 20 mM phosphate, pH 7.2 at 298 K.

	θ (deg)	rHb-R δ (ppm)	rHb-A δ (ppm)	H117A rHbCN δ (ppm)	rHb-DPIX δ (ppm)
1-CH_3	106.3	15.03	10.60	12.60	19.2
2-CH_3	73.2	-	-	-	23.9
3-CH_3	16.8	9.99	13.14	15.06	9.8
4-CH_3	343.2	-	-	-	6.9
5-CH_3	286.7	21.28	17.84	13.76	21.4
8-CH_3	163.5	10.33	12.66	8.28	8.4

5.3.1.1 Evaluation of Axial Ligand Orientation Using Methyl Chemical Shifts for S6803 rHb-R and rHb-DPIX

Bertini and co-workers have proposed empirical Karplus-like equations relating heme methyl ^{1}H chemical shifts to axial ligand orientation (1999). The methyl ^{1}H shifts of S6803 rHb-R were used to determine the orientation of the axial ligands as predicted by Equation 2. Fitting of the data (Figure 5.3) resulted in β and φ values of 70° and −23° respectively. Incorporation of heme in rHb only yields four methyl shifts for use in Equation 2. Fe(III) 2,4-dimethyldeuteroporphyrin IX (2,4-DPIX) is a symmetrical heme substitute with methyl groups in place of the 2- and 4- vinyl positions. This compound provides two additional values in determining axial ligand orientation. 2,4-DPIX was incorporated into rHb-R to increase the number of useful shifts. Substitution of methyl

groups for the vinyl group is not expected to alter the overall structure of the protein. The resulting complex, rHb-DPIX, was examined by ^{1}H NMR spectroscopy and the methyl group assignments listed in Table 5.1 The data resulted in $\beta = 68°$ and $\varphi = -16°$, similar to that of rHb-R . Examination of 20 low-energy structures of rHb-R determined by NMR spectroscopy provides two values for β and φ: $\beta = 80°$ and $\varphi = 20°$ and $\beta = 20°$ and $\varphi = -20°$ (Falzone et al. 2002). In the first case, β is close to the predicted value, while φ is comparable. The value of β in Equation 2, relies on a number of assumptions derived from bis-histidine complexes such as cytochromes. In these systems the axial ligand tilt is minimal and contributions of each ligand to the electronic structure are treated equally (Bertini et al. 1999, Shokhirev & Walker 1998b). Among Hbs, the tilt of the proximal ligand varies and modulates the energetic barrier resulting from out of plane movements of the heme iron (Das et al. 2000, Neya & Morishima 1981, Perutz et al. 1998).

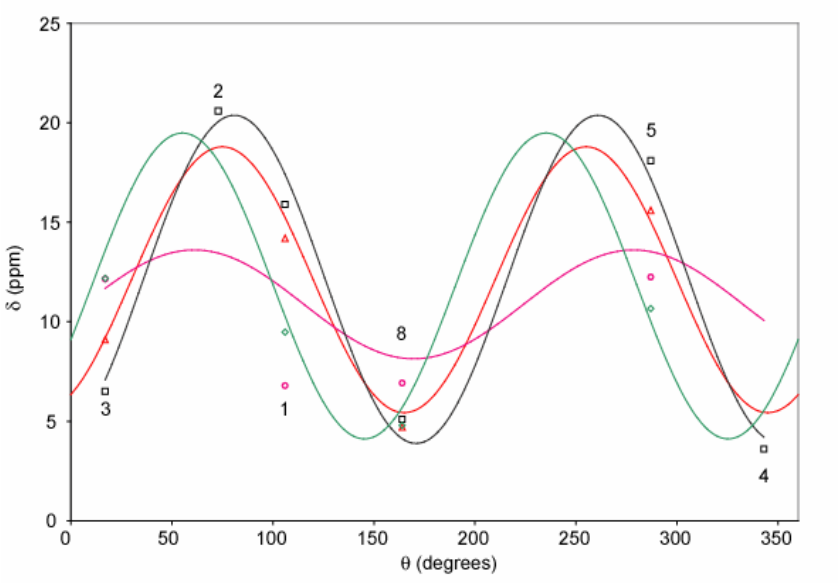

Figure 5.3 Fit of porphyrin methyl chemical shifts. The chemical shifts (open symbols) are plotted versus θ, the angular displacement of the methyl group from the Fe-NC axis. Equation 2 was used to fit the chemical shifts from S6803 Hbs rHb-R (orange), rHb-A (pink), rHb-DPIX (black) and Equation 3 for S6803 H117A HbCN (green). The solid lines represent the fitted curves. The methyl positions are shown above or below the data points.

5.3.1.2 Evaluation of Axial Ligand Orientation Using Methyl Chemical Shifts for S6803 rHb-A

S6803 rHb-A methyl chemical shifts were also studied using Equation 2 and yielded $\beta = 78°$ and $\varphi = -40°$. The crystal structure of rHb-A shows that the orientation of the proximal and distal ligands is similar to that calculated for rHb-A. Again, a disparity in the values of β and φ are observed between the crystal structure ($\beta \sim 65°$ and $\varphi \sim -20°$) and the value calculated from the methyl chemical shift. Covalent attachment

in rHb-A exerts a significant effect on the methyl ^{1}H chemical shift and reflect changes in the relationship between the ^{1}H chemical shift and the axial ligand orientation.

5.3.1.3 Evaluation of Axial Ligand Orientation Using Methyl Chemical Shifts for H117A S6803 rHbCN

The NMR data on H117A S6803 rHbCN, though partial, was useful in the characterizing the orientation of the proximal ligand. Application of Equation 3, which is calibrated for His/CN^{-} complexes (Bertini et al. 1999), returned a value of ~ –35° for φ, aligning the projection of the axial imidazole ring on the heme plane close to the δ-β meso axis (lying at –45°, Figure 3). This axial histidine orientation is consistent with that of His70 in the wild-type protein (Falzone et al. 2002, Vu et al. 2004b) and of the proximal histidine in other trHbs (Milani et al. 2001, Milani et al. 2003b). This orientation is also comparable to that in certain heme oxygenases (Friedman et al. 2003) and presumed to strengthen the Fe(II)-His bond by relieving steric strain with the pyrrole nitrogens (Samuni et al. 2004).

5.3.2 Evaluation of Contact Shifts

5.3.2.1 Evaluation of the ^{1}H Contact Shift in S6803 rHb-R and rHb-A

Although the heme methyl ^{1}H chemical shifts are strongly influenced by the orientation of the axial ligand, the contact shift remains a large contribution to the overall chemical shift. The meso ^{1}H chemical shift is dominated by the contact shift. The contact shift reflects contributions from the paramagnetic susceptibility tensor (La Mar et al. 1999). Upon forming the His117-heme linkage, the spread of the methyl ^{1}H chemical

shifts decreases and that of the meso shifts increases (Figure 5.4). This trend can be explained by a readjustment of the in-plane magnetic axes (Shokhirev & Walker 1998b). However, the average of the meso shifts remains near 0 ppm, a value lower than usual (2–5 ppm) and seen in cases, such as *Glycera* metHbCN (Alam & Satterlee 1994), where the cyanide ligand is unusually tilted from the heme normal (Park et al. 2002). The difference in shift between the α and γ meso protons and the β and δ meso protons (Δmeso) is related to the orientation of the magnetic axes in the heme plane (Lee et al. 1993, Shokhirev & Walker 1998b). The near zero value in all four cases indicates an orientation near the NA-Fe-NC axis. Counter rotation, which relates the in-plane χ_{xx} magnetic axis (−φ, Figure 5.2) to the molecular geometry (Shokhirev & Walker 1998a), places the axial imidazole bisector at a similar location. The meso order (α > δ > β > γ) is contrary to predictions (α ~ γ and β ~ δ) and supports unequal contact contributions due to a tilt of the z axis (Lee et al. 1993). The variation in shifts between rHb-R and rHb-A suggests that cross-linking affects this tilt.

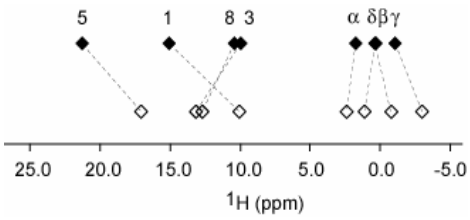

Figure 5.4 Representation of the heme methyl and meso ^{1}H shifts in S6803 rHb-R (filled symbols) and rHb-A (open symbols). The ^{1}H shifts are listed in table 5.1.

A possible role for the His117-heme cross-link is the modulation of axial ligation strength via constraints imposed on heme placement. NMR observables do not report

directly on the planarity of the porphyrin ring, the Nε–Fe bond length and the Nε–Fe–Nε bond angle. The rHb-R NMR model was therefore generated with set geometries for the heme and its axial ligands (Falzone et al. 2002). Thus, on the basis of this model and forthcoming NMR models of rHb-A, it is not possible to assess subtle changes in axial bonding. Insight into the effect of the cross-link can be gained instead from inspecting the NMR spectral properties of the heme group and axial histidines.

5.3.2.2 Evaluation of ^{13}C Contact Shift in S6803 rHb-R and rHb-A

The near zero value of the meso ^{1}H shift in rHb-R and rHb-A indicates an orientation near the NA-Fe-NC axis, as inferred from the methyl ^{13}C shifts. Figure 5.6 maps the contact contribution according to its magnitude and the location of the nucleus in the heme skeleton. Although inversion symmetry was not strictly observed by all pairs of positions, the trend is recognizable. The 4-α-CH/8-CH_3 contact shift ratio was closest to 1 (between 1.01 and 1.05) whereas the 5-CH_3/1-CH_3 ratio is between 1.2 and 1.3 in rHb-R and larger (~1.5) in rHb-A. In rHb-R, the electronic density was larger on pyrroles B and D than A and C; consistent with conclusions based on heme methyl proton shifts (Bertini et al. 1999, Falzone et al. 2002). The density difference was apparently attenuated in rHb-A. The substituents at positions 3, 4, 7, and 8, which exhibited the smallest shifts, were minimally affected by the nature of the protein and the presence of the cross-link. Overall, the constancy of the contact patterns suggested a relatively unchanged orbital hole (*i.e.*, $(d_{xz},d_{yz})^1$), and the orientation of the bisector of the two imidazole planes (or the determinant imidazole) is predicted to be lying near the NA-Fe-NC axis. In addition, the small spread of the shifts about the average value indicated

that, if the two histidines contribute equally, the angle between the planes (β, Figure 5.2) is large and the energy gap between the two orbitals is small (Turner 2000).

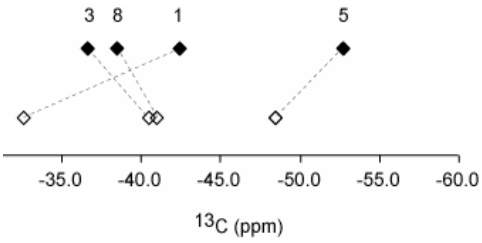

Figure 5.5 Representation of the heme methyl ^{13}C shifts in S6803 rHb-R (filled symbols) and rHb-A (open symbols). The ^{13}C shifts are listed in Table 3.1.

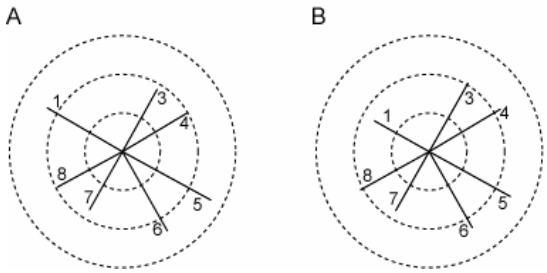

Figure 5.6 Representation of the ^{13}C contact shift in (A) rHb-R and (B) rHb-A. The solid lines represent the magnitude of the contact shift listed in table 3.1 after diamagnetic correction. The orientation of each line illustrates the vector the α heme substituent with respect to the iron (center). The scale (dotted lines) shown is 20 ppm (inner circle), 40 ppm (middle circle), and 60 ppm (outer circle). Inversion symmetry about the heme iron is approximately observed.

5.3.3 Axial Histidine Equivalence

Additional assessment of axial histidine equivalence can be obtained from the hyperfine shift experienced by the β protons (La Mar et al. 1999). The values listed in Table 5.2 are similar in both the rHb-R and rHb-A forms. The averages appeared in a

narrow range (9 – 11 ppm), with smaller values for rHb-R than rHb-A, and within each protein, smaller values for His70 than His46. The variations may point to subtle differences in bond strength but do not suggest major strain. Another indicator of the electronic structure is provided by the CδH and CεH of the axial histidines (Emerson & La Mar 1990). These nuclei experienced dipolar and contact shifts, and variations in the values originate mostly from the dipolar contribution, which is affected by the tilt of the magnetic z-axis with respect to the heme plane. Assignments were not obtained for the four protons because of overlap in the ^{1}H data. However, even a conservative interpretation of the shifts reported in Table 5.1 reveals that these values change markedly upon formation of the cross-link.

Table 5.2 ^{1}H chemical shifts for axial histidines in S6803 rHb[a]

		rHb-R	rHb-A
His46			
	NH	10.71	11.15
	Cα	77.7	80.6
	CαH	7.70	9.41
	Cβ	24.3	24.5
	CβH	10.82	11.65
	CβH	9.20	9.28
	NδH	13.2	14.13
His70			
	NH	9.90	9.75
	Cα	69.1	71.9
	CαH	6.75	6.53
	Cβ	23.8	22.2
	CβH	8.92	10.26
	CβH	9.62	10.02
	NδH	15.0	15.9
	m	11.7[b]	17.2
	n	5.4[b]	9.1
	o	–1.7[b]	–5.6
	z	–10.8 [b,c]	–11.3

[a] in H_2O, pH 7.2-7.5, 298 K. [b] As reported in Lecomte et al. (2001) at 308K. [c] Assigned as His46 CεH (Scott & Lecomte 2000).

5.4 Conclusion

Heme methyl ^{1}H chemical shift analysis using the method by Bertini and co-workers (1999) returned values for β and φ which differed slightly from values determined from the structures of S6803 rHb-R and rHb-A. The differences in β values suggest the axial histidines are tilted from the heme normal. In the case of rHb-A, the differences may also reflect perturbations to heme electronic structure resulting from covalent modification. The rHb-A data were fitted to the equation corresponding to a bis-histidyl axial ligation scheme. Data analysis allows for a correction of the contribution of adjacent vinyl groups on methyl chemical shifts. However, among the proteins used to determine Equation 2, modification of a single vinyl group is not observed and thus unaccounted for in the derivation (Bertini et al. 1999). Despite this consideration, the calculations provided insight into the orientation of the axial ligands. In the case of His70, the calculated imidazole orientation is comparable to other trHbs as well as that found in some heme peroxidases (Friedman et al. 2003). The orientation of the proximal ligand likely strengthens the iron-histidine bond by minimizing steric interaction with the heme pyrrole nitrogens.

Examination of the meso shifts reveal non-equivalence of the α/γ and β/δ pairs. This suggested tilting of the axial ligands and was confirmed by ^{13}C contact shift data. The contact shift data also indicate the heme electronic structure in rHb-A is moderately altered versus rHb-R. In both cases, data indicate minor differences between the binding strength of the axial histidines. Comparison of the axial ligand bond strength among a number of pentacoordinate Hbs, bis-histidyl cytochromes and S6803 rHb-A suggests the bond is modulated by axial ligand tilt and bond length (Hoy et al. 2004). Modulation of

axial bond strength in hxHbs may represent a mechanism to modulate function in globin fold. Additional NMR and crystal data on hxHbs are needed to assess a functional relationship between heme electronic structure and ligand binding.

Chapter 6

Characterization of Zn-Porphyrin Reconstituted S6803 rHb

5.1 Introduction

Structural studies on hemoproteins have often used Zn (II) protoporphyrin IX (ZnPPIX) a substitute to study protein motions and ligand diffusion (Fujii et al. 1993, Furukawa et al. 2000, Leonard et al. 1974, McNaughton et al. 2003, Papp et al. 1990, Sudhakar et al. 1994). ZnPPIX is well suited for fluorescence and phosphorescence spectroscopy owing to the high quantum yield and long lifetime in the triplet state. When ZnPPIX is incorporated into Hbs, it serves as a deoxy mimic in ligand diffusion studies. Studies on hybrid Zn substituted human Hb show the zinc metal adopts the same out of plane distortion as observed for heme in the T state. ZnPPIX reconstituted Hbs have also been used in NMR experiments as low spin mimics of the deoxy state (Anni et al. 1995, Dalvit et al. 1986, Qian et al. 2003). In the pentacoordinate state, the heme Fe(II) center has a spin state of S = 2. NMR studies of high-spin Fe(II) are complicated by strong Curie relaxation effects which yield poorer spectra at high field (La Mar et al. 1999). The closed shell metal center of ZnPPIX provides a heme mimic to study pentacoordinate hemoproteins by NMR spectroscopy.

Formation of rHb-A in the presence of sodium dithionite raised the question of the role of the heme iron in protein reactivity. To probe the involvement of the iron center, ZnPPIX was used to reconstitute the protein in place of heme. The resulting protein, rHb-ZnPPIX, was inert to cross-link forming chemistry (Chapter 3). Beyond addressing reactivity issues, the Zn-substituted protein is expected to yield unique

insights into the geometry and bonding properties of the Hb. Specifically, the zinc may be pentacoordinate, in which case, the protein would allow an opportunity to study a mimic of the deoxy form of S6803 rHb, presumably with His46 in the dissociated state. However, limited evidence also exists to support that Zn may form hexacoordinate complexes (Anni et al. 1995). In this case, the protein may provide a diamagnetic species that could be used for further structural characterization and to obtain shift information. This chapter describes the preliminary characterization of ZnPPIX-reconstituted S6803 rHb (rHb-ZnPPIX) by NMR spectroscopy, the determination of the coordination state of the zinc ion, and an examination of the strength of the axial histidine bonds.

6.2 Materials and Methods

6.2.1 Protein Preparation and Purification

S6803 rHb was reconstituted with ZnPPIX as described in Chapter 2. When uniformly labeled ^{15}N protein was required, the apoprotein was expressed in media containing $^{15}NHCl_4$ using established methods (Lecomte et al. 2001). Holoprotein concentrations were estimated based on the apoprotein before reconstitution. Characterization was carried out by NMR methods. Where necessary, the protein was lyophilized and dissolved in the phosphate buffer (^1H_2O or ^2H_2O, pH 7.2) for NMR spectroscopy.

6.2.2 NMR Spectroscopy

1D proton data were collected with a 1.2-s presaturation of the water signal (256 to 1024 transients, 8192 points over 10 kHz). Variable temperature spectra were collected between 278 and 313 K. Spectra were also recorded at 298 K after adjusting

the pH of the sample to 6.46. The raw data were zero-filled to twice the number of points and the FID was filtered with squared-sine bell window functions shifted by 90°.

Homonuclear NOESY (Kumar et al. 1980), DQF-COSY (Rance et al. 1983) and TOCSY (Cavanagh & Rance 1992) spectra were collected with spectral widths of 10 kHz in both dimensions. The number of points in the indirect dimension was either 512 real (TPPI) or 256 complex (States-TPPI). Mixing times for NOESY and TOCSY data were 100 ms and 45 ms, respectively. TOCSY data were collected using a relaxation compensated DIPSI-2 locking sequence with a 25 μs $\pi/2$ pulse (Cavanagh & Rance 1992). Suppression of the water signal was achieved by presaturation of the water line or a WATERGATE scheme (Piotto et al. 1992). Quadrature detection was achieved either by the TPPI (Marion & Wüthrich 1983) or States method (States et al. 1982). Homonuclear data were zero-filled in the indirect dimension. A squared-cosine bell window was applied in both dimensions.

6.3 Results

6.3.1 Assignment of ZnPPIX ^{1}H Signals

The ^{1}H spectrum of rHb-ZnPPIX is shown in Figure 6.1; it indicates that the protein is well folded upon incorporation of the zinc-substituted porphyrin. ZnPPIX ^{1}H assignments for ZnPPIX were obtained using methods described in (La Mar et al. 1999). NOE connectivities between the meso protons and methyl groups, Figure 6.2, served as starting points. Assignments for the majority of the ZnPPIX protons are listed in Table 6.1.

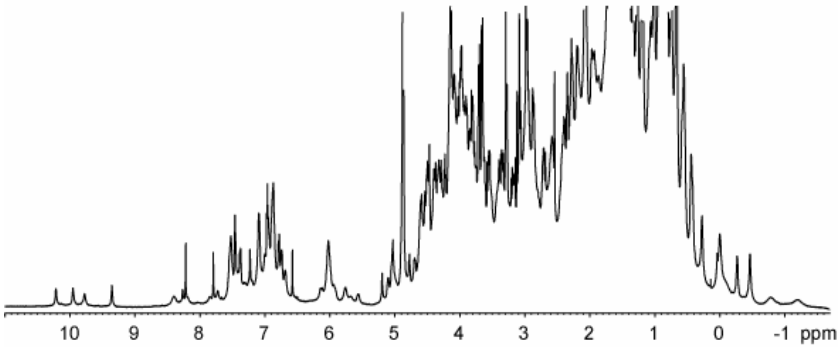

Figure 6.1 ^{1}H spectrum of rHb-ZnPPIX in 20 mM phosphate (100% $^{2}H_2O$) buffer, pH 7.2, 298 K. Assignments for the ZnPPIX substituents are in Table 6.1.

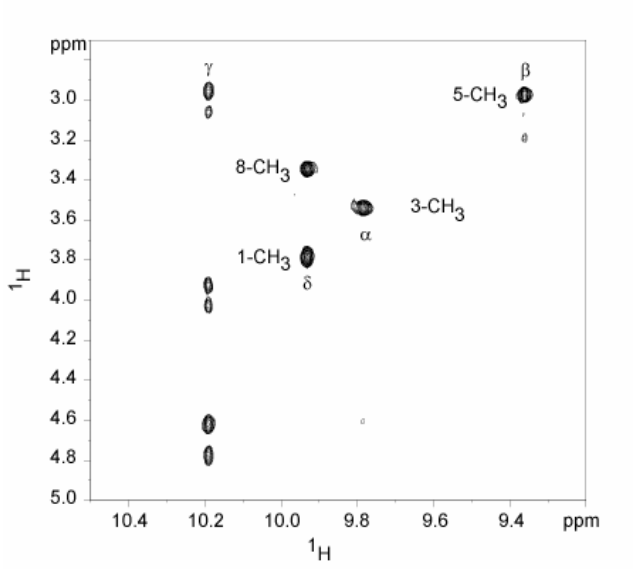

Figure 6.2 A portion of the ^{1}H-^{1}H NOESY data of rHb-ZnPPIX showing distinct effects involving the meso and methyl protons. Methyl groups were used to identify vinyl groups though NOE connectivities. The 1-CH_3 was distinguished from the 8-CH_3 by NOE connectivities to the adjacent 2-vinyl group.

Table 6.1 Assignment for the porphyrin substituents in S6803 rHb-ZnPPIX

	^{1}H (ppm)
1-CH_3	3.75
2-α-vinyl	8.35
2-β-vinyl-cis	6.00
2-β-vinyl-trans	6.12
3-CH_3	3.53
4-α-vinyl	7.52
4-β-vinyl-cis	5.54
4-β-vinyl-trans	5.93
5-CH_3	2.99
8-CH_3	3.34
α- meso	9.81
β-meso	9.38
γ-meso	10.16
δ-meso	9.93

Heme-protein contacts were identified using the structure of S6803 rHb-R as a reference. NOEs were found between Val87 and the 2-vinyl, Val121 and the α-meso proton and 3-CH_3, Phe34 and His83 as well as His33, Phe34 and Phe35, Phe34 and the 4-α vinyl, and Phe35 and the β-meso proton. Interestingly, a strong NOE between Val87(G8) and Phe35(CD1) but not Val87 and the β-meso proton was observed. The hemichrome structure showed these residues were farther than 6 Å apart. The *Ce*

trHbCN structure reveals that Phe33(CD1) and Tyr32 are in an orientation different from that observed in the S6803 hemichrome. The position of Phe33(CD1) in this structure is expected to lead to observable NOEs to the β-meso proton as well as Val83(G8). The NOE in S6803 rHb-ZnPPIX suggested Phe35(CD1) adopted a position similar to that observed in *Ce* trHb (as opposed to the hemichrome), but further structural data are needed to confirm this observation.

6.3.2 Identification of Axial Zinc Ligand(s)

To determine the coordination state of the zinc ion, NMR spectra were collected on uniformly ^{15}N-labeled protein Figure 6.3 shows a ^{1}H-^{15}N HMQC with parameters optimized for detection of long range coupling in histidine rings. Six histidines, labeled A to F, were observed, five in the NεH tautomer and only one in the NδH tautomer. The latter histidine had a shifted CεH expected for an axial histidine under the ring current influence of the porphyrin macrocycle. Additionally, a NδH proton was observed downfield from the other histidine signals; the characteristics of this NδH were consistent with those of a residue coordinated to the porphyrin metal (Lukin et al. 2000). The absence of a second shifted histidine residue in the NδH tautomeric state, in conjunction with five histidines appearing at normal chemical shifts, suggested that S6803 rHb-ZnPPIX was a pentacoordinate species with His46 oriented away from the porphyrin macrocycle. His A and B have been assigned to 83 and 33 respectively. His D and E were similar to His77 and 117 in the hemichrome. By default, His C was likely His46. Triple resonance data will be used to confirm the identity of His C through E.

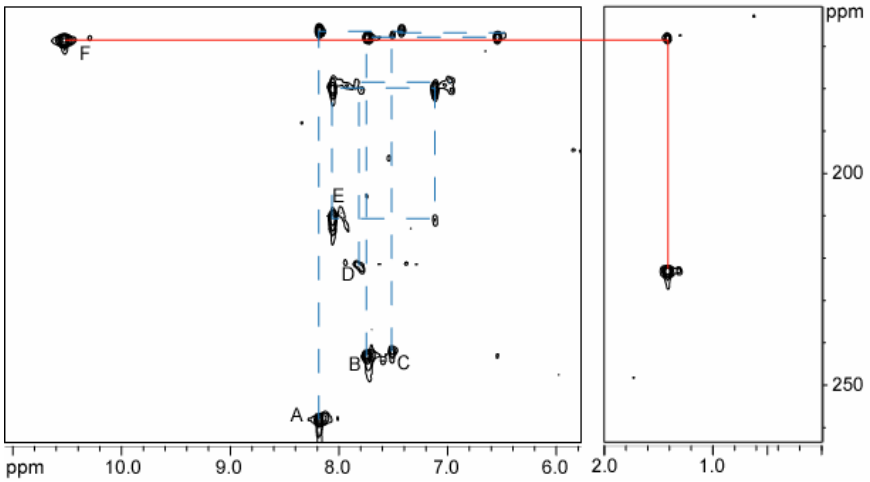

Figure 6.3 ^{1}H-^{15}N HMQC collected at 298 K (20 mM phosphate, pH 7.2, 95% $^{1}H_2O$: 5% $^{2}H_2O$). A total of 6 histidine residues were expected for S6803 rHb-ZnPPIX. His A-E appeared at shifts typical for unliganded histidines. His F displayed shifted CεH proton expected for a histidine residue under the influence of porphyrin macrocycle ring current (Lukin et al. 2000).

6.3.3 Probing the Structure of the Distal Pocket

Data on H117A S6803 rHbCN suggested that in the absence of distal coordination by His46, that the structure adopted a hydrogen bond network similar to that in *Ce* trHb (Chapter 4). If this was the case, Tyr22(B10), Gln43(E7) and Gln47(E11) were expected to be rotated inwards and facing the zinc atom. The ring current effect from the porphyrin should shift their resonances upfield. Figure 6.4 illustrates the ^{1}H-^{15}N HSQC collected on S6803 rHb-ZnPPIX. Examination of the proton dimension upfield of the water line did not reveal any shifted side chain NH_2 groups. The inset of Figure 6.4 clearly indicates all that 7 NH_2 groups expected for S6803 rHb-ZnPPIX were observed in the usual proton chemical shift region. Inspection of TOCSY data (not shown) did not

reveal any abnormally shifted tyrosine residues. At current, the data do not support a distal pocket arrangement as in *Ce* trHb or H117A S6803 rHbCN. One possible explanation is that the presence of the cyanide ligand at the distal site is required to recruit Tyr22, Gln43, and Gln47 and to stabilize the hydrogen bonding network observed in trHbs. The absence of His46 near the porphyrin suggested hexacoordination in the ferric state is strained at the distal site and is relieved upon decoordination or incorporation of pentacoordinate metal centers in the porphyrin. Additional examination of triple-resonance data is underway to confirm the observations reported here.

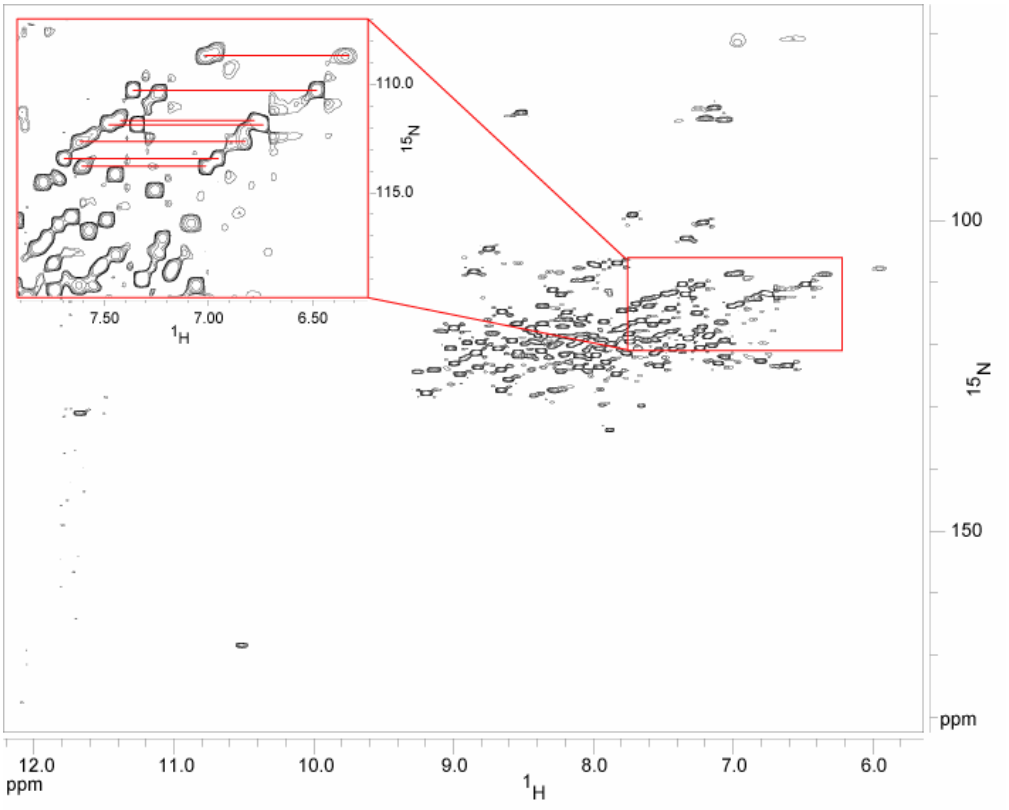

Figure 6.4 ^{1}H-^{15}N HSQC of S6803 rHb-ZnPPIX collected at 298 K (20 mM phosphate, pH 7.2, 95% $^{1}H_2O$: 5% $^{2}H_2O$). Here the NδH of His70 is observed at 10.5 ppm (^{15}N, 168 ppm). A shifted NH is also observed at 11.6 ppm (^{15}N, 131 ppm), and is likely the backbone NH of His70. The inset shows the 7 NH_2 groups in the S6803 Hb structure.

6.3.4 Variable Temperature and pH Data

A non-uniform temperature response was observed for the ^{1}H spectra of rHb-ZnPPIX (Figure 6.5). At high temperature, all the meso-H lines were sharp, but as the temperature was lowered, the α-meso signal broadened more significantly than the other meso protons, suggesting that this resonance reported on a local dynamic process. Similar behavior was observed for the methyl groups of Val121 in the H-helix; however, in this case, a maximum broadening was reached at 288 K.

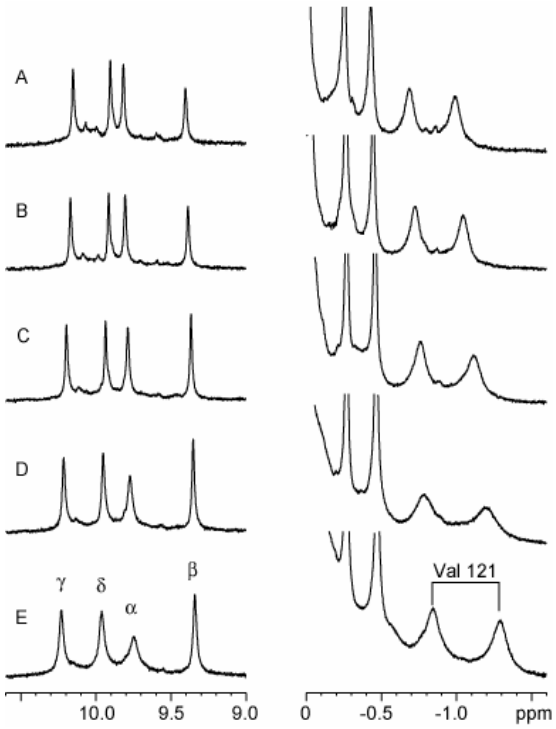

Figure 6.5 Portions of the rHb-ZnPPIX ^{1}H spectrum at (A) 313 K, (B) 308 K, (C) 298 K, (D) 288 K, and (E) 278 K. The meso protons are labeled in the left hand panel; the right hand panel illustrates the methyl groups of Val121.

The signals of Val121 and the α-meso proton resonance also broadened in response to decreased pH (Figure 6.6). Only a single set of resonances was observed for Val121 under these conditions and indicated a process near the slow limit of fast exchange. The structure of S6803 rHb-R showed this residue is near His117 and the 2-vinyl group (Figure 6.7).

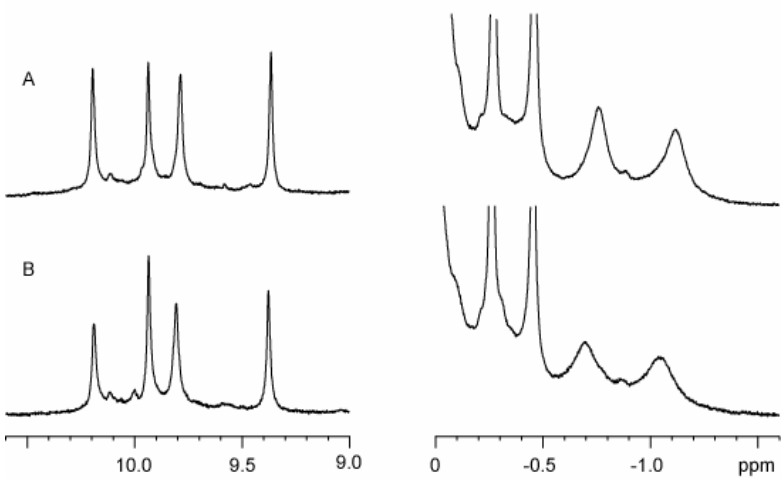

Figure 6.6 Portions of the rHb-ZnPPIX ^{1}H spectra at pH (a) 7.2 and (b) 6.46 (20 mM phosphate, 100% $^{2}H_2O$). As in Figure 6.3, the meso protons and Val121 methyl groups are shown.

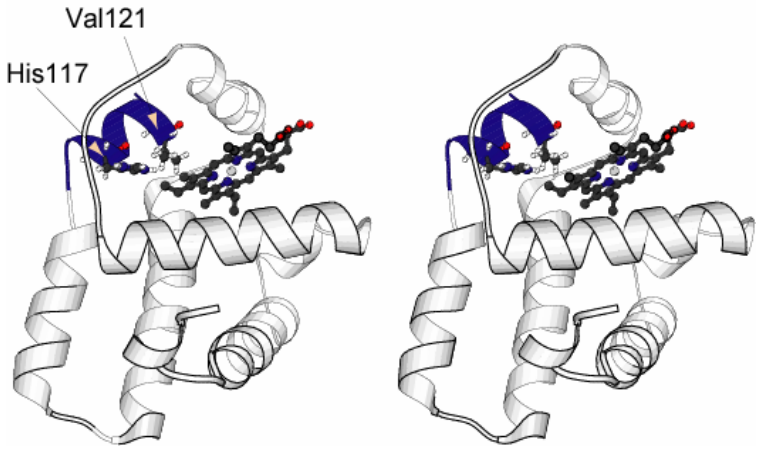

Figure 6.7 Stereoview of the structure of S6803 rHb-R (1mwb) showing the region of the helix sensitive to temperature and pH changes. His117 and Val121 are shown in proximity to the 2-vinyl group.

Temperature and pH broadening near the 2-vinyl group may also be present in the hemichrome and metcyano forms of rHb. However the diagnostic resonances were not detected and the manifestation more difficult to detect.

6.4 Conclusions

S6803 rHb-ZnPPIX did not form the covalent linkage as described in Chapter 3. Heteronuclear NMR data revealed only one axial histidine residue was present, assigned to His70. In the pentacoordinate state, His46 of rHb-ZnPPIX moved away from the influence of the porphyrin ring. The NOE data suggested that the hydrogen bonding network observed in H117A S6803 rHbCN was not present in rHb-ZnPPIX. Temperature and pH broadening indicated exchange processes near the 2-vinyl group. The dynamics appeared limited to this region near the heme and may indicate conformational exchange or titration of His117, which contribute to the reactivity in the hemichrome state. Additional analysis of the NMR data will clarify spatial relationship between the the porphyrin and its environment in rHb-ZnPPIX and may provide a model of the His46 dissociated state for ligand binding analysis.

REFERENCES

Acampora, G., and Hermans, J., Jr. (1967) *J Am Chem Soc 89*, 1543.

Alam, S. L., and Satterlee, J. D. (1994) *Biochemistry 33*, 4008.

Alei, M. J., Morgan, L. O., Wageman, W. E., and Whaley, T. W. (1980) *J Am Chem Soc 102*, 2881.

Allen, J. W., Daltrop, O., Stevens, J. M., and Ferguson, S. J. (2003) *Philos Trans R Soc Lond B Biol Sci 358*, 255.

Altman, J., Lipka, J. J., Kuntz, I., and Waskell, L. (1989) *Biochemistry 28*, 7516.

Anderson, S. L., and McIntosh, L. (1991) *J Bacteriol 173*, 2761.

Angeloni, S. V., and Potts, M. (1994) *Gene 146*, 133.

Anni, H., Vanderkooi, J. M., and Mayne, L. (1995) *Biochemistry 34*, 5744.

Antonini, E., and Brunori, M. (1971) *Hemoglobin and myoglobin in their reactions with ligands*, Vol. 12, North-Holland, Amsterdam.

Arnao, M. B., Sanchez-Bravo, J., and Acosta, M. (1996) *Biochem Mol Biol Int 39*, 1125.

Arrendondo-Peter, R., Hargrove, M. S., Sarath, G., Moran, J. F., Lohrman, J., Olson, J. S., and Klucas, R. V. (1997) *Plant Physiol 115*, 1259.

Barker, P. D., and Ferguson, S. J. (1999) *Structure Fold Des 7*, R281.

Barrick, D., Ho, N. T., Simplaceanu, V., Dahlquist, F. W., and Ho, C. (1997) *Nat Struct Biol 4*, 78.

Bashford, D., Chothia, C., and Lesk, A. M. (1987) *J Mol Biol 196*, 199.

Bertini, I., Luchinat, C., Parigi, G., and Walker, F. A. (1999) *J Biol Inorg Chem 4*, 515.

Bodenhausen, G., and Ruben, D. G. (1980) *Chem Phys Lett 69*, 185.

Bolognesi, M., Bordo, D., Rizzi, M., Tarricone, C., and Ascenzi, P. (1997) *Prog Biophys Mol Biol 68*, 29.

Bourgeois, D., Vallone, B., Schotte, F., Arcovito, A., Miele, A. E., Sciara, G., Wulff, M., Anfinrud, P., and Brunori, M. (2003) *Proc Natl Acad Sci U S A 100*, 8704.

Burmester, T., Ebner, B., Weich, B., and Hankeln, T. (2002) *Mol Biol Evol 19*, 416.

Burmester, T., Weich, B., Reinhardt, S., and Hankeln, T. (2000) *Nature 407*, 520.

Carver, T. E., Brantley, R. E., Jr., Singleton, E. W., Arduini, R. M., Quillin, M. L., Phillips, G. N., Jr., and Olson, J. S. (1992) *J Biol Chem 267*, 14443.

Cavanagh, J., Fairbrother, W. J., Palmer, A. G. I., and Skelton, N. J. (1996) *Protein NMR Spectroscopy. Principles and Practice*, Academic Press, San Diego, USA.

Cavanagh, J., and Rance, M. (1992) *J Magn Reson 96*, 670–678.

Cocco, M. J., Kao, Y. H., Phillips, A. T., and Lecomte, J. T. (1992) *Biochemistry 31*, 6481.

Conti, E., Moser, C., Rizzi, M., Mattevi, A., Lionetti, C., Coda, A., Ascenzi, P., Brunori, M., and Bolognesi, M. (1993) *J Mol Biol 233*, 498.

Couture, M., Chamberland, H., St-Pierre, B., Lafontaine, J., and Guertin, M. (1994) *Mol Gen Genet 243*, 185.

Couture, M., Das, T. K., Lee, H. C., Peisach, J., Rousseau, D. L., Wittenberg, B. A., Wittenberg, J. B., and Guertin, M. (1999a) *J Biol Chem 274*, 6898.

Couture, M., Das, T. K., Savard, P. Y., Ouellet, Y., Wittenberg, J. B., Wittenberg, B. A., Rousseau, D. L., and Guertin, M. (2000) *Eur J Biochem 267*, 4770.

Couture, M., and Guertin, M. (1996) *Eur J Biochem 242*, 779.

Couture, M., Yeh, S. R., Wittenberg, B. A., Wittenberg, J. B., Ouellet, Y., Rousseau, D. L., and Guertin, M. (1999b) *Proc Natl Acad Sci U S A 96*, 11223.

Cowley, A. B., Altuve, A., Kuchment, O., Terzyan, S., Zhang, X., Rivera, M., and Benson, D. R. (2002) *Biochemistry 41*, 11566.

Cowley, A. B., Lukat-Rodgers, G. S., Rodgers, K. R., and Benson, D. R. (2004) *Biochemistry 43*, 1656.

Dalvit, C., Tennant, L., and Wright, P. E. (1986) *J Inorg Biochem 28*, 303.

Das, T. K., Couture, M., Ouellet, Y., Guertin, M., and Rousseau, D. L. (2001) *Proc Natl Acad Sci U S A 98*, 479.

Das, T. K., Weber, R. E., Dewilde, S., Wittenberg, J. B., Wittenberg, B. A., Yamauchi, K., Van Hauwaert, M. L., Moens, L., and Rousseau, D. L. (2000) *Biochemistry 39*, 14330.

DePillis, G. D., Ozaki, S., Kuo, J. M., Maltby, D. A., and Ortiz de Montellano, P. R. (1997) *J Biol Chem 272*, 8857.

Dewilde, S., Kiger, L., Burmester, T., Hankeln, T., Baudin-Creuza, V., Aerts, T., Marden, M. C., Caubergs, R., and Moens, L. (2001) *J Biol Chem 276*, 38949.

Dickerson, R. E., and Geis, I. (1983) *Hemoglobin : structure, function, evolution, and pathology*, Benjamin/Cummings Pub. Co., Menlo Park, Calif.

Dill, K. A. (1990) *Biochemistry 29*, 7133.

Dou, Y., Olson, J. S., Wilkinson, A. J., and Ikeda-Saito, M. (1996) *Biochemistry 35*, 7107.

Du, W., Syvitski, R., Dewilde, S., Moens, L., and La Mar, G. N. (2003) *J Am Chem Soc 125*, 8080.

Duff, S. M., Wittenberg, J. B., and Hill, R. D. (1997) *J Biol Chem 272*, 16746.

Emerson, S. D., and La Mar, G. N. (1990) *Biochemistry 29*, 1556.

Falzone, C. J., and Lecomte, J. T. (2002) *J Biomol NMR 23*, 71.

Falzone, C. J., Vu, B. C., Scott, N. L., and Lecomte, J. T. (2002) *J Mol Biol 324*, 1015.

Friedman, J., Lad, L., Deshmukh, R., Li, H., Wilks, A., and Poulos, T. L. (2003) *J Biol Chem 278*, 34654.

Fujii, M., Hori, H., Miyazaki, G., Morimoto, H., and Yonetani, T. (1993) *J Biol Chem 268*, 15386.

Furukawa, Y., Ishimori, K., and Morishima, I. (2000) *Biochemistry 39*, 10996.

Gibson, Q. H., Regan, R., Elber, R., Olson, J. S., and Carver, T. E. (1992) *J Biol Chem 267*, 22022.

Gibson, Q. H., and Smith, M. H. (1965) *Proc R Soc Lond B Biol Sci 163*, 206.

Hardison, R. (1998) *J Exp Biol 201*, 1099.

Hargrove, M. S. (2000) *Biophys J 79*, 2733.

Hargrove, M. S., Barrick, D., and Olson, J. S. (1996) *Biochemistry 35*, 11293.

Hargrove, M. S., Brucker, E. A., Stec, B., Sarath, G., Arredondo-Peter, R., Klucas, R. V., Olson, J. S., and Phillips, G. N. (2000) *Structure Fold Des 8*, 1005.

Hargrove, M. S., Krzywda, S., Wilkinson, A. J., Dou, Y., Ikeda-Saito, M., and Olson, J. S. (1994) *Biochemistry 33*, 11767.

Hermans, J., Jr., and Acampora, G. (1967) *J Am Chem Soc 89*, 1547.

Herold, S., Fago, A., Weber, R. E., Dewilde, S., and Moens, L. (2004) *J Biol Chem 279*, 22841.

Hoy, J. A., Kundu, S., Trent, J. T., 3rd, Ramaswamy, S., and Hargrove, M. S. (2004) *J Biol Chem 279*, 16535.

Hu, B., Hauksson, J. B., Tran, A. T., Kolczak, U., Pandey, R., Rezzano, I. N., Smith, K. M., and La Mar, G. N. (2001) *J Am Chem Soc 123*, 10063.

Hunt, P. W., Watts, R. A., Trevaskis, B., Llewelyn, D. J., Burnell, J., Dennis, E. S., and Peacock, W. J. (2001) *Plant Mol Biol 47*, 677.

Hvitved, A. N., Trent, J. T., 3rd, Premer, S. A., and Hargrove, M. S. (2001) *J Biol Chem 276*, 34714.

Jue, T., Krishnamoorthi, R., and La Mar, G. N. (1983) *J Am Chem Soc 105*, 5701.

Kaneko, T., Sato, S., Kotani, H., Tanaka, A., Asamizu, E., Nakamura, Y., Miyajima, N., Hirosawa, M., Sugiura, M., Sasamoto, S., Kimura, T., Hosouchi, T., Matsuno, A., Muraki, A., Nakazaki, N., Naruo, K., Okumura, S., Shimpo, S., Takeuchi, C., Wada, T., Watanabe, A., Yamada, M., Yasuda, M., and Tabata, S. (1996) *DNA Res 3*, 109.

Kay, L. E., Keifer, P., and Saarinen, T. (1992) *J Am Chem Soc 114*, 10663.

Kendrew, J. C., Dickerson, R. E., Strandberg, B. E., Hart, R. G., Phillips, D. C., and Shore, V. C. (1960) *Nature 185*, 422.

Kooter, I. M., Moguilevsky, N., Bollen, A., van der Veen, L. A., Otto, C., Dekker, H. L., and Wever, R. (1999) *J Biol Chem 274*, 26794.

Kraulis, P. J. (1991) *J Appl Crystalography 24*, 946.

Krzywda, S., Murshudov, G. N., Brzozowski, A. M., Jaskolski, M., Scott, E. E., Klizas, S. A., Gibson, Q. H., Olson, J. S., and Wilkinson, A. J. (1998) *Biochemistry 37*, 15896.

Kumar, A., Ernst, R. R., and Wuthrich, K. (1980) *Biochem Biophys Res Commun 95*, 1.

Kundu, S., Premer, S. A., Hoy, J. A., Trent, J. T., 3rd, and Hargrove, M. S. (2003) *Biophys J 84*, 3931.

La Mar, G. N., Cutnell, J. D., and Kong, S. B. (1981) *Biophys J 34*, 217.

La Mar, G. N., Satterlee, J. D., and de Ropp, J. S. (1999) in *The Porphyrins Handbook* (Smith, K. M., Kadish, K., and Guilard, R., Eds.) pp 185, Academic Press, Burlington, MA.

La Mar, G. N., Toi, H., and Krishnamoorthi, R. (1984) *J Am Chem Soc 106*, 6395.

LeBrun, L. A., Xu, F., Kroetz, D. L., and Ortiz de Montellano, P. R. (2002) *Biochemistry 41*, 5931.

Lecomte, J. T., and La Mar, G. N. (1985) *Biochemistry 24*, 7388.

Lecomte, J. T., Scott, N. L., Vu, B. C., and Falzone, C. J. (2001) *Biochemistry 40*, 6541.

Lecomte, J. T. J., and La Mar, G. N. (1987) *J Am Chem Soc 109*, 7219.

Lee, K. B., La Mar, G. N., Mansfield, K. E., Smith, K. M., Pochapsky, T. C., and Sligar, S. G. (1993) *Biochim Biophys Acta 1202*, 189.

Leesch, V. W., Bujons, J., Mauk, A. G., and Hoffman, B. M. (2000) *Biochemistry 39*, 10132.

Leonard, J. J., Yonetani, T., and Callis, J. B. (1974) *Biochemistry 13*, 1460.

Lill, H., and Nelson, N. (1991) *Plant Mol Biol 17*, 641.

Liong, E. C., Dou, Y., Scott, E. E., Olson, J. S., and Phillips, G. N., Jr. (2001) *J Biol Chem 276*, 9093.

Louro, R. O., Correia, I. J., Brennan, L., Coutinho, I. B., Xavier, A. V., and Turner, D. L. (1998) *J Am Chem Soc 120*, 13240.

Lukin, J. A., Simplaceanu, V., Zou, M., Ho, N. T., and Ho, C. (2000) *Proc Natl Acad Sci U S A 97*, 10354.

Marion, D., and Wüthrich, K. (1983) *Biochem Biophys Res Commun 113*, 967.

Massiot, D., Fayon, F., Capron, M., King, I., Le Calve, S., Alonso, B., Durand, J. O., Bujoli, B., Gan, Z. H., and Hoatson, G. (2002) *Magnetic Resonance in Chemistry 40*, 70.

McNaughton, L., Hernandez, G., and LeMaster, D. M. (2003) *J Am Chem Soc 125*, 3813.

Milani, M., Ouellet, Y., Ouellet, H., Guertin, M., Boffi, A., Antonini, G., Bocedi, A., Mattu, M., Bolognesi, M., and Ascenzi, P. (2004a) *Biochemistry 43*, 5213.

Milani, M., Pesce, A., Ouellet, H., Guertin, M., and Bolognesi, M. (2003a) *IUBMB Life 55*, 623.

Milani, M., Pesce, A., Ouellet, Y., Ascenzi, P., Guertin, M., and Bolognesi, M. (2001) *Embo J 20*, 3902.

Milani, M., Pesce, A., Ouellet, Y., Dewilde, S., Friedman, J., Ascenzi, P., Guertin, M., and Bolognesi, M. (2004b) *J Biol Chem 279*, 21520.

Milani, M., Savard, P. Y., Ouellet, H., Ascenzi, P., Guertin, M., and Bolognesi, M. (2003b) *Proc Natl Acad Sci U S A 100*, 5766.

Mintorovitch, J., and Satterlee, J. D. (1988) *Biochemistry 27*, 8045.

Mueller, L. (1979) *J Am Chem Soc 101*, 4481–4484.

Mukai, M., Ouellet, Y., Ouellet, H., Guertin, M., and Yeh, S. R. (2004) *Biochemistry 43*, 2764.

Neya, S., and Morishima, I. (1981) *J Biol Chem 256*, 11612.

Nienhaus, K., Deng, P., Kriegl, J. M., and Nienhaus, G. U. (2003) *Biochemistry 42*, 9647.

Ouellet, H., Juszczak, L., Dantsker, D., Samuni, U., Ouellet, Y. H., Savard, P. Y., Wittenberg, J. B., Wittenberg, B. A., Friedman, J. M., and Guertin, M. (2003) *Biochemistry 42*, 5764.

Ouellet, H., Ouellet, Y., Richard, C., Labarre, M., Wittenberg, B., Wittenberg, J., and Guertin, M. (2002) *Proc Natl Acad Sci U S A 99*, 5902.

Oxvig, C., Thomsen, A. R., Overgaard, M. T., Sørensen, E. S., Højrup, P., Bjerrum, M. J., Gleich, G. J., and Sottrup-Jensen, L. (1999) *J Biol Chem 274*, 16953.

Papp, S., Vanderkooi, J. M., Owen, C. S., Holtom, G. R., and Phillips, C. M. (1990) *Biophys J 58*, 177.

Park, H. J., Yang, C., Treff, N., Satterlee, J. D., and Kang, C. (2002) *Proteins 49*, 49.

Pelton, J. G., Torchia, D. A., Meadow, N. D., and Roseman, S. (1993) *Protein Sci 2*, 543.

Perutz, M. F. (1970) *Nature 228*, 726.

Perutz, M. F., Kendrew, J. C., and Watson, H. C. (1965) *J Mol Biol 13*, 669.

Perutz, M. F., Wilkinson, A. J., Paoli, M., and Dodson, G. G. (1998) *Annu Rev Biophys Biomol Struct 27*, 1.

Pesce, A., Couture, M., Dewilde, S., Guertin, M., Yamauchi, K., Ascenzi, P., Moens, L., and Bolognesi, M. (2000) *EMBO J 19*, 2424.

Pesce, A., Nardini, M., Ascenzi, P., Geuens, E., Dewilde, S., Moens, L., Bolognesi, M., Riggs, A. F., Hale, A., Deng, P., Nienhaus, G. U., Olson, J. S., and Nienhaus, K. (2004) *J Biol Chem*.

Pesce, A., Nardini, M., Dewilde, S., Geuens, E., Yamauchi, K., Ascenzi, P., Riggs, A. F., Moens, L., and Bolognesi, M. (2002) *Structure (Camb) 10*, 725.

Pierattelli, R., Banci, L., and Turner, D. L. (1996) *J Biol Inorg Chem 1*, 320.

Piotto, M., Saudek, V., and Sklenár, V. (1992) *J Biomol NMR 2*, 661.

Polyakov, N. E., Leshina, T. V., Konovalova, T. A., and Kispert, L. D. (2001) *Free Radic Biol Med 31*, 398.

Ptitsyn, O. B., and Ting, K. L. (1999) *J Mol Biol 291*, 671.

Qian, C., Yao, Y., Tong, Y., Wang, J., and Tang, W. (2003) *J Biol Inorg Chem 8*, 394.

Qin, J., La Mar, G. N., Cutruzzola, F., Allocatelli, C. T., Brancaccio, A., and Brunori, M. (1993) *Biophys J 65*, 2178.

Quillin, M. L., Arduini, R. M., Olson, J. S., and Phillips, G. N., Jr. (1993) *J Mol Biol 234*, 140.

Quillin, M. L., Li, T., Olson, J. S., Phillips, G. N., Jr., Dou, Y., Ikeda-Saito, M., Regan, R., Carlson, M., Gibson, Q. H., Li, H., and et al. (1995) *J Mol Biol 245*, 416.

Rance, M., Sørensen, O. W., Bodenhausen, G., Wagner, G., Ernst, R. R., and Wüthrich, K. (1983) *Biochem Biophys Res Commun 117*, 479.

Reeder, B. J., Svistunenko, D. A., Sharpe, M. A., and Wilson, M. T. (2002) *Biochemistry 41*, 367.

Rizzi, M., Wittenberg, J. B., Coda, A., Ascenzi, P., and Bolognesi, M. (1996) *J Mol Biol 258*, 1.

Sambrook, J., and Russell, D. W. (2001) *Molecular cloning : a laboratory manual*, 3rd ed., Cold Spring Harbor Laboratory Press, Cold Spring Harbor, N.Y.

Samuni, U., Dantsker, D., Ray, A., Wittenberg, J. B., Wittenberg, B. A., Dewilde, S., Moens, L., Ouellet, Y., Guertin, M., and Friedman, J. M. (2003) *J Biol Chem 278*, 27241.

Samuni, U., Ouellet, Y., Guertin, M., Friedman, J. M., and Yeh, S. R. (2004) *J Am Chem Soc 126*, 2682.

Sawai, H., Kawada, N., Yoshizato, K., Nakajima, H., Aono, S., and Shiro, Y. (2003) *Biochemistry 42*, 5133.

Schmid, F. X. (1989) in *Protein structure A Practical Approach* (Creighton, T. E., Ed.) pp 251, IRL Press, New York.

Schotte, F., Lim, M., Jackson, T. A., Smirnov, A. V., Soman, J., Olson, J. S., Phillips, G. N., Jr., Wulff, M., and Anfinrud, P. A. (2003) *Science 300*, 1944.

Schulz, H., Hennecke, H., and Thöny-Meyer, L. (1998) *Science 281*, 1197.

Scott, N. L., Falzone, C. J., Vuletich, D. A., Zhao, J., Bryant, D. A., and Lecomte, J. T. (2002) *Biochemistry 41*, 6902.

Scott, N. L., and Lecomte, J. T. (2000) *Protein Sci 9*, 587.

Shokhirev, N. V., and Walker, F. A. (1998a) *J Am Chem Soc 120*, 981.

Shokhirev, N. V., and Walker, F. A. (1998b) *J Biol Inorg Chem 3*, 581.

Shulman, R. G., Glarum, S. H., and Karplus, M. (1971) *J Mol Biol 57*, 93.

Silchenko, S., Sippel, M. L., Kuchment, O., Benson, D. R., Mauk, A. G., Altuve, A., and Rivera, M. (2000) *Biochem Biophys Res Commun 273*, 467.

Springer, B. A., Egeberg, K. D., Sligar, S. G., Rohlfs, R. J., Mathews, A. J., and Olson, J. S. (1989) *J Biol Chem 264*, 3057.

States, D. J., Haberkorn, R. A., and Ruben, D. J. (1982) *J Magn Reson 48*, 286.

Stevens, J. M., Daltrop, O., Higham, C. W., and Ferguson, S. J. (2003) *J Biol Chem 278*, 20500.

Sudhakar, K., Loe, S., Yonetani, T., and Vanderkooi, J. M. (1994) *J Biol Chem 269*, 23095.

Sun, Y., Jin, K., Mao, X. O., Zhu, Y., and Greenberg, D. A. (2001) *Proc Natl Acad Sci U S A 98*, 15306.

Teeter, M. M. (2004) *Protein Sci 13*, 313.

Thöny-Meyer, L. (2003) *Biochemistry 42*, 13099.

Thorsteinsson, M. V., Bevan, D. R., Ebel, R. E., Weber, R. E., and Potts, M. (1996) *Biochim Biophys Acta 1292*, 133.

Thorsteinsson, M. V., Bevan, D. R., Potts, M., Dou, Y., Eich, R. F., Hargrove, M. S., Gibson, Q. H., and Olson, J. S. (1999) *Biochemistry 38*, 2117.

Tilton, R. F., Jr., Kuntz, I. D., Jr., and Petsko, G. A. (1984) *Biochemistry 23*, 2849.

Tilton, R. F., Jr., Singh, U. C., Kuntz, I. D., Jr., and Kollman, P. A. (1988) *J Mol Biol 199*, 195.

Tomlinson, E. J., and Ferguson, S. J. (2000a) *Proc Natl Acad Sci U S A 97*, 5156.

Tomlinson, E. J., and Ferguson, S. J. (2000b) *J Biol Chem 275*, 32530.

Tran-Dinh, S., Fermandjian, S., Sala, E., Mermet-Bouvier, R., and Fromageot, P. (1975) *J Am Chem Soc 97*, 1267.

Trent, J. T., 3rd, and Hargrove, M. S. (2002) *J Biol Chem 277*, 19538.

Trent, J. T., 3rd, Hvitved, A. N., and Hargrove, M. S. (2001a) *Biochemistry 40*, 6155.

Trent, J. T., 3rd, Kundu, S., Hoy, J. A., and Hargrove, M. S. (2004) *J Mol Biol 341*, 1097.

Trent, J. T., 3rd, Watts, R. A., and Hargrove, M. S. (2001b) *J Biol Chem 276*, 30106.

Turner, D. L. (1995) *Eur J Biochem 227*, 829.

Turner, D. L. (2000) *J Biol Inorg Chem 5*, 328.

Turner, D. L., Brennan, L., Messias, A. C., Teodoro, M. L., and Xavier, A. V. (2000) *Eur Biophys J 29*, 104.

Vu, B. C., Jones, A. D., and Lecomte, J. T. (2002) *J Am Chem Soc 124*, 8544.

Vu, B. C., Nothnagel, H. J., Vuletich, D. A., Falzone, C. J., and Lecomte, J. T. J. (2004a) *Biochemistry*, *in press*.

Vu, B. C., Vuletich, D. A., Kuriakose, S. A., Falzone, C. J., and Lecomte, J. T. (2004b) *J Biol Inorg Chem 9*, 183.

Warshel, A. (1977) *Proc Natl Acad Sci U S A 74*, 1789.

Weber, R. E., and Vinogradov, S. N. (2001) *Physiol Rev 81*, 569.

Wink, D. A., Wink, C. B., Nims, R. W., and Ford, P. C. (1994) *Environ Health Perspect 102 Suppl 3*, 11.

Wishart, D. S., Bigam, C. G., Yao, J., Abildgaard, F., Dyson, H. J., Oldfield, E., Markley, J. L., and Sykes, B. D. (1995) *J Biomol NMR 6*, 135.

Wittenberg, J. B., Bolognesi, M., Wittenberg, B. A., and Guertin, M. (2002) *J Biol Chem 277*, 871.

Yeh, S. R., Couture, M., Ouellet, Y., Guertin, M., and Rousseau, D. L. (2000) *J Biol Chem 275*, 1679.

VITA

Bao-Han Christie Vu

BORN: Oklahoma City, Oklahoma November 15, 1976

EDUCATION:

B.S., Chemistry, Creighton University	May 1998
M.S., Chemistry, The Pennsylvania State University	August 2001
Ph.D., Chemistry, The Pennsylvania State University	December 2004

PUBLICATIONS

Vu, B.C., Nothnagel, H.J., Vuletich, D.A., Falzone, C.J., Lecomte, J.T.J (2004) Cyanide Binding to Hexacoordinate Cyanobacterial Hemoglobins: Hydrogen Bonding Network and Heme Pocket Rearrangement in Ferric H117A Synechocystis Hb. *Biochemistry*, *in press*.

Vu, B. C., Vuletich, D.A., Kuriakose, S.A., Falzone, C.J., and Lecomte, J.T.J. (2004) Characterization of the Heme-Histidine Cross-Link in Cyanobacterial Hemoglobins from *Synechocystis* sp. PCC 6803 and *Synechococcus* sp. PCC 7002. *J. Biol. Inorg. Chem.* **9**, 183-194.

Lecomte, J. T. J., Vuletich, D.A., Vu, B. C., Kuriakose, S. A., Scott, N. L., and Falzone, C. J. (2004) Structural Properties of Cyanobacterial Hemoglobins: the Unusual Heme-Protein Cross-Link of *Synechocystis* sp. PCC 6803 Hb and *Synechococcus* sp. PCC 7002 Hb. *Micron*, **35**, 69-70.

Falzone, C. J., Vu, B. C., Scott, N. L., Lecomte, J. T. J. (2002) The Solution Structure of the Recombinant Hemoglobin from the Cyanobacterium *Synechocystis* sp. PCC 6803 in its Hemichrome State. *J. Mol. Biol*, **324**, 1015-1029.

Vu, B. C., Jones, A. D., Lecomte, J. T. J. (2002) Novel Histidine-Heme Covalent Linkage in a Hemoglobin. *J. Am. Chem. Soc.*, **124,** 8544-8545.

Lecomte, J. T. J., Scott, N. L., Vu, B. C., and Falzone, C. J. (2001) Binding of Ferric Heme by the Recombinant Globin from the Cyanobacterium *Synechocystis* sp. PCC 6803. *Biochemistry,* **40,** 6541-6552.

Falzone, C. J., Wang, Y., Vu, B. C., Scott, N. L., Bhattacharya, and Lecomte, J. T. J. (2001) Structural and Dynamic Perturbations Induced by Heme Binding in Cytochrome b_5 *Biochemistry,***40**, 4879-91.

AWARDS

Apple Fellowship	2003
Clare Booth Luce Women in Science Scholar	1997-1998